

UNIVERSITY OF OKLAHOMA

GRADUATE COLLEGE

POLYMER ELECTROLYTE CONDUCTIVITY AND THE VOGEL EQUATION

A Dissertation

SUBMITTED TO THE GRADUATE FACULTY

in partial fulfillment of the requirements for the

degree of

Doctor of Philosophy

By

Frederick W. McKenna

Norman, Oklahoma

2004

UMI Number: 3148979



UMI Microform 3148979

Copyright 2005 by ProQuest Information and Learning Company.
All rights reserved. This microform edition is protected against
unauthorized copying under Title 17, United States Code.

ProQuest Information and Learning Company
300 North Zeeb Road
P.O. Box 1346
Ann Arbor, MI 48106-1346

POLYMER ELECTROLYTE CONDUCTIVITY AND THE VOGEL EQUATION

A Dissertation APPROVED FOR THE
DEPARTMENT OF PHYSICS AND ASTRONOMY

BY

John E. Furneaux

Roger Frech

Kieran Mullen

Neil Shafer-Ray

Ralph Wheeler

©Copyright by Frederick W. McKenna 2004

All Rights Reserved

Acknowledgments

I would like to thank Drs. John Furneaux, Roger Frech, Kieran Mullen, Neil Shafer-Ray, and Ralph Wheeler for serving on my committee. I am also grateful to Dr. Masood Khan for X-ray structure work and to Dr. Vito Di Noto for reviewing this thesis.

During my research I was fortunate to work with and learn from many members of Dr. Frech's research group. It is therefore a pleasure to acknowledge Dr. Chris Rhodes, Dr. Shawna York, Dr. Rebecca Sanders, Dr. Varuni Seneviratne, Chris Burba, Matt Petrowski, Nathalie Rocher, Rachel Mason, and Gwen Giffin.

Finally, I would like to thank my parents, James and Lois, for their constant support.

Contents

1	Introduction to Polymer Electrolytes	1
1.1	Thermodynamics of Dissolution	4
1.2	Ionic species in polymer electrolytes	5
1.3	Structure and Morphology of polymer electrolytes	7
1.3.1	Semicrystalline Polymer Morphology	8
1.3.2	Salt-polymer structures in PEO LiCF ₃ SO ₃	8
1.4	Polymer motion and conductivity	11
1.5	Thesis Outline	13
2	Experimental	20
2.1	Sample Preparation	20
2.2	Infrared Spectroscopy	22
2.3	Impedance Spectroscopy	22
2.3.1	Introduction	22
2.3.2	Equipment Setup	28

2.3.3	Operation of HP 4192 LF	30
2.3.4	Circuit Modelling and Data Presentation	31
2.3.5	Non-linear Curve Fitting	39
3	Frequency-Dependent Conductivity of Polymer Electro-	
	lytes	42
3.1	Introduction	42
3.2	Conductivity properties of disordered solids	44
3.3	Scaling properties of polymer electrolytes	46
3.4	Theoretical treatments of conductivity scaling and frequency dispersion	57
3.4.1	The macroscopic model	58
3.4.2	The symmetric hopping model	62
3.4.3	Site energy disorder and Coulomb interactions	67
3.5	Summary	68
4	The Vogel Equation and Polymer Electrolytes	73
4.1	Approaches to the Vogel equation	74
4.1.1	Free volume theories	74
4.1.2	The configuration entropy approach	76
4.2	Polymer Electrolytes and the Vogel equation	79
4.2.1	Partially crystalline polymer electrolytes	79
4.2.2	Amorphous polymer electrolytes	85

4.2.3	Low temperature behavior of polymer electrolytes	88
4.3	The Vogel equation and non-polymer electrolyte ionic conductors . .	90
4.4	Summary	92
5	Semi-Crystalline Polymer Electrolytes	96
5.1	Examination of the two mechanisms seen in partially crystalline poly- mer electrolytes	98
5.2	Application of the two Arrhenius equation to the PEO LiTFSI system	103
5.3	New parameters for the two Arrhenius equation	108
5.4	Summary	116
6	The Compensation Effect	119
6.1	Introduction to the compensation effect	119
6.2	Heat bath excitations and the compensation effect	121
6.2.1	The theory of Peacock-Lopez and Suhl	121
6.2.2	The theory of Yelon and co-workers	124
6.2.3	The theory of Linert	126
6.2.4	The compensation effect and the melting temperature	130
6.3	The compensation effect and polymers	134
6.4	Summary	138
7	A microscopic picture of polymer electrolyte conductiv- ity	142

7.1	Microscopic pictures of ion transport	143
7.1.1	hydrodynamic model	144
7.1.2	Dynamic Bond Percolation	145
7.1.3	Requirements of a microscopic interpretation based on partially cystalline polymer electrolytes	146
7.1.4	Models of transport in non-polymer electrolyte ionic conductors	148
7.1.5	Polymer electrolytes	154
7.1.6	The microscopic basis of the compensation effect	161
7.2	Summary	164
8	Generalization and glass phenomenology	168
8.1	Generalization to a Distribution of Activation Energies	169
8.2	Some theories of glass phenomenology	177
8.3	Some comments on polymer electrolytes	182
8.4	Summary	184
8.5	Mathematical Appendix	185
8.5.1	Derivation of $g_V(E)$	185
8.5.2	Characteristic Function	190
9	Summary and Future Work	194
9.1	Summary	194
9.2	Future Work	198

Abstract

Polymer electrolytes are ion conducting solids with possible applications to rechargeable batteries. Despite great interest much remains unknown about the conductivity of polymer electrolytes. A number of topics concerned with polymer electrolyte conductivity are discussed in this work.

The frequency-dependent conductivity of an amorphous polymer electrolyte is examined. It is shown that the frequency-dependent conductivity of polymer electrolytes exhibit many of the same properties as ion conducting glasses. This suggests similarities in the mechanism of ion conduction between polymer electrolytes and ionic glasses.

The conductivity of semi-crystalline polymer electrolyte systems are also investigated. This work demonstrates that at least two separate ion conduction mechanisms are occurring in semi-crystalline polymer electrolytes. A proposal is made for understanding the discontinuities seen in the conductivity of semi-crystalline polymer electrolytes.

An examination of conductivity prefactors reveals the possible presence of the compensation effect. While great care must be taken before reporting a compensation effect, this work and the work of other researchers suggests that there is relation between the conductivity prefactors and the activation energy. Various theories of the compensation effect are discussed, and consistent with Linert's theory a connection is made between the compensation effect and the vibrational spectra of the polymer.

The free volume theory of the Vogel equation is discussed. Some of the weaknesses

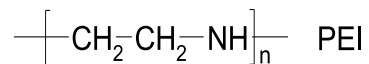
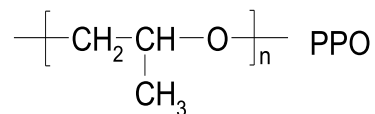
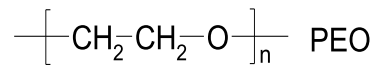
of this theory as applied to polymer electrolytes are pointed out. A theory of the Vogel equation in terms of hopping models is presented. This theory is consistent with the results of the frequency-dependent conductivity and semi-crystalline polymer electrolytes.

Chapter 1

Introduction to Polymer Electrolytes

This thesis is concerned with the conductivity of polymer electrolytes. A polymer is a large molecule made by stringing together smaller molecules. Some examples of polymers of interest for polymer electrolytes are shown in table 1.1. The polymers shown in table 1.1 include polyethylene oxide(PEO), polypropylene oxide(PPO), and polyethylene imine(PEI). The large molecules that make up the polymer mean that polymer electrolytes have physical properties that differ greatly from liquid electrolytes. A polymer electrolyte is formed by dissolving a salt into the polymer. Not all polymers are capable of dissolving salts. Those shown in table 1.1 are capable of dissolving salts. The salt starts to dissolve when one or more of the atoms that make up the polymer interact with the salt. This interaction may cause the salt to separate into positively charged cations and negatively charged anions. Examples of salts that have been used in polymer electrolytes are lithium bromide(LiBr), lithium trifluoromethanesulfonate(also called lithium triflate)(LiCF₃SO₃), and lithium perchlorate(LiClO₄). While lithium is the most interesting cation for applications, other

Table 1.1: Some common polymers used for polymer electrolytes



cations such a sodium and magnesium can also be used.

The conductivity of polymer electrolytes was first investigated by P. V. Wright and co-workers in 1973[1]. Widespread interest in polymer electrolytes began in 1979 when Armand and co-workers[2] pointed out the potential application of polymer electrolytes in solid state batteries. Since then a wide variety of techniques including NMR[3], EXAFS[4], vibrational spectroscopy[5], DSC[6], X-ray[7], and neutron scattering[8] in addition to conductivity measurements have been performed to better understand polymer electrolytes. Some of the fundamental questions these studies try to address are: (1) what are the salt polymer interactions?, (2) what are the ion-ion interactions?, (3) what phases appear in polymer electrolytes?, and (4) what is the ion transport mechanism? The knowledge needed to answer the last question depends heavily on the knowledge needed to answer the other questions.

As mentioned above, polymer electrolytes have different physical properties than liquid electrolytes. It is these different physical properties that fuel technological interest in polymer electrolytes. This technological interest stems mainly from the potential applications of polymer electrolytes in rechargeable solid state batteries[9, 10].

A solid state plastic separator would solve many problems associated with battery construction. In batteries using a liquid electrolyte, elaborate precautions are necessary in order to ensure that there is no leakage of the electrolyte. The containers necessary to ensure that there are no leaks decrease the energy density (energy/weight) of the battery. A solid state battery would largely eliminate this problem. On the otherhand, solid state separators such as ionically conducting crystals introduce different problems. When a battery is charged or discharged, the anode and cathode change volume as ions enter or leave. A plastic solid separator would be able to accommodate these volume changes better than a crystalline separator. A further advantage of an polymer electrolyte would be the ability to process the polymer in wide variety of shapes allowing many different battery configurations.

There are however many obstacles that must be overcome before polymer electrolytes see widespread use. The most serious obstacle is the conductivity of polymer electrolytes. For widespread applications, a conductivity greater than 10^{-3}S/cm at room temperature is desired. This is about two orders of magnitude greater than what is achieved with the better polymer electrolytes. Another problem with polymer electrolytes is that both the cations and anions conduct. For battery applications it is desirable that only the cations conduct since only the electrodes are reactive with the cations. Anion conduction can lead to polarization effects in the battery which reduce battery performance. These severe challenges must be overcome before polymer electrolyte batteries see wide spread use.

The main part of this chapter briefly reviews aspects of polymer electrolytes rele-

vant to the main body of the this thesis. Reviews going into more depth or covering different aspects of polymer electrolytes can be found in references [11, 12, 9, 13, 14, 15, 16, 17, 18, 10, 19, 20, 7].

1.1 Thermodynamics of Dissolution

In order for a polymer to dissolve a salt, the free energy change going from undissolved to dissolved must to negative. Thermodynamics says that the change in free energy is given by

$$\Delta G = \Delta H - T\Delta S \quad (1.1)$$

where ΔG is the change in free energy, ΔH is the change in enthalpy, and ΔS is the change in entropy. The change in enthalpy will depend on such factors as the lattice energy of the salt and the bonds formed between the polymer and the ions[9]. For example, polyethylene is very poor at dissolving salts. The reason is that the carbons along the backbone do not interact with the ions. There is therefore no way to overcome the lattice energy of the salt. Polyethylene oxide on the other hand dissolves certain salts quite well. This is because the ether oxygens along the PEO backbone coordinate with the cations of the salt. The coordination of the cations to the polymer allows the salt to be dissolved.

Since $\Delta G \propto T\Delta S$, the change in free energy will depend increasingly on the change in entropy as the temperature is increased. As the salt is dissolved, the ions are seperated from each other. This leads to a increase in entropy. However, as the

polymer coordinates to the cations, the polymer segments around the cations become more ordered. This ordering restricts the conformations of the polymer, and the entropy decreases. In PPO, it is seen that at high temperatures the salt precipitates out of the polymer[21]. This suggests that ΔS is negative for polymer electrolytes, and that at high temperatures the decrease in enthalpy on dissolution is outweighed by the increase in entropy that results when the salt precipitates. It will be seen later that the entropy changes due to cation-polymer coordination will effect the conductivity.

1.2 Ionic species in polymer electrolytes

Even though the salts are dissolved by the polymer, this does not mean that cations and anions are well separated from each other. There is ample evidence that the ions interact with each other. These interactions lead to the formation of ion pairs and ion aggregates.

The most direct evidence for ion-ion interactions is probably from vibrational spectroscopy. To use vibrational spectroscopy it is necessary to use an anion that has a set of vibrational modes. These vibrational modes will be sensitive to the association of the anion with the cation. A vibrational peak associated with the free anion will be in a slightly different location than a peak associated with an anion that is paired with a cation. The reason the peaks shift is that the electron distribution around the anion is perturbed when the cation is paired with the anion. Figure 1.1

illustrates these statements with the triflate anion. The peaks in the figure relates to a vibration of the CF_3 group on the triflate anion. While the peak resolution in figure 1.1 is not ideal, it is sufficient to reveal the presence of at least three peaks. Through a combination of experiment and calculations the three peaks in the figure have been assigned[22]. The lowest wavenumber peak around 752 cm^{-1} has been assigned to the free anion. The peak around 758 cm^{-1} has been assigned a cation-anion pair. The peak around 763 cm^{-1} has been assigned to a salt aggregate. The term aggregate will be used to refer to any salt structure involving three or more ions. The aggregate illustrated in the figure is a minimum aggregate structure that gives a peak around 763 cm^{-1} . A more complex aggregate structure involving multiple cations and anions will also give a peak around 763 cm^{-1} . A proposed aggregate structure will be mentioned below.

In speaking of ionic species it would be a mistake to think of the species as static entities. The vibrational spectrum of the anion is a time average spectrum over a relatively long period. During that time the ionic species are not static but are changing from free to pair, pair to free, aggregate to pair, etc.

The simultaneous presence of free ions, pairs, and aggregates has important consequences for polymer electrolyte conductivity. Since pairs are charge neutral, an applied electric field will not cause translational motion of a pair. While an aggregate can have a charge associated with it, a large aggregate structure such as the one shown in figure 1.4 is unlikely to contribute to charge transport. Instead what is likely necessary for charge transport is the dissociation of pairs into free ions or for a

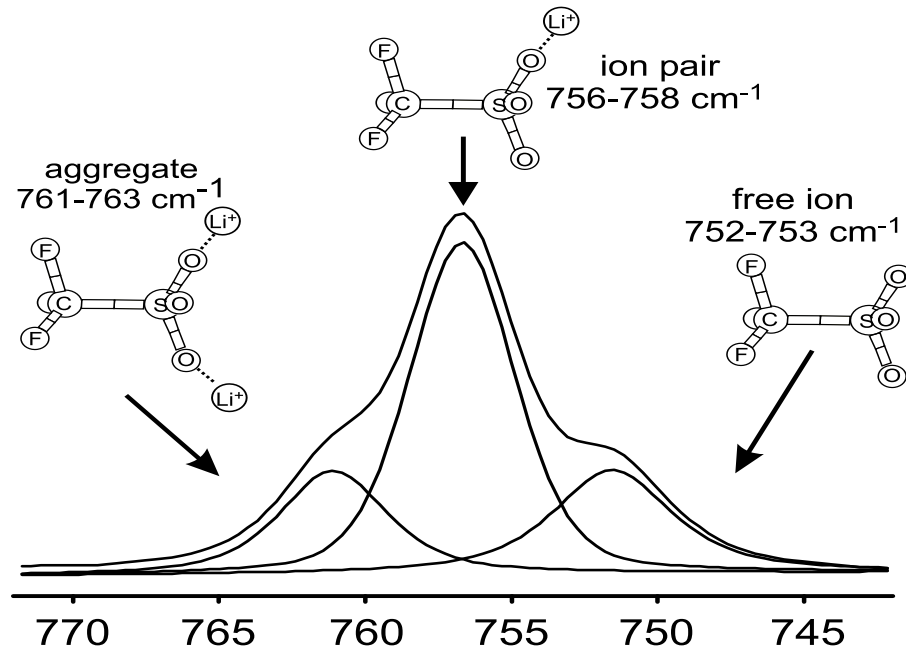


Figure 1.1: Ion association peaks seen in Raman spectra ($\delta_s(CF_3)$ vibrational mode of the triflate anion). Figure courtesy of Chris Rhodes.

ion to dissociate from a aggregate structure.

1.3 Structure and Morphology of polymer electrolytes

PPO is a amorphous polymer because of the bulky CH_3 side group which prevents the polymer from crystallizing. PEO has an identical backbone structure as PPO. PEO, however, lacks the CH_3 side group and is able to crystallize. When salts are dissolved in a polymer, small locally ordered structures can be identified in the polymer electrolyte.

1.3.1 Semicrystalline Polymer Morphology

Because polymers are long linear molecules, polymers such as PEO are not able to crystallize completely. Instead, polymers crystallize in layers[23]. A schematic picture of this situation is shown in figure 1.2. Regions of amorphous polymer lie between the crystalline layers. It has been shown that ion conduction takes place primarily in these amorphous regions[24]. The ion transport in the crystalline regions is negligible. Ideally these crystalline layers would not be present since they restrict the number of pathways an ion can travel. Amorphous and semi-crystalline polymers can be distinguished by their macroscopic properties. Amorphous polymers are usually clear and flexible whereas semi-crystalline polymers are usually more rigid and opaque. Also the DSC of semi-crystalline polymers shows peaks corresponding to melting transitions whereas no peaks are seen in amorphous polymers. PEO melts around 60°C [24], and as will be seen later melting leads to a dramatic change in the conductivity.

For later reference, the crystalline structure of PEO is shown in figure 1.3 [25]. The helix shown in figure 1.3 is a 7_2 helix(7 monomer units in 2 revolutions of the helix). The CCOC dihedral angles are trans and the OCCO dihedral angles are gauche.

1.3.2 Salt-polymer structures in PEO LiCF_3SO_3

By studying the spectra of crystalline model compounds and comparing these to the spectra of polymer electrolytes, Rhodes and Frech have proposed a number of salt-polymer structures for the PEO LiCF_3SO_3 system[5]. The structure proposed

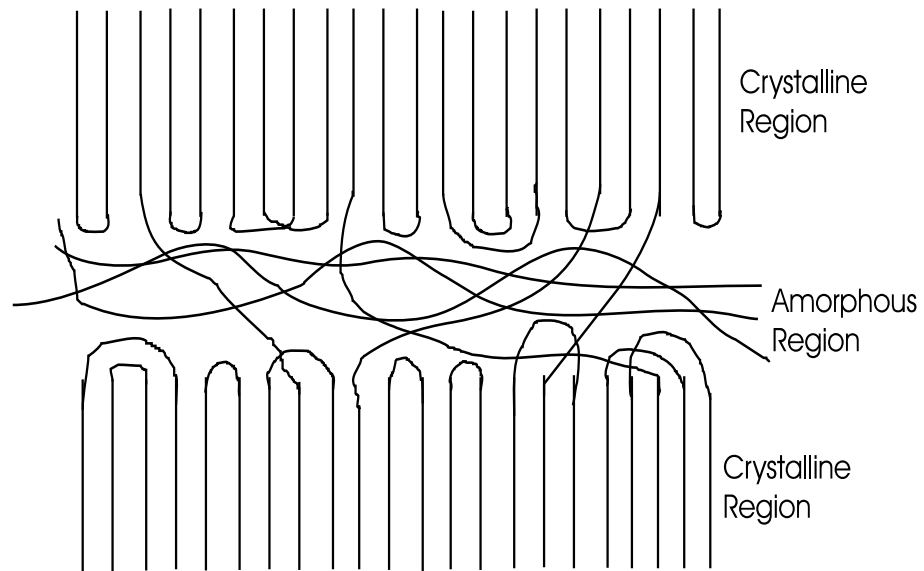


Figure 1.2: Polymers usually crystallize as spherulites. The spherulites are made up of alternating layers of crystalline and amorphous regions

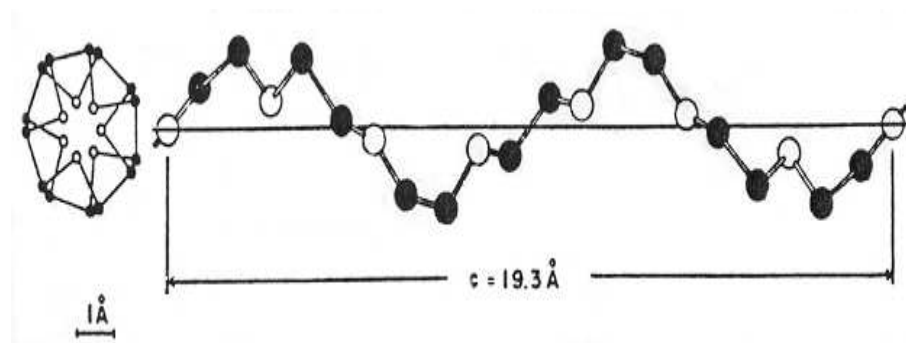


Figure 1.3: Structure of crystalline PEO [25]

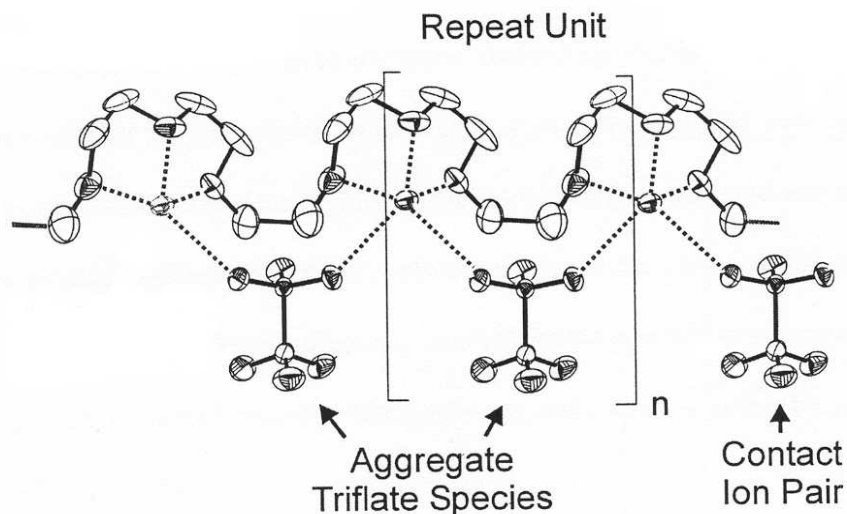


Figure 1.4: Proposed aggregate structure in PEO LiCF_3SO_3 [5]

for the aggregate is shown in figure 1.4. The structure shown in figure 1.4 will give two different peaks in the vibrational spectra. Anions that are in the middle of the aggregate structure will give peaks around 762 cm^{-1} . Anions at the ends of the aggregate structure will show spectral signatures characteristic of ion pairs. Note that in this proposed aggregate structure that the cations are coordinated to both the anions and the ether oxygens along the PEO backbone. The cations cause the PEO backbone to adopt a crystal like helical configuration. The aggregate structure is located in the amorphous regions of the PEO, so the salt causes the PEO to assume locally ordered structures even in the amorphous region. The aggregate structure shown in figure 1.4 makes it very unlikely that the aggregate itself can be a charge carrier. Instead free cations and anions must dissociate from the aggregate structure in order for there to be charge transport.

As the salt concentration is increased, the aggregate structure becomes larger and larger. Eventually crystalline domains will form. The salt-polymer crystalline domains are distinguishable from the pure PEO crystalline domains by DSC and x-ray. These salt-polymer crystalline domains are undesirable since the salt is trapped in the domain and cannot contribute to the conductivity.

While the structure discussed here has been for PEO LiCF₃SO₃, it is likely that other salt-polymer systems will have their own locally ordered structures embedded in the amorphous phase.

1.4 Polymer motion and conductivity

One of the unique features of solid polymer electrolytes is the close relation between structural relaxations in the polymer and the ion conductivity. In other solid ionic conductors such as ionic glasses, conductivity and structural relaxations are not as closely coupled.

One way of demonstrating the relation between structural relaxations and ion conductivity is through Angell's decoupling index [26, 27, 28]. Angell's decoupling index is defined as

$$R_\tau = \frac{\tau_s}{\tau_\sigma} \tag{1.2}$$

where τ_s is a characteristic structural relaxation time and τ_σ is a characteristic time associated with the conductivity. One possibility for τ_σ is

$$\tau_\sigma = \frac{\epsilon_0 \epsilon_\infty}{\sigma_{dc}} \tag{1.3}$$

where ϵ_0 is the permittivity of free space, ϵ_∞ is the infinite frequency dielectric constant, and σ_{dc} is the DC conductivity. A value for τ_s can be obtained from ultrasonic measurement, Brillouin scattering, or the microscopic viscosity. The decoupling index has been measured for some polymer electrolyte systems. The measurements give $R_\tau \sim 10^{-2}$ at low values of salt concentration[26]. This says that structural relaxations are a bit quicker than the time scale associated with conductivity. The decoupling index, however, increases as salt concentration increases[28]. R_τ is not unity as would be expected for perfect coupling between conductivity and structural relaxations. The influence of ion-ion interactions has been discussed as a reason for R_τ being less than one[27].

Another demonstration of the connection between conductivity and structural relaxations is the comparison of the α -relaxation and the conductivity. The α -relaxation is a term for a prominent peak seen in plots of the imaginary part of the frequency-dependent dielectric constant. Higher frequency peaks have been termed β -relaxations and γ -relaxations. These peaks involve the rotation of dipoles in the polymer. The α -relaxation probably involves dipoles along the polymer backbone, so the presence of the α -relaxation entails some movement of the polymer backbone. The temperature dependence of the α -relaxation compares well with the temperature dependence of polymer electrolyte conductivity at low salt concentrations[29] which suggests the importance of polymer segmental motion to conductivity. This comparison is shown in figure 1.5. Higher salt concentrations do not scale as well as the concentration seen in the figure.

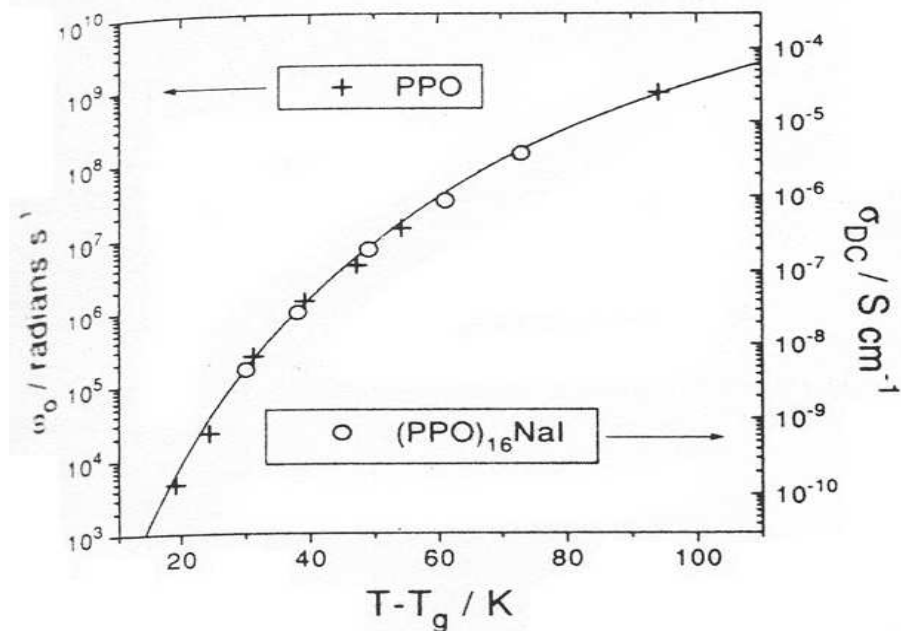


Figure 1.5: Comparison of the α relaxation and conductivity[29]. The x-axis has been shifted by the glass transition temperature.

The above experiments emphasize the importance of polymer motion to conductivity. Unfortunately, the experiments use PPO rather than PEO. PEO is a better solvent than PPO and yields higher conductivities. However, the semicrystalline nature of PEO makes it much harder to perform the experiments performed above. Some of the results might be different for PEO than for PPO.

1.5 Thesis Outline

This thesis is concerned primarily with polymer electrolyte conductivity. The primary equation used to model polymer electrolyte conductivity is the Vogel equation. The Vogel equation is often associated with the concept of free volume, so free volume

is proposed as a basis for understanding ion transport in polymer electrolytes. This study argues that polymer electrolyte conductivity and the Vogel equation should be understood in terms of hopping models. The thesis is divided as follows.

Chapter 2: *Experimental* discusses the materials, techniques and equipment used in this study. Since this study deals with polymer electrolyte conductivity and impedance spectroscopy is the main tool used to measure polymer electrolyte conductivity, a fairly lengthy review is given on impedance spectroscopy.

Chapter 3 discusses the frequency-dependent conductivity of polymer electrolytes. It is shown that polymer electrolytes exhibit frequency-dependent properties similar to other disordered solid ionic conductors such as ionic glasses. The models that have been proposed to understand the frequency-dependent properties of disordered solid ionic conductors are discussed. These models are based on hopping models and involve a distribution of hopping barriers. Since polymer electrolytes show the same frequency-dependent properties as ionically conducting glasses and ionically conducting glasses are modelled with hopping models, the chapter argues that polymer electrolyte conductivity should also be understood in terms of hopping models.

Chapter 4 discusses the Vogel equation. Since the Vogel equation is the primary empirical equation used to model conductivity in amorphous polymer electrolytes, the chapter presents the two main arguments used to justify the Vogel equation. These two models are known as the free volume model and the configurational entropy model. Neither of these models are hopping models, and it would be difficult to present any discussion of the frequency-dependent conductivity in terms of them.

While the Vogel equation is widely used to fit polymer electrolyte DC conductivity, there are instances where the Vogel equation fails to model the observed behavior. These failures occur in semi-crystalline polymer electrolytes and in certain amorphous polymer electrolytes that show Arrhenius behavior at low temperatures. The next chapter proposes an equation that can deal with semi-crystalline polymer electrolytes and the low temperature Arrhenius behavior.

In Chapter 5: *Semi-Crystalline Polymer Electrolytes*, an equation based on fitting the frequency-dependent impedance of semi-crystalline polymer electrolytes is suggested. This equation is based on the recognition that there are at least two mechanisms operating in semi-crystalline polymer electrolytes. The equation is tested on the PEO LiTFSI polymer salt system. While this equation was suggested by semi-crystalline polymer electrolytes, it can also fit amorphous polymer electrolytes over a limited temperature range. An examination of the conductivity prefactors suggests the compensation effect.

Chapter 6: *The Compensation Effect* discusses the compensation effect and reviews a number of theories that have been put forth to understand it.

Chapter 7: *Microscopic Interpretation* discusses a possible physical basis for the equation proposed in chapter 5. The proposed microscopic picture is highly speculative, but it points out that ion-ion and ion-polymer interactions could be the source of the hopping barriers. Also, a correlation is made between the compensation effect parameter and vibrational peaks seen in the far IR spectra of the polymer electrolytes.

In Chapter 8: *Generalization*, a hopping model approach to the Vogel equation

is discussed. The reasoning for discussing the Vogel equation in terms of a hopping model is: (1) In chapter 3 it was shown that hopping models can be used to understand the frequency-dependent conductivity of polymer electrolytes. The DC conductivity should also be understood in terms of a hopping model. (2) In chapter 5 it was argued that the DC conductivity of semi-crystalline polymer electrolytes can be understood with a equation involving two Arrhenius factors. This equation can also be used for amorphous polymer electrolytes over a limited temperature range. The obvious generalization of the two Arrhenius equation is to a distribution of activation energies. The generalization is shown to be equivalent to the Vogel equation (but with a different physical interpretation). Some theories of viscosity in supercooled liquids which involve hopping are briefly discussed.

Finally, a summary is given.

Bibliography

- [1] D. E. Fenton, J. M. Parker, and P. V. Wright. *Polymer*, 14:589, 1973.
- [2] M. B. Armand, J. M. Chabagno, and M. J. Duclot. *Fast Ion Transport in Solids*, pages 131–136. Elsevier, 1989.
- [3] K. Hayamizu, Y. Aihara, and W. S. Price. *J. Chem. Phys.*, 113:4785, 2000.
- [4] R. G. Linford. *Chem. Soc. Rev.*, page 267, 1995.
- [5] C. P. Rhodes and R. Frech. *Macromolecules*, 34:2660, 2001.
- [6] C. Vachon, C. Labreche, A. Vallee, S. Besner, M. Dumont, and J. Prud'homme. *Macromolecules*, 28:5585, 1995.
- [7] Y. G. Andreev and P. G. Bruce. *J. Phys.:Condens. Matter*, 13:8245, 2001.
- [8] P. Carlsson. *J. Chem. Phys.*, 114:9645, 2001.
- [9] F. M Gray. *Solid Polymer Electrolyte: Fundamentals and Technological Applications*. VCH Publishers, New York, 1991.
- [10] W. H. Meyer. *Advanced Materials*, 10:439, 1998.

- [11] J. R. MacCallum and C. A. Vincent, editors. *Polymer Electrolyte Reviews*, volume 1. Elsevier, New York, 1987.
- [12] J. R. MacCallum and C. A. Vincent, editors. *Polymer Electrolyte Reviews*, volume 2. Elsevier, New York, 1989.
- [13] M. B. Armand. *Ann. Rev. Mater. Sci.*, 16:245, 1986.
- [14] C. A. Vincent. *Chemistry in Britain*, April:391, 1989.
- [15] M. A. Ratner and A. Nitzan. *Faraday Discuss. Chem. Soc.*, 88:19, 1989.
- [16] P. G. Bruce. *Synthetic Metals*, 45:267, 1991.
- [17] L. M. Torell, P. Jacobsson, and G. Petersen. *Polymer for Advanced Technologies*, 4:152, 1993.
- [18] P. G. Bruce and C. A. Vincent. *J. Chem. Soc. Faraday Trans.*, 89:3187, 1993.
- [19] A. Ferry. *Recent Res. Devel. Macromol. Res.*, 4:79, 1999.
- [20] M. A. Ratner, P. Johansson, and D. F. Shriver. *MRS Bulletin*, March:31, 2000.
- [21] G. G. Cameron and M. D. Ingram. *Polymer Electrolyte Reviews*, volume 2, chapter 5. Elsevier, 1989.
- [22] W. Huang, R. Frech, and R. A. Wheeler. *J. Phys. Chem.*, 98:100, 1994.
- [23] P. C. Painter and M. M. Coleman. *Fundamentals of Polymer Science: An Introductory Text*. Technomic, Lancaster, PA, 1997.

- [24] M. Minier, C. Berthier, and W. Gorecki. *J. Physique*, 45:739, 1984.
- [25] T. Yoshihara, H. Tadokoro, and S. Murahashi. *J. Chem. Phys.*, 41:2902, 1964.
- [26] L. M. Torell and C. A. Angell. *Br. Polym. J.*, 20:173, 1988.
- [27] M. G. McLin and C. A. Angell. *J. Phys. Chem.*, 95:9464, 1991.
- [28] M. G. McLin and C. A. Angell. *Solid State Ionics*, 53-56:1027, 1992.
- [29] A. L. Tipton, M. C. Lonergan, M. A. Ratner, D. F. Shriver, T. T. Y. Wong, and K. Han. *J. Phys. Chem.*, 98:4148, 1994.

Chapter 2

Experimental

2.1 Sample Preparation

The polymers used in this study are polyethylene oxide(PEO) and a epichlorohydrin elastomer. PEO ($M_w = 10^5$) was acquired from Aldrich. As purchased, PEO is a white powder. Prior to use, the PEO was heated to 50°C for 24 to 48 hrs. in a vacuum oven. Following the vacuum oven, the PEO was placed in a nitrogen glovebox. The chemical structure of PEO is $\text{CH}_3\text{O}-(\text{CH}_2\text{CH}_2\text{O})_n-\text{CH}_3$. The epichlorohydrin elastomer was a gift from Zeon chemicals. The tradename for the epichlorohydrin elastomer is C2000. C2000 will be used to designate the elastomer in the rest of this study. The chemical structure of C2000 is $(\text{CH}_2\text{CHCH}_2\text{ClOCH}_2\text{CH}_2\text{O})_n$. C2000 resembles a copolymer of PEO and polypropylene oxide (PPO), but the CH_3 group of the PPO has been replaced by CH_2Cl . The reason that C2000 is used instead of PPO is that PPO is only easily available in low molecular weights. At these low molecular weights, PPO is a viscous liquid instead of a solid. C2000 on the otherhand is a solid with a

Mooney viscosity between 90 and 102. As received, C2000 comes as a solid somewhat flexible block. Small pieces were cut from the block and placed in a vacuum oven at 120°C for 48 hours. Following the vacuum oven, the C2000 was placed in a nitrogen glovebox.

The salts used in this study include lithium trifluoromethanesulfonate (LiTF), lithium-(bis)trifluoromethanesulfonate imide (LiTFSI), and lithium bromide (LiBr). The chemical formula of LiTF, also called lithium triflate, is $LiCF_3SO_3$. The chemical formula of LiTFSI is $Li(N(SO_2CF_3)_2)$. The salts were dried in a vacuum oven at 120°C for 48 hours. After drying, the salts were placed in a nitrogen glovebox.

The polymer electrolyte were prepared by mixing appropriate amounts of salt and polymer. Acetonitrile was used to dissolve the salt and polymer mixture, and the subsequent solution was allowed to stir for a least 24 hours. The concentration of salt in the polymer is usually expressed in terms of the ether oxygen to metal cation ratio(O:M). Ether oxygens are the oxygens on the polymer and so do not include oxygens on the anion. The desired O:M ratio is converted to a weight ratio so that the appropriate amounts of salt and polymer can be mixed. A polymer electrolyte made of PEO and LiTF with ether oxygen to metal cation ratio of 10 to 1 will be designated as PEO LiTF 10-1.

In preparing polymer electrolytes for impedance spectroscopy, the polymer-salt-acetonitrile solution was poured into a teflon cup inside the nitrogen glovebox. The acetonitrile was allowed to evaporate over a period to two to three days. The resulting polymer electrolyte films were usually between 250 and 500 microns. The polymer

electrolyte films were then cut to size and placed inside a impedance cell inside the glovebox.

2.2 Infrared Spectroscopy

Far infrared spectra were collected on a Bruker IFS66V FT-IR. A mylar beam splitter was used in the far IR region. The resolution was set to 1 cm^{-1} . Spectra were collected by casting films on polyethylene windows.

2.3 Impedance Spectroscopy

This section explores the basics of impedance spectroscopy. Since impedance spectroscopy is the primary experimental technique used in this thesis, a review of the technique is given below.

2.3.1 Introduction

The primary use of impedance spectroscopy is to find the conductivity of samples such as polymer electrolyte films. In order to find the conductivity of a sample, typically the resistance is first found using Ohm's law:

$$R = \frac{V}{I} \tag{2.1}$$

where V is the applied(measured) voltage and I is the measured(applied) current.

The conductivity can then be found with

$$R = \frac{l}{\sigma A} \quad (2.2)$$

where σ is the sample conductivity, l is the sample length, and A is the sample area.

In principle all that is required is to apply a DC voltage and measure the subsequent DC current. This procedure will not lead to the desired sample resistance. Consider the situation where a sample, such as a polymer electrolyte film, is placed between two stainless steel electrodes. On applying a voltage, the ions in the polymer electrolyte will move, and a current will be measured. Once the ions reach the steel electrodes, they can not move further, and ions will accumulate at the electrodes. The sample becomes polarized, and an internal electric field builds up to oppose the applied electric field. Assuming that electron conduction in the polymer electrolyte is insignificant and ion transfer to the stainless steel electrodes is insignificant, the measured current will approach zero.

This situation can be improved somewhat by using electrodes made from the same metal as the metal cations in the polymer electrolytes. If, for example, the polymer electrolyte uses a lithium based salt, then lithium metal foil can be used as the electrodes. In this case ions can transfer from the polymer electrolyte to the lithium metal electrodes or vice versa. There will be a non-zero current that can be measured. However, along with the sample resistance there will also be a resistance associated with the transfer of ions between the lithium metal and the polymer electrolyte. This charge transfer resistance can be substantial and is impossible to separate from the

sample resistance using DC methods.

While DC measurements can not distinguish between the bulk resistance and interface effects, AC measurements allow such discrimination. Impedance spectroscopy involves the use of AC measurements to find the frequency-dependent impedance of a sample and test fixture. From these AC measurements the resistance of a sample can be found.

If an AC current of the form $I = I_0 \cos(\omega t)$ is applied, the resulting voltage will be

$$V = Z'(\omega)I_0 \cos(\omega t) - Z''(\omega)I_0 \sin(\omega t). \quad (2.3)$$

A part of the voltage will be in phase with the applied current, and a part of the voltage will be out of phase with the applied current. $Z'(\omega)$ and $Z''(\omega)$ are the in phase and out of phase impedances. Impedance spectroscopy is used to measure $Z'(\omega)$ and $Z''(\omega)$.

Instead of referring to the in phase and out of phase impedances, it is helpful to consider $Z'(\omega)$ and $Z''(\omega)$ as the real and imaginary part of a complex number.

$$\mathbf{Z}(\omega) = Z'(\omega) + iZ''(\omega) \quad (2.4)$$

The currents and voltages are also considered as complex quantities, $\mathbf{I} = I_0 e^{i\omega t}$ and $\mathbf{V} = V_0 e^{i\omega t}$. The complex form of Ohm's law can then be written as $\mathbf{V} = \mathbf{Z}\mathbf{I}$. Considering the impedance as a complex quantity greatly simplifies the mathematics associated with calculating impedances.

The complex formulation of voltages, currents, and impedances is easily demon-

strated to be equivalent to equation 2.3. Physical measurements obviously entail measuring the real parts of complex quantities. The real part of the applied current is $Re(\mathbf{I}) = I_0 \cos(\omega t)$. The real part of the voltage, \mathbf{V} , is

$$\begin{aligned}
 Re(\mathbf{V}) &= Re(\mathbf{Z}\mathbf{I}) \\
 &= Re((Z' + iZ'')I_0 e^{i\omega t}) \\
 &= Re((Z' + iZ'')(I_0 \cos(\omega t) + iI_0 \sin(\omega t))) \\
 &= Re(Z'I_0 \cos(\omega t) - Z''I_0 \sin(\omega t) + iZ''I_0 \cos(\omega t) + iZ'I_0 \sin(\omega t)) \\
 &= Z'I_0 \cos(\omega t) - Z''I_0 \sin(\omega t). \tag{2.5}
 \end{aligned}$$

The complex formulation is equivalent to the in phase/out of phase formulation.

While the complex formulation is helpful, it is the in phase and out of phase components that are actually measured. The impedance of a ideal resistor in complex notation is $\mathbf{Z} = R$. The impedance of a ideal capacitor in complex notation is $\mathbf{Z} = -i/\omega C$ where C is the capacitance. The impedance of an ideal inductor is $\mathbf{Z} = i\omega L$ where L is the inductance. The ideal resistor only has a real component. The ideal capacitor and inductor only have a imaginary component. An impedance that has a real component results in a input signal and a output signal with the same phase. An impedance that has a imaginary component results in a input signal and a output signal with a $\pm\pi/2$ phase difference. An impedance with real and imaginary components results in phases differences between 0 and $\pm\pi/2$.

Though $Z'(\omega)$ and $Z''(\omega)$ might appear independent of each other, they are actu-

ally connected. The connection is given by the Kramers-Kronig relations[1]:

$$\begin{aligned} Z'(\omega) - Z'(\infty) &= \frac{2}{\pi} \int_0^\infty \frac{xZ''(x) - \omega Z''(\omega)}{x^2 - \omega^2} dx \\ Z''(\omega) &= -\frac{2\omega}{\pi} \int_0^\infty \frac{Z'(x) - Z'(\omega)}{x^2 - \omega^2} dx. \end{aligned} \quad (2.6)$$

The Kramers-Kronig relations result from the requirement that input and output signals be related by causality. In principle, $Z'(\omega)$ could be measured by itself, and $Z''(\omega)$ could be calculated with Kramers-Kronig relations. Because of practical difficulties such as finite frequency ranges and errors in measured data, it is always preferable to measure both $Z'(\omega)$ and $Z''(\omega)$.

Before discussing a modern technique of measuring frequency-dependent impedance, a more traditional technique using a Wheatstone bridge is presented. The Wheatstone bridge is usually studied in introductory physics classes where it is learned that a Wheatstone bridge can be used to find unknown resistances. Figure 2.1 illustrates a Wheatstone bridge with complex impedances instead of real impedances. \mathbf{Z}_{s1} and \mathbf{Z}_{s2} are two standard impedances whose impedance is known with high precision. \mathbf{Z}_{var} is a variable impedance whose real and imaginary values can be changed. For example, \mathbf{Z}_{var} might be made up of a variable resistor and a variable capacitor in series. \mathbf{Z}_{unk} is the unknown impedance to be found. In order to find the unknown impedance, a sinusoidal voltage is applied to the circuit. The variable impedance is then adjusted until there is a null voltage reading on the volt meter. The condition of a null voltage reading between the two nodes of the circuit leads to the following

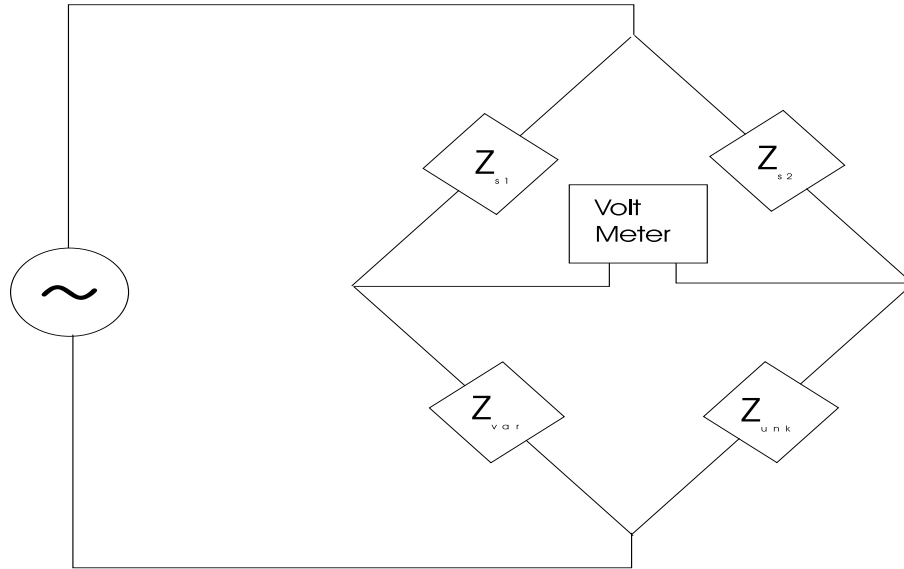


Figure 2.1: Basic layout of Wheatstone bridge

relation among the impedances:

$$\mathbf{Z}_{unk} = \frac{\mathbf{Z}_{s2}}{\mathbf{Z}_{s1}} \mathbf{Z}_{var}. \quad (2.7)$$

Since the other impedances are known, the unknown impedance can be found.

One shortcoming of the Wheatstone bridge and related bridge techniques is that the useable frequency is usually limited to tens of kilohertz. Another problem is that each frequency requires that the variable impedance be readjusted. This is a slow process making the collection of data a very tedious process. A modern technique discussed later greatly extends the frequency range and automatically finds the impedance without having to manually readjust a variable impedance.

2.3.2 Equipment Setup

The block diagram shown in figure 2.2 illustrates the various components used in taking impedance measurements. The core component is the HP 4192 LF impedance analyzer. The impedance analyzer applies the frequency-dependent voltages and measures the frequency-dependent current from which it finds the frequency-dependent impedance. Coaxial lines lead from the impedance analyzer to the impedance cell test fixture. The test fixture consists of stainless steel electrodes one-half inch in diameter in an enclosed casing. The test fixture also includes a micrometer to measure the film thickness. The HP 4192 LF impedance analyzer is controlled by a computer through a GPIB port. An Isotemp 1013 P refrigerated circulator is used for variable temperature measurements. The Isotemp 1013 P is controlled by the computer through a RS 232 port. The bath fluid used is a mixture of ethylene glycol and water. A thermocouple, attached to the impedance cell and close to the sample, is connected to a digital multimeter. The digital multimeter is connected to the computer through a GPIB port.

The computer controls the impedance analyzer, temperature bath, and digital multimeter. The software to do this was written in the Labview programming environment (a product of National Instruments). One program allows a single temperature frequency sweep. The program allows the user to specify the frequency range, the AC voltage, and the DC bias. The frequency range of the HP 4192 is 5 Hz to 13 MHz. The applied AC voltage can be from 5 mV to 1.1 V. The DC bias can range from -35 V to 35 V. The frequency sweep is a logarithmic sweep. Upon completion

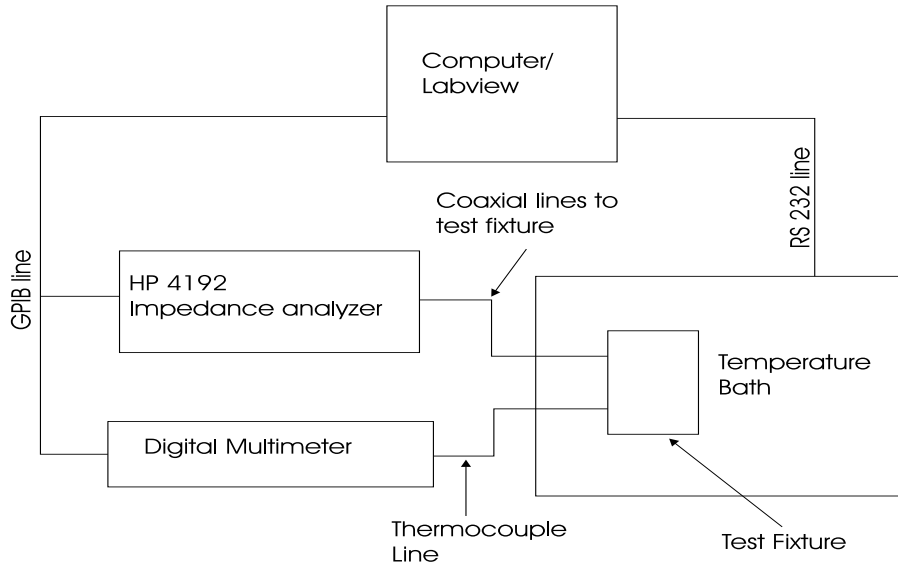


Figure 2.2: Block diagram for experimental setup

of the frequency sweep, the impedance is displayed as $-\text{Im } Z$ vs. $\text{Re } Z$. A separate program performs the temperature variable measurements. The temperature range of the refrigerated circulator is from -30°C to 200°C . However, due to the ethylene glycol/water bath fluid, a temperature range of 0°C to 90° is about the maximum that can be used. A third program provides a user friendly graphical interface to the LEVM non-linear curve fitting program discussed in a later section.

A typical data run would include the following. The temperature range would be set from 0°C to 90°C , and the temperature step size would be 10°C . The frequency range would be from 5 Hz to 10 MHz, and the DC bias would be set to zero. The AC voltage was set to 50 mV. It is actually desirable to set the AC voltage as low as possible in order to reduce non-linear effects that might be introduced. Due to the operation of the HP 4192, setting the AC voltage much below 50 mV results in

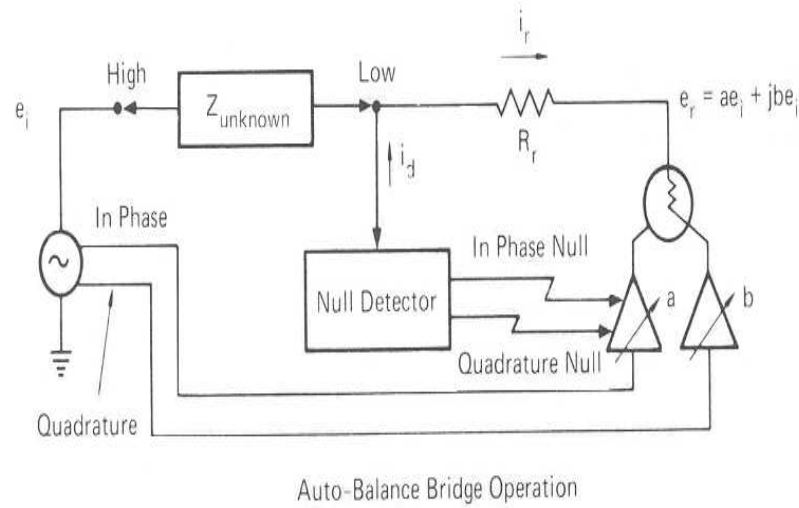


Figure 2.3: Figure illustrating basic operating principles of HP 4192 impedance analyzer. Figure taken from reference [1]

significant reduction in the precision of the measured data. A full temperature run from 0°C to 90°C would typically take between 9 to 10 hours.

2.3.3 Operation of HP 4192 LF

The Wheatstone bridge method of finding an unknown impedance was discussed above. In this study, the HP 4192 LF was used to measure impedance. The HP 4192 LF uses a auto-balance bridge method[1][2] shown schematically in figure 2.3.

A sinusoidal voltage, e_i , is applied to one end of the unknown impedance. A different sinusoidal voltage, e_r , having the same frequency as e_i is applied to the right of the reference resistor, R_r . At a certain value of e_r , the node labelled Low will be zero. The current, i_d , will also be zero so that the current in the unknown

impedance will be the same as the current in R_r :

$$i_r = \frac{\mathbf{e}_i}{\mathbf{Z}_{unknown}} = \frac{\mathbf{e}_r}{R_r}. \quad (2.8)$$

With this condition the unknown impedance is given by

$$\mathbf{Z}_{unknown} = R_r \frac{\mathbf{e}_i}{\mathbf{e}_r} \quad (2.9)$$

The voltages \mathbf{e}_i and \mathbf{e}_r are fed into phase sensitive detectors that determine in-phase and out of phase components from which the real and imaginary parts of the impedance can be found.

The above result depends on the Low node being zero. If this not the case, the null detector uses the phase and amplitude information contained in i_d to alter \mathbf{e}_r so that the Low node will be zero. This feedback process ensures that the bridge is auto-balanced.

2.3.4 Circuit Modelling and Data Presentation

The HP 4192 LF is used to collect the real and the imaginary part of the impedance versus frequency. Once the data is collected it must be interpreted. For proper interpretation, a model is required. Models are usually specified by specifying a mathematical equation. The mathematical equation should then be able to reproduce the qualitative and quantitative features of the experimental data. In impedance analysis instead of directly specifying a mathematical equation, a circuit model is specified. This is of course equivalent to specifying a mathematical equation, but the

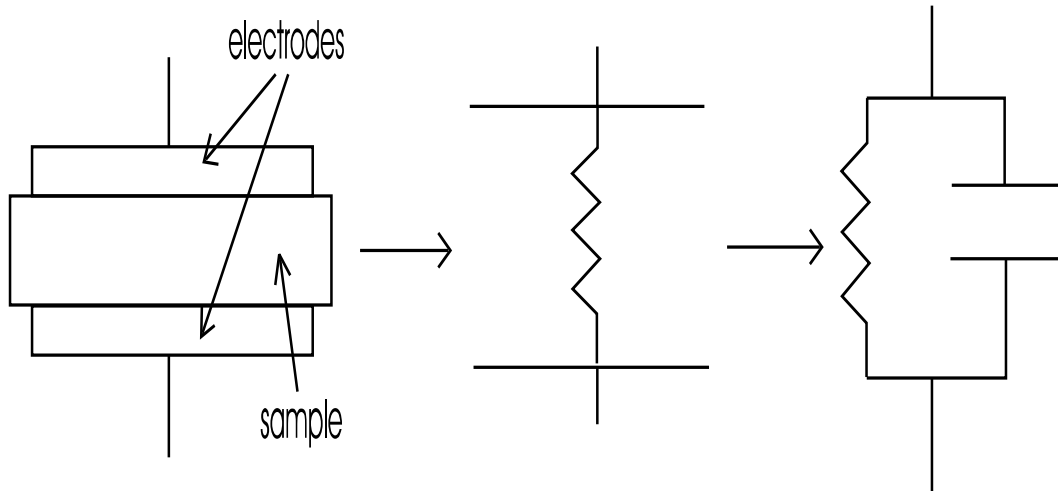


Figure 2.4: Circuit model of polymer electrolyte between electrodes

model is more easily visualized and understood in terms of circuit components rather than a mathematical equation.

Consider the following experimental situation. A polymer electrolyte film is placed between two stainless steel electrodes. This situation is illustrated in figure 2.4. The polymer electrolyte film between the stainless steel electrodes can be modeled by a capacitor and resistor in parallel. The capacitor represents the capacitance of the parallel stainless steel electrodes with the polymer as a dielectric. The polymer electrolyte film is represented by a resistor. As illustrated in figure 2.4, the polymer electrolyte resistor is in parallel with the electrode capacitor.

The impedance of a resistor is $\mathbf{Z} = R$. The impedance of a capacitor is $\mathbf{Z} = 1/i\omega C$. The total impedance of two impedances in parallel is found analogously to two resistors in parallel:

$$\frac{1}{\mathbf{Z}_{tot}} = \frac{1}{R} + \frac{1}{1/i\omega C}$$

$$\mathbf{Z}_{tot} = \frac{R}{1 + i\omega RC}. \quad (2.10)$$

A standard method of presenting impedance data is to graph $-\text{Im } \mathbf{Z}$ vs. $\text{Re } \mathbf{Z}$. From equation 2.10, $\text{Re } \mathbf{Z}$ and $-\text{Im } \mathbf{Z}$ for the parallel resistor and capacitor are

$$\begin{aligned} \text{Re}\mathbf{Z} &= \frac{R}{1 + (\omega RC)^2} \\ -\text{Im}\mathbf{Z} &= \frac{\omega R^2 C}{1 + (\omega RC)^2}. \end{aligned} \quad (2.11)$$

For real ω , both $\text{Re } \mathbf{Z}$ and $-\text{Im } \mathbf{Z}$ are non-negative. It is easy to show that the following relation holds for the real and imaginary parts of the impedance as given in equation 2.11.

$$(\text{Re}\mathbf{Z} - R/2)^2 + (-\text{Im}\mathbf{Z})^2 = (R/2)^2 \quad (2.12)$$

Equation 2.12 is just the equation for a circle centered on the real axis at $R/2$ with a radius of $R/2$. This is illustrated in figure 2.5. Assuming a parallel resistor/capacitor captures the important features of the physical problem, the resistance of a sample can be found by plotting $-\text{Im } \mathbf{Z}$ vs. $\text{Re } \mathbf{Z}$ and finding the point where the semicircle approaches the non-zero real axis.

The parallel resistor and capacitor fails to model the fact that the stainless steel electrodes are largely blocking to the ionic currents in the sample. How would this blocking effect be modeled? When an excess of, say, positive charge accumulates in the sample next to the electrodes, a excess of negative charge will accumulate on the electrode. This situation can be modelled approximately with a capacitor. Figure 2.6 shows two circuits that can model the blocking effect of the electrodes. The two circuits are mathematically equivalent though the capacitor values will be somewhat

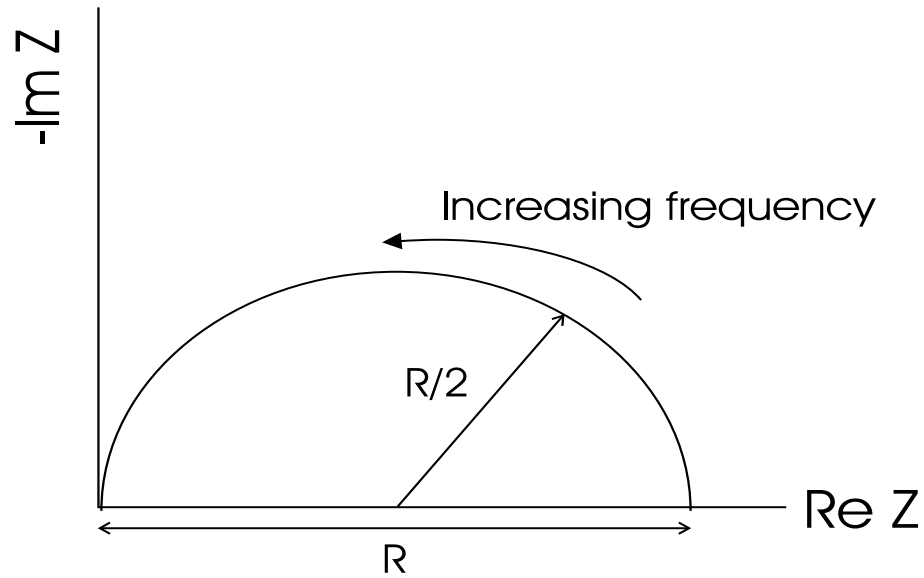


Figure 2.5: $-\text{Im } Z$ versus $\text{Re } Z$ for parallel resistor and capacitor

different for the two circuits. With the two capacitors, there can be no DC current through the circuit which is expected for blocking electrodes. The relative values of the capacitor will determine the shape of the $-\text{Im } Z$ vs. $\text{Re } Z$ plot. Physically, however, one expects the blocking capacitor to be much larger than the capacitance associated with the two electrodes separated by the sample. This is because capacitance goes like $C \sim 1/\text{length}$. The distance between the two electrodes is much larger than the distance between the accumulated charge in the sample and the electrode. The capacitance of the blocking capacitor is therefore larger than the capacitance associated with the two electrodes. The $-\text{Im } Z$ vs. $\text{Re } Z$ for this situation is shown in figure 2.7. Figure 2.7 resembles figure 2.5 except now there is a low frequency vertical spike. The vertical spike is due to the blocking capacitor, and it ensures that at zero frequency the magnitude of the impedance will be infinite.

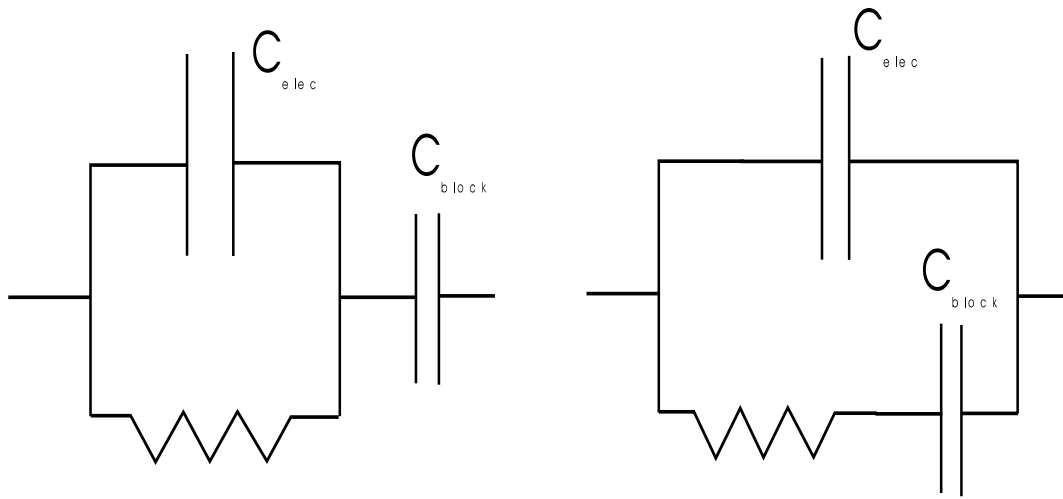


Figure 2.6: Two model circuit to account for blocking electrodes

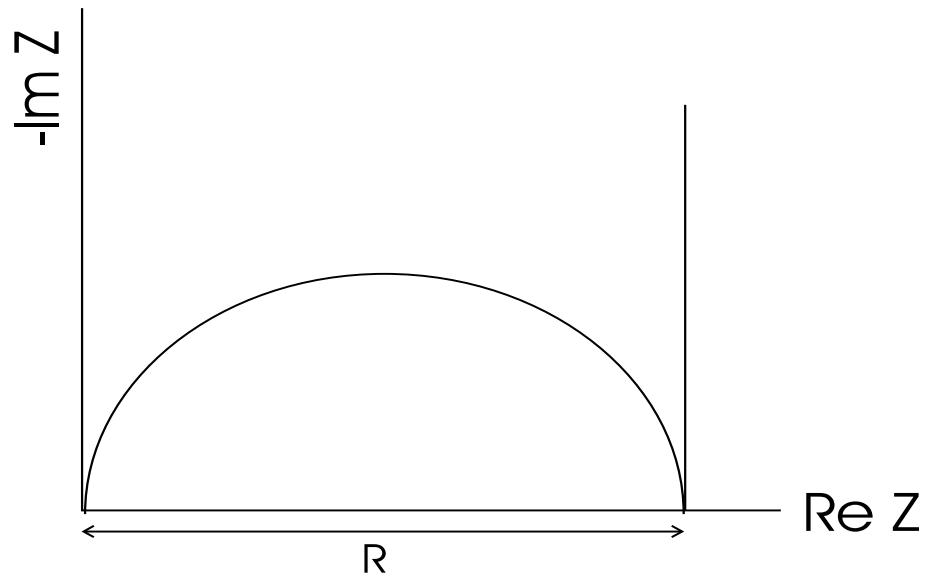


Figure 2.7: $-\text{Im } Z$ versus $\text{Re } Z$ for circuit models shown in figure 2.6

An ideal capacitor and resistor in parallel give a perfect half circle with radius $R/2$ when plotted as $-\text{Im } \mathbf{Z}$ vs. $\text{Re } \mathbf{Z}$. However, a perfect semicircle is rarely seen experimentally. What is often seen experimentally is flattened and/or skewed semicircles. As the name suggests, flattened semicircles appear to have been compressed so that the vertical height of the semicircle is less than $R/2$. Skewed semicircles appear asymmetric in a $-\text{Im } \mathbf{Z}$ vs. $\text{Re } \mathbf{Z}$ plot. It has been found empirically that flattened semicircles can be accounted for by replacing the ideal resistor by what is called a Cole-Cole element[3]. The impedance of the Cole-Cole element is given by

$$Z_{CC} = \frac{R}{1 + (i\tau_{CC}\omega)^\alpha} \quad (2.13)$$

where τ_{CC} is a characteristic time and α is related to the flatness of the semicircle. A skewed semicircle can be accounted for empirically with a Cole-Davidson element. The impedance of the Cole-Davidson element[4] is given by

$$Z_{CD} = \frac{R}{(1 + i\tau_{CD}\omega)^\beta} \quad (2.14)$$

where τ_{CD} is a characteristic time and β is related the asymmetry of the semicircle. The Cole-Cole and Cole-Davidson elements can be combined to form the Havriliak-Negami element[5]. The impedance of the Havriliak-Negami element is given by

$$Z_{HN} = \frac{R}{(1 + (i\tau_{HN}\omega)^\alpha)^\beta} \quad (2.15)$$

where τ_{HN} is a characteristic time and α and β are related to flatness and skewness respectively. While the Cole-Cole, Cole-Davidson, and Havriliak-Negami elements have been succesful in fitting experimental data, a full theoretical justification for

these equations is not available. One possible interpretation of these fitting elements is that they represent a distribution of relaxation times[6, 7]. A single parallel RC circuit has a single relaxation time. A distribution of relaxation times could therefore be represented by a distribution of parallel RC circuits. Depending on the distribution, this approach would give similar impedances as the Cole-Cole, Davidson-Cole, or Havriliak-Negami elements. Whatever the theoretical justification of these equations might be(distribution of relaxation times or not), they can be used to model the experimentally data. The DC resistance is the quantity to be extracted from the experimental data, and this is given by the R parameter in equations 2.13,2.14,2.15.

Impedance data has been presented as $-\text{Im } \mathbf{Z}$ vs. $\text{Re } \mathbf{Z}$. There are other methods of presenting experimental data. The choice of data presentation depends on what information is to be extracted and to a lesser extent personal taste. Along with the impedance formalism data can be presented in the conductivity, dielectric, and modulus formalisms.

The conductivity can be calculated from the impedance with $\sigma(\omega) = 1/\mathbf{Z}(\omega)$. (Technically the inverse of the impedance is the admittance. The conductivity is then calculated from the admittance and the length/area ratio. The term conductivity will be used instead of admittance with the understanding that factors of length/area need to be taken into account.) The conductivity is simply the inverse of the impedance. Bauerle [8] has plotted experimental data as $-\text{Im } \sigma$ vs. $\text{Re } \sigma$, but this method of data presentation is rarely used. What is more commonly done is to plot $\sigma'(\omega) = \text{Re}\sigma(\omega)$ vs. log frequency. Consider again the resistor and capacitor in parallel. The complex

conductivity of this circuit is

$$\sigma = \frac{1}{R} + i\omega C. \quad (2.16)$$

If σ' is plotted versus log frequency, the plot will be a horizontal line with a y-axis value of $1/R$. A parallel resistor and capacitor is usually too simple to model a wide range of experimental data. As will be seen in a later chapter, real experimental data will exhibit dispersion at higher frequencies.

The dielectric formalism can be related to the conductivity formalism by $\sigma(\omega) = i\omega\epsilon(\omega)$. Naturally enough, the dielectric formalism is used for dielectric materials. Pure dielectric materials do not exhibit a DC conductivity. If a material does exhibit DC conductivity, the DC conductivity can be subtracted from $\sigma(\omega)$ before calculating $\epsilon(\omega)$ in order to get the dielectric response. A resistor and capacitor in series gives the classic Debye dielectric response and results in a perfect semicircle when $-\text{Im } \epsilon$ is plotted versus $\text{Re } \epsilon$.

The modulus formalism is related to the dielectric formalism by $\epsilon(\omega) = 1/\mathbf{M}(\omega)$ where $\mathbf{M}(\omega)$ is the modulus function. Experimental data is usually presented in the Modulus formalism as $M''(\omega) = \text{Im}\mathbf{M}(\omega)$ versus log frequency. One reason for the popularity of the modulus formalism is that the modulus function can be related to a function $\phi(t)$ [9] which describes the decay of the electric field when a constant displacement field is applied:

$$\mathbf{M}(\omega) = M'(\infty) \left[1 + \int_0^\infty \frac{d\phi(t)}{dt} e^{-i\omega t} dt \right]. \quad (2.17)$$

A function that is often used for $\phi(t)$ is the stretched exponential, $\phi(t) = e^{-(t/\tau)^n} 0 <$

$n \leq 1$.

In this study data will be presented as $-\text{Im } \mathbf{Z}$ vs. $\text{Re } \mathbf{Z}$ and as $\text{Re } \sigma(\omega)$ versus the logarithm of frequency.

2.3.5 Non-linear Curve Fitting

Once a circuit model is chosen, it is necessary to fit this model to the experimental data. Non-linear curve fitting must be used to fit the complicated circuit models to the data. The non-linear curve fitting package used in this study is the LEVM program written by J. Ross MacDonald and co-workers[1]. The LEVM was written specifically for fitting circuit models to impedance data. The LEVM program supports a wide range of circuit elements such as resistors, capacitors, inductors, Cole-Cole elements, Cole-Davidson elements, Havriliak-Negami elements, and many others. These diverse elements can be organized into many different configurations.

Let $y(\omega, \mathbf{P})$ represent the mathematical equation associated with the circuit model. The vector \mathbf{P} represents the free parameters in the equation. The experimental data is represented by $y_i(\omega_i)$. Fitting programs usually search for the set of parameters, \mathbf{P} , that minimize the following sum.

$$\chi^2 = \sum_i w_i [y_i(\omega_i) - y(\omega_i, \mathbf{P})]^2 \quad (2.18)$$

A weight factor, w_i , can be included in the sum if a standard deviation is associated with each data point. This ensures that points with a large standard deviation are weighed less than points with a small standard deviation. If a standard deviation is

not associated with each data point, unity weighting in which $w_i = 1$ can be used.

For complex impedance data, there are two sets of data: the real impedance and the imaginary impedance. While these two sets can be fit independently, it is preferably to fit them together. The sum of squares to be minimized then is

$$\chi^2 = \sum_i w'_i [Z'_i - Z'(\omega_i, \mathbf{P})]^2 + w''_i [Z''_i - Z''(\omega_i, \mathbf{P})]^2. \quad (2.19)$$

Even though it is known that the sum of squares is to be minimized, it is a far from simple task to determine just how to do this. The reason for this difficulty is that the space represented by the free parameters, \mathbf{P} , will have many local minimum. A program such as LEVM that searches the parameter space might find a local minimum instead of the desired global minimum. It is therefore important to have good initial guesses for the free parameters. The algorithm that the LEVM program uses to search the parameter space is based on the Levenberg-Marquardt algorithm hence the name LEVM.

Bibliography

- [1] J. R. Macdonald, editor. *Impedance Spectroscopy-Emphasizing Solid Materials and Systems*. Wiley-Interscience, New York, 1987.
- [2] *HP 4192A LF Manual*.
- [3] K. S. Cole and R. H. Cole. *J. Chem. Phys.*, 9:341, 1941.
- [4] D. W. Davidson and R. H. Cole. *J. Chem. Phys.*, 19:1484, 1951.
- [5] S. Havriliak and S. Negami. *J. Polym. Sci. C*, 14:99, 1966.
- [6] J. Ross Macdonald. *J. Appl. Phys.*, 58:1955, 1985.
- [7] R. L. Hurt and J. Ross Macdonald. *Solid State Ionics*, 20:111, 1986.
- [8] J. E. Bauerle. *J. Phys. Chem. Solids*, 30:2657, 1969.
- [9] F. S. Howell, R. A. Bose, P. B. Macedo, and C. T. Moynihan. *J. Phys. Chem.*, 78:639, 1974.

Chapter 3

Frequency-Dependent Conductivity of Polymer Electrolytes

3.1 Introduction

The purpose of this chapter is to investigate the frequency-dependent conductivity of polymer electrolytes. It will be seen that the frequency-dependent properties of polymer electrolytes are similar to those of other disordered solids such as ion conducting glasses. Some of the models that have been used to understand the frequency-dependent conductivity of disordered solids are discussed. These models usually involve some distribution of hopping barriers/activation energies which suggests that polymer electrolytes might also involve a distribution of activation energies.

In the last chapter various methods of presenting data measured by an impedance analyser were discussed. This chapter presents data in terms of $\sigma(\omega)$. In particular, the real part of $\sigma(\omega)$ as function of frequency is used.

Consider the simple parallel resistor/capacitor discussed in the previous chapter. The impedance of that circuit was $Z(\omega) = R/(1 + i\omega RC)$. The conductivity(ignoring

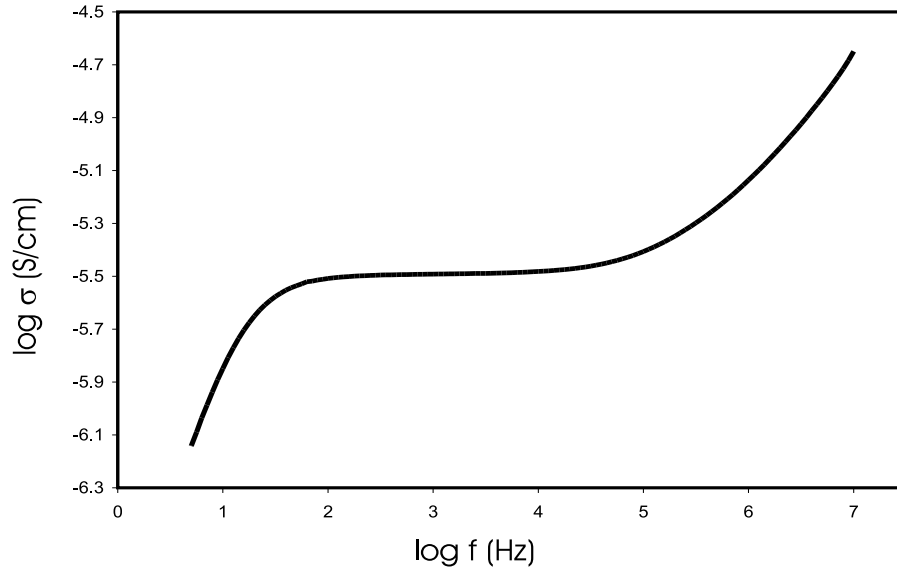


Figure 3.1: Frequency-dependent conductivity curve illustrating general behavior. At low frequencies electrode blocking effects cause a decrease in conductivity. At high frequencies, frequency dispersion occurs. The flat region gives the DC conductivity.

factors of area/length) is therefore $\sigma(\omega) = 1/Z(\omega) = 1/R + i\omega C$. The real part of the conductivity is just $\text{Re}(\sigma(\omega)) = 1/R$. For the simple parallel resistor/capacitor circuit, if the real part of the conductivity is plotted versus frequency the plot will just be a flat horizontal line whose value is $1/R$. For polymer electrolytes and other disordered systems the frequency plots can be a bit more complicated. Figure 3.1 shows a typical plot of which more examples will be seen later. The plot can be divided up into three regions. At low frequencies, the real part of the conductivity decreases as the frequency decreases. At high frequencies, the real part of the conductivity increases as the frequency increases. In between the high and low frequencies the conductivity is fairly flat. This flat frequency independent part is reminiscent of the simple parallel

resistor/capacitor which also gives a flat real part of the conductivity. In fact the value of the conductivity along this flat part is the DC conductivity. The downward curve of the conductivity at low frequency is not inherent to the sample itself but to the blocking electrodes. At low frequencies, the sample can become polarized due to a build up of charge at the electrodes. The polarization reduces the current, and therefore the conductivity is reduced. This polarization effect will not be of further interest in this work.

The high frequency conductivity dispersion is of further interest. While some work has been done investigating this region for polymer electrolytes[1, 2, 3], this high frequency dispersion has been extensively studied for ionic conductors such as glass electrolytes, electron conductors such as amorphous semiconductors, and other disordered solids. This chapter will compare the results of these systems with polymer electrolytes. It will be shown that there are striking similarities which suggest that there are similarities in the ionic transport mechanism also.

3.2 Conductivity properties of disordered solids

The real part of the conductivity versus frequency for disordered solids such as ionic glasses and amorphous semiconductors exhibit many similarities. Dyre and Schroder [4, 5] listed a number of properties that are often seen in these systems. One of these properties is that at high frequencies the real part of the conductivity goes like a power law in frequency i.e. $\sigma'(\omega) = Re(\sigma(\omega)) \propto \omega^n$. This behavior is similar to that pointed

out by Jonscher [6] for dielectric systems. The n in ω^n is usually between .6 and 1. As discussed in the previous section, another characteristic property is that the frequency dispersion ceases and becomes frequency independent as frequency decreases. Also, the property known as the Barton-Nakajima-Namikawa(BNN) relation[4] is found to hold. The BNN relation states that $\sigma_{dc} = p\Delta\epsilon\epsilon_0\omega_m$ where ω_m is the frequency at which the frequency dispersion begins, p is of the order unity, and $\Delta\epsilon\epsilon_0$ is the dielectric loss. Probably the most remarkable property, however, is that the conductivity curves can often be scaled onto a master curve. This demonstrates that disordered solids exhibit a degree of universality.

To perform this scaling the y-axis is scaled by the DC conductivity so that the y-axis becomes $\log(\sigma/\sigma_{DC})$. The conductivity curves must also be shifted along the frequency axis. A number of recent papers have discussed how to perform this frequency shift. Ghosh and Sural [7] looked at the scaling behavior of fluoride glasses. The frequency was scaled by the peak frequency of $M''(\omega)$ versus ω . Recall that $M^* = 1/\epsilon^* = M' + iM''$. Using this peak frequency Ghosh and Sural were able to scale fluoride glasses both at different temperatures and different concentrations. The peak frequency in the M'' is usually where the frequency dispersion begins in the $\sigma'(\omega)$ spectrum. The peak frequency is then basically equivalent to the ω_n of the BNN relation. Roling et al. [8] investigated the scaling behavior of the glass $xNa_2O \cdot (1-x)B_2O_3$. They found that for a given concentration x the temperature dependent conductivity curves could be scaled onto a master curve by using the scaling $\omega/\sigma_{DC}T$ where T is the temperature. The $\sigma_{DC}T$ scaling has been found to work

on many systems. However, for different concentrations x , the $\sigma_{DC}T$ scaling failed. The scaling behavior for concentration was regained by using $\omega x/\sigma_{DC}T$. Sidebottom [9, 10, 11] showed that the scaling $\omega x/\sigma_{DC}T$ failed for the $(Na_2O)_x(GeO_2)_{1-x}$ system. Sidebottom then argued for a frequency scaling of the form $\omega\epsilon_0\Delta\epsilon/\sigma_{DC}$ and with this was able to scale the $(Na_2O)_x(GeO_2)_{1-x}$ system. Schroder and Dyre [12] soon afterward argued that if scaling is at all possible the scaled frequency should be given by $\omega\epsilon_0\Delta\epsilon/\sigma_{DC}$. The scaling $\omega x/\sigma_{DC}T$ and $\omega\epsilon_0\Delta\epsilon/\sigma_{DC}$ are equivalent if $\Delta\epsilon \propto x/T$. This will be seen not to be the case for polymer electrolytes.

When conductivity curves scale, a master equation of the form

$$\frac{\sigma(\omega)}{\sigma_{DC}} = F\left(\frac{\omega}{\omega_s}\right) \quad (3.1)$$

where ω_s is the scaling frequency, applies. The existence of a master curve indicates that the system obeys the time-temperature superposition principle. If the master curve is known, the individual conductivity curves can be characterized by two parameters: σ_{DC} and ω_s . As will be seen below, the study of these two parameters and how they are related yields valuable information.

3.3 Scaling properties of polymer electrolytes

In the previous section the characteristic features of conductivity in disordered materials were discussed. Emphasis, however, was placed on the scaling behavior of the conductivity. It was seen that by scaling the y-axis by the DC conductivity and the x-axis by a characteristic frequency, the conductivity spectrum of ionic glasses and

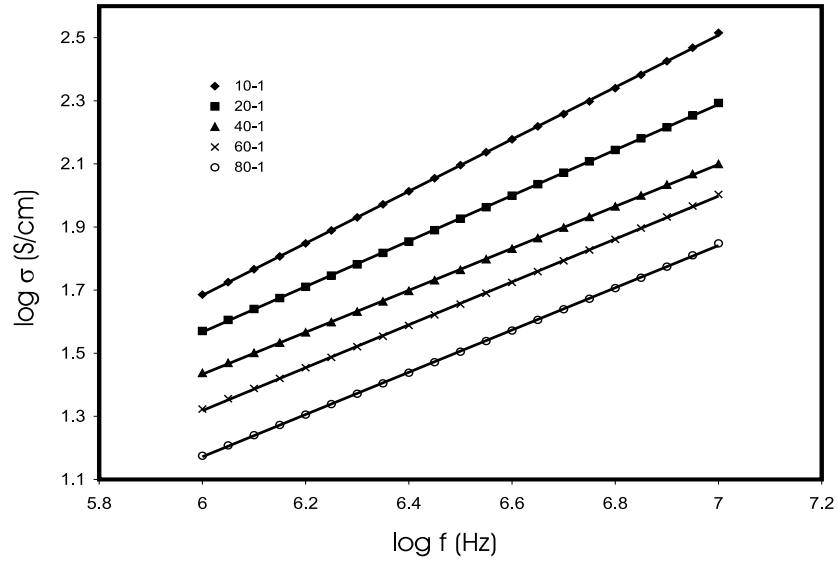


Figure 3.2: High frequency behavior of polymer electrolyte conductivity. Some of the curves have been vertically displaced for clarity.

amorphous semiconductors can often be made to collapse onto a single master curve. In this section, it is demonstrated that similar behavior is seen in polymer electrolyte conductivity.

The polymer salt conductivity data that will be presented is for C2000-LiTFSI. C2000, $([CH_2CH_2OCH_2CHCClH_2O]_n)$, is a amorphous elastomeric polymer. LiTFSI ($LiN(SO_2CF_3)_2$) is a common salt used in polymer electrolytes. Conductivity data were collected for polymer oxygen to lithium ratios of 80:1, 60:1, 40:1, 30:1, 20:1, and 10:1. The temperature range used is 0°C to 90°C in 10° steps.

In the previous section, it was mentioned that an often observed result of conductivity in disordered materials at high frequencies is $\sigma'(\omega) \propto \omega^n$ where n is usually between .6 and 1. Figure 3.2 shows $\log \sigma(f)$ versus $\log f$ in the frequency range from 1

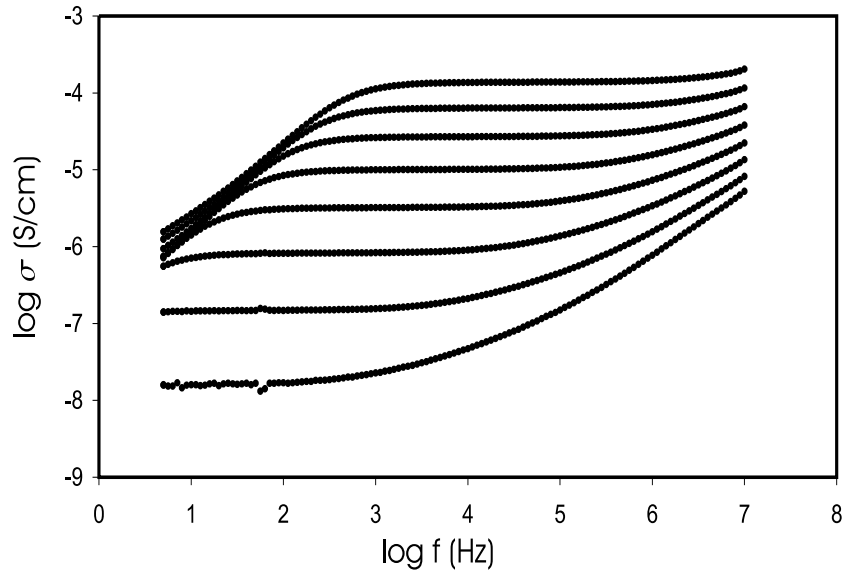


Figure 3.3: Real part of conductivity versus frequency for C2000-LiTFSI 10:1. The bottom curve is at a temperature of 0°C. The temperature interval between curves is 10 degrees.

MHz to 10 MHz. The different lines correspond to different concentrations but at the same temperature of 0°C. The lines appear linear with n values between about .6 and .8. Dyre [13], however, cautions about the pure power law form since an exponent such as $n = 1 - 2/\ln(\omega\tau)$, where τ is some microscopic time, can be used to fit the data, and this form for n can be derived theoretically from a barrier hopping picture.

It will now be seen whether polymer electrolytes can be scaled to a master curve. To this end the conductivity spectrum of the 10:1 concentration is first examined. Figure 3.3 shows conductivity spectrum of C2000-LiTFSI 10:1 in the temperature range of 0°C to 70°C. The 80 and 90°C curves are not shown since they show very little frequency dispersion at the higher frequencies. It is seen that the lower the temperature the lower the frequency at which the dispersion region begins. As the

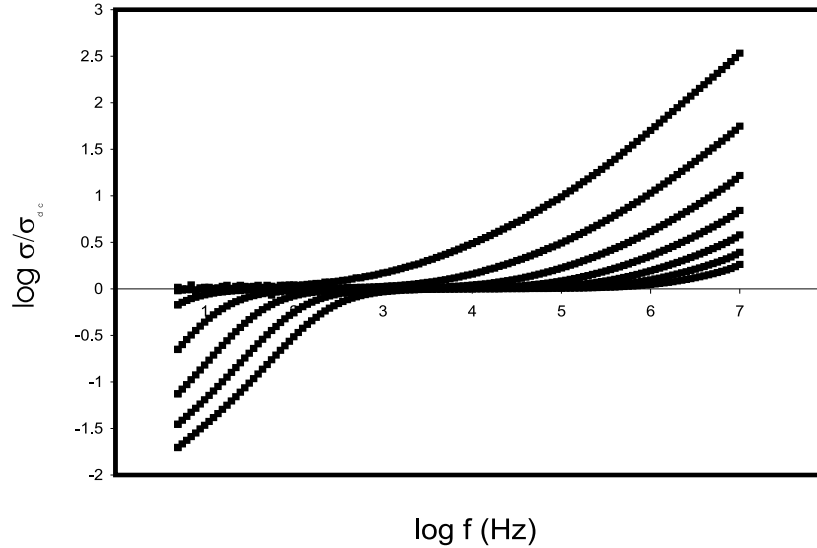


Figure 3.4: Frequency spectrum curve of fig. 3.3 scaled by DC conductivity

temperature increases the start of the dispersion region shifts to higher frequencies. Correspondingly the frequency dispersion becomes less pronounced at higher temperatures. As a first test of scaling, $\log(\sigma/\sigma_{DC})$ is plotted versus unscaled frequency in figure 3.4. It appears that the frequency dispersion regions do resemble each other and that curves will collapse onto a single curve with the proper shift along the frequency axis.

What is the proper shift along the frequency axis? The previous section mentioned two possibilities for the scaled frequency: $f/\sigma_{DC}T$ and $f\Delta\epsilon\epsilon_0/\sigma_{DC}$. The first possibility is just the second with $\Delta\epsilon \propto 1/T$. To aid in the determination of the proper frequency shift factor, the start of the frequency dispersion region was arbitrarily chosen to be the frequency at which each of the curve in figure 3.4 reached the y-axis value of 0.1. These frequencies plotted versus the DC conductivity are shown

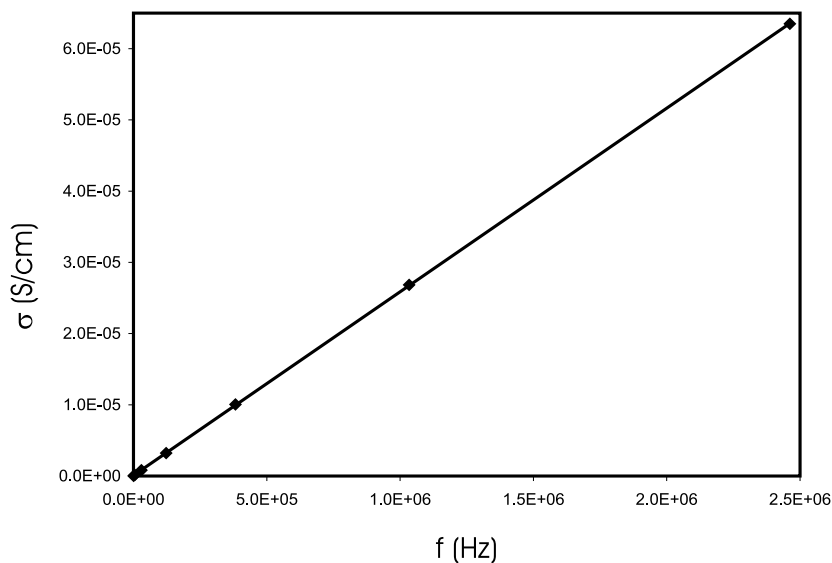


Figure 3.5: DC conductivity plotted versus the frequency at which dispersion begins. The polymer electrolyte is C2000-LiTFSI 10:1.

in figure 3.5 where a linear relation is seen. This suggest that the x-axis scaling should be given by f/σ_{DC} .

The curves from figure 3.4 can now be collapsed onto a master curve. Figure 3.6 shows the master curve attained from figure 3.4 by using the scaled frequency f/σ_{DC} . It is seen that there is a good collapse onto a single curve. Though not of primary interest, the electrode blocking effects at low frequency even collapse somewhat.

As a further example of polymer electrolyte scaling behavior, the C2000-LiTFSI 80:1 is also shown to scale. Figure 3.7 shows the real part of the conductivity versus frequency for various temperatures. The 80:1 displays some somewhat unusual behavior. The 80:1 conductivity curves start flat and curves upwards qualitatively similar to the 10:1. However, as the frequency increases a bend appears in the con-

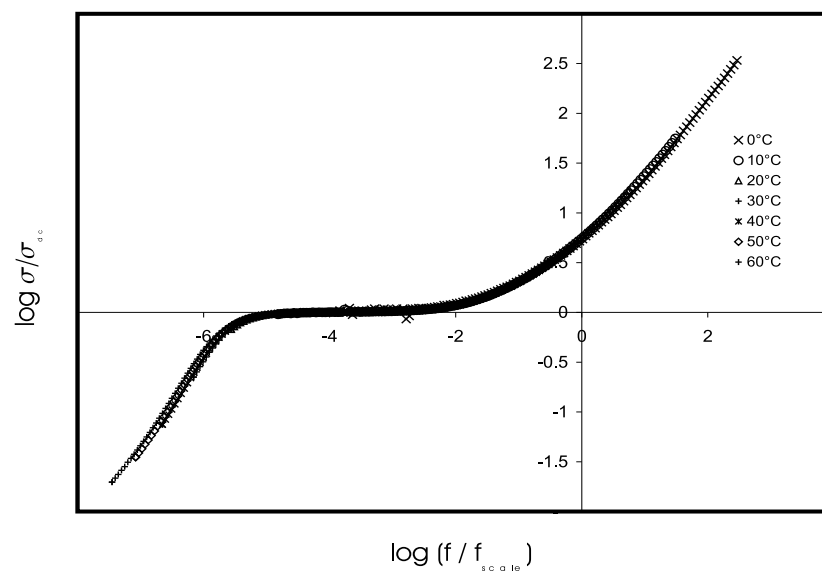


Figure 3.6: Master curve for C2000-LiTFSI 10:1.

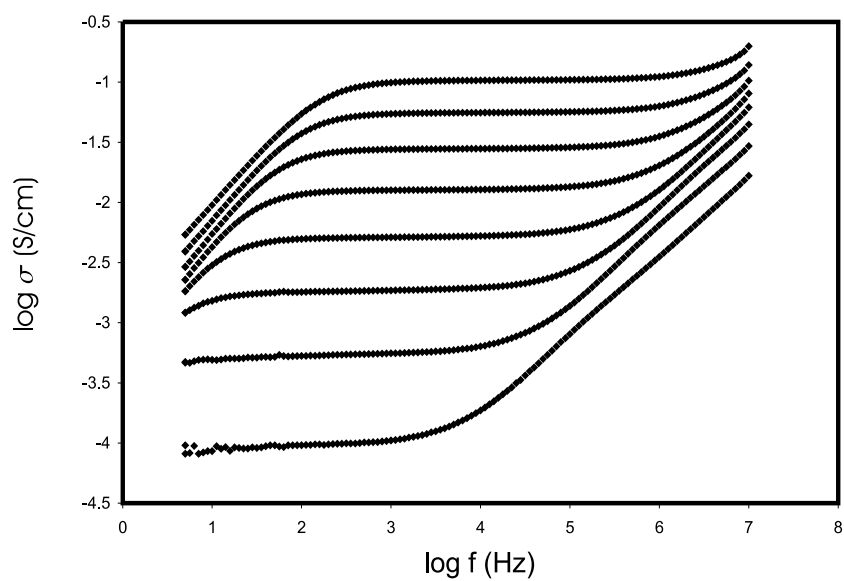


Figure 3.7: Real part of conductivity versus frequency for C2000-LiTFSI 80:1. The bottom curve is at a temperature of 0°C. The temperature interval between curves is 10 degrees

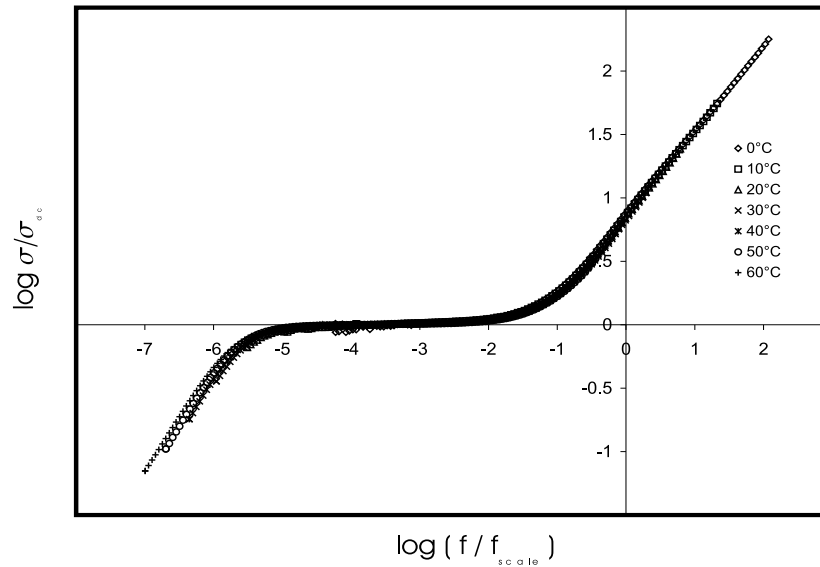


Figure 3.8: Master curve for C2000-LiTFSI 80:1.

ductivity. Below the bend the the curve appears not to have yet reached a constant slope. Above the bend, the slope appears constant but smaller than the curve below the bend would suggest. While noteworthy this bend does not appear to effect the scaling properties. Figure 3.8 shows the master curve of C2000-LiTFSI 80:1. The same frequency scaling that was used for the 10:1 has been used for the 80:1. Again the collapse onto a single curve is quite good.

It has been shown that the temperature dependent curves for both the 10:1 and the 80:1 C2000-LiTFSI concentrations collapse onto a master curve. The next question becomes: will curves of different concentrations also collapse onto a single master curve? Figure 3.9 shows scaled conductivity versus unscaled frequency. Each curve was taken at $0^{\circ}C$. While the frequency has not been scaled, it is obvious from the figure that no frequency shift will scale the curves onto a single master curve. This

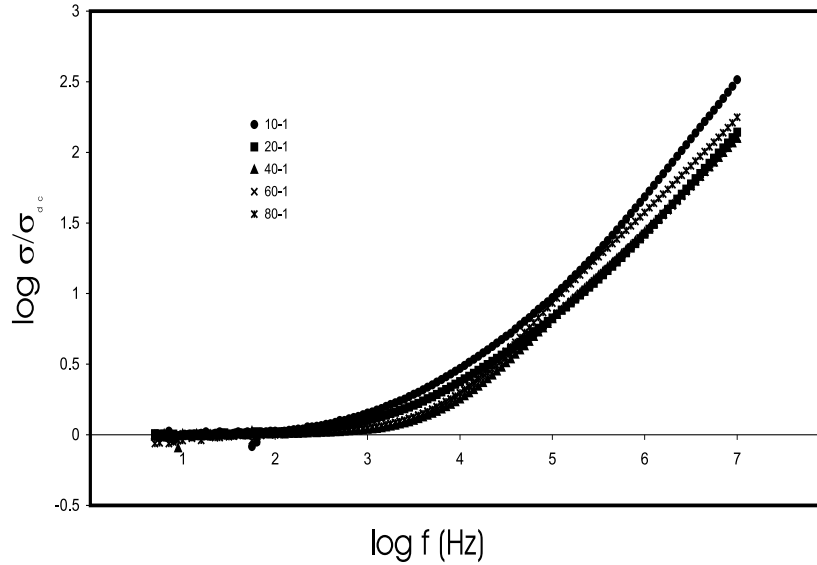


Figure 3.9: Scaled conductivity versus unscaled frequency for various concentrations.

contrasts to glass ionic conductors where a master curve for both concentration and temperature is often found to exist.

The BNN relation will now be investigated as this will provide further insight into polymer electrolyte conductivity. The BNN relation says that $\sigma_{DC} = p\Delta\epsilon\epsilon_0\omega_m$ (we will assume $p = 1$) where $\Delta\epsilon$ is the dielectric loss strength ($\epsilon_s - \epsilon_\infty$) and ω_m is the frequency at which frequency dispersion begins. To test this relation it is necessary to have the dielectric loss strength. There can be a number of contributions to the dielectric loss strength. Because there are dipoles along the polymer backbone, there is a dielectric loss due to the polymer. This loss is usually rather weak ($\epsilon_{polymer} < 10$) and occurs at frequencies greater than the frequency range of this study. There is also a dielectric loss due to the motion of the ions. Considering ion motion only, the

frequency-dependent conductivity can be written as

$$\sigma(\omega) = \sigma(0) + i\omega(\epsilon(\omega) - \epsilon_\infty)\epsilon_0. \quad (3.2)$$

The dielectric loss can be found with

$$\Delta\epsilon\epsilon_0 = \lim_{\omega \rightarrow 0} \text{Im} \frac{\sigma(\omega) - \sigma(0)}{\omega}. \quad (3.3)$$

It can be difficult to apply equation 3.3. The reason is that at low frequencies there is a large dielectric effect due to electrode polarization. This effect is so large that it obscures the smaller relaxation due to ion motion. To extract a reliable estimate for the dielectric loss due to ion motion, circuit modelling was performed. The circuit model used is shown in figure 3.10. Also shown in the figure is an example of the impedance data that was fitted with the circuit model. The circuit model consists of capacitor in parallel with a Havriliak-Negami impedance(see Experimental section). These two elements are then in series with a constant-phase element(CPE). The CPE represents the electrode polarization effects.

The circuit model in the figure 3.10 gives good fits to the experimental data. Strictly speaking, a dielectric loss strength does not exist for the Havriliak-Negami impedance since if $\sigma_{HN}(\omega) = 1/Z_{HN}(\omega)$ is inserted into equation 3.3 the resulting expression diverges for $\alpha, \beta < 1$. If $\alpha, \beta = 1$ then the dielectric loss strength is given by

$$\Delta\epsilon\epsilon_0 = \frac{\tau_{HN}l}{RA} \quad (3.4)$$

where l and A are the length and area of the sample. Even though the fits yield α and β values that are less than one, equation 3.4 will still be used as a estimate for

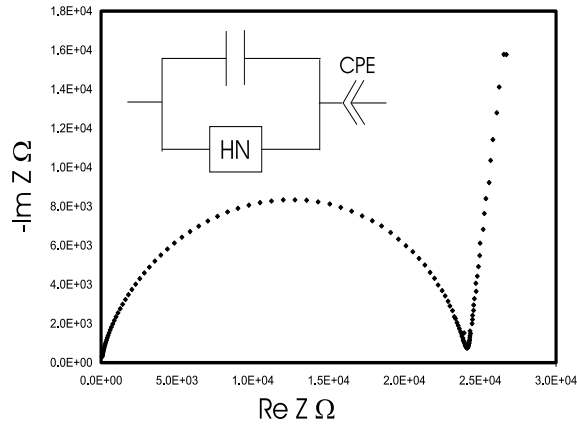


Figure 3.10: Circuit model used to fit impedance data and impedance data for C2000 LiTFSI 10:1 at 20°C .

the dielectric loss strength.

Figure 3.11 shows the dielectric loss strength as a function of temperature. The dielectric loss strength was found using the curve fitting discussed above. Three concentrations are shown. The 80:1 and 40:1 concentrations are largely independent of temperature. The 10:1 shows a distinct temperature dependence. The 10:1, however, is problematic at high temperatures. The reason for this is that at high temperatures the 10:1 shows an incomplete semicircle in the imaginary impedance versus real impedance plots. Since the semicircles are less complete than at the lower temperatures the fits are less reliable. The value of the capacitor in figure 3.10 for the 10:1 is fairly constant in the 0°C to 40°C range but starts increasing at 50°C . If this capacitor is fixed to its value in the 0°C to 40°C range then the dielectric loss is given by the triangles in figure 3.11. This suggests the dielectric loss might also be approximately constant for the 10:1.

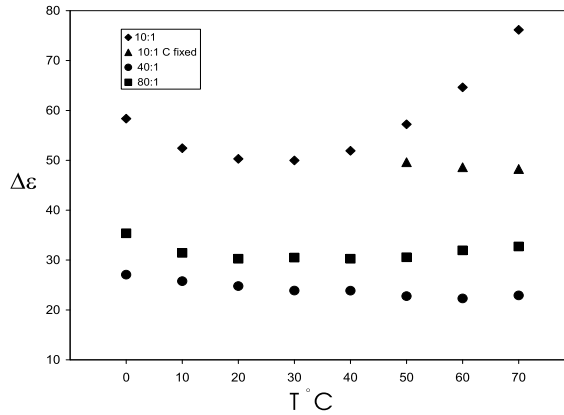


Figure 3.11: Dielectric loss as a function of temperature. The concentrations 10:1, 40:1, and 80:1 are shown.

In figure 3.5 it was seen that the DC conductivity versus the frequency at which dispersion starts is linear. According to the BNN relation the slope of DC conductivity versus the frequency at which dispersion begins should be $\Delta\epsilon\epsilon_0$. If the BNN relation applies to polymer electrolytes this gives a second method to find the dielectric loss due to ion motion. In figure 3.12, the dielectric loss found by scaling the conductivity (i.e. the BNN relation) is compared to the dielectric loss found by curve fitting. The curve fitting values of $\Delta\epsilon$ were taken from fits to the impedance at 20°C . The BNN values of $\Delta\epsilon$ were taken from the slopes of plots similar to figure 3.5 but for different concentrations. There is a systematic difference between the two methods for finding $\Delta\epsilon$. This systematic difference could be due to an additional dielectric process included in the curve fitting method. It could be due to the use of equation 3.3 even though $\alpha, \beta \neq 1$, or it could be due to the assumption that $p = 1$. The two methods do, however, show the same general behavior as concentration is varied.

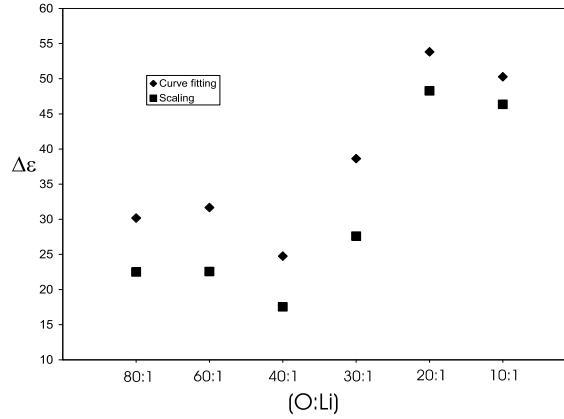


Figure 3.12: Comparison of dielectric derived from curve fitting and dielectric loss from BNN relation.

Since $\Delta\epsilon$ is due to ion motion, it might be expected that $\Delta\epsilon \propto$ concentraion. However, figure 3.12 shows that this is not the case. Figure 3.12 shows a more complex dependence on concentration than a simple linear relation. This complex relation is not unexpected due to the ion pairing and aggregation seen spectroscopically in polymer electrolytes(see Introduction).

3.4 Theoretical treatments of conductivity scaling and frequency dispersion

A variety of different approaches have been used to understand the remarkable conductivity scaling properties of disordered solids. The approaches discussed below include the macroscopic model, the symmetric hopping model, and monte carlo simulations of a lattice with site disorder in which the ions are interacting.

3.4.1 The macroscopic model

The macroscopic model posits a macroscopic conductivity $\mathbf{J} = g(r) \mathbf{E} = -g(r) \nabla\phi$. Inserting this into the equation for charge conservation, $\frac{d\rho}{dt} = \nabla \cdot \mathbf{J}$, gives $\frac{d\rho}{dt} = \nabla \cdot (-g(r)\nabla\phi)$. The fields and free charge density are considered periodic in t so that $\rho(r, t) = \rho(r)e^{i\omega t}$ and $\frac{d\rho}{dt} = i\omega\rho$. Inserting this result into the Maxwell equation,

$$\nabla \cdot \mathbf{D} = \rho, \quad (3.5)$$

gives with $\mathbf{D} = \epsilon_\infty\epsilon_0\mathbf{E}$

$$\nabla \cdot ([i\omega\epsilon_\infty\epsilon_0 + g(r)]\nabla\phi) = 0 \quad (3.6)$$

Consider now a two dimensional discretization of the equation 3.6. Between the lattice points (j,k) and $(j,k+1)$ would be an admittance $i\omega\epsilon_\infty\epsilon_0 + g_{j,k+1/2}$ where $g_{j,k+1/2}$ corresponds to the conductivity between the points (j,k) and $(j,k+1)$. The admittance $i\omega\epsilon_\infty\epsilon_0 + g_{j,k+1/2}$ corresponds to the impedance of a capacitor and resistor in parallel with the resistance given by $1/g_{j,k+1/2}$ and the capacitance by $1/i\omega\epsilon_\infty\epsilon_0$. A two dimensional discretization would therefore correspond to the circuit model shown in figure 3.13. Though not obvious from the circuit model, equation 3.6 takes into account the interactions of the free ions. This comes about from the use of equation 3.5, i.e. Gauss's law, in deriving equation 3.6. In using ϵ_∞ for the dielectric behavior of the bound charge instead of a frequency-dependent dielectric, $\epsilon(\omega)$, it is assumed that the bound charge reacts nearly instantaneously compared to the frequencies ω of interest. The values of the conductivity g used between two lattice points are given by some distribution $f(g)$, and the different g 's are assumed to be uncorrelated.

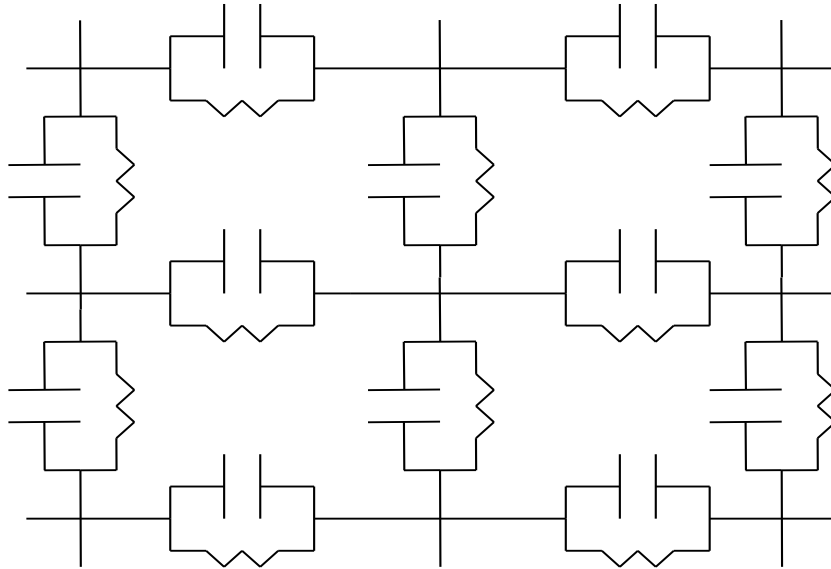


Figure 3.13: Circuit representing macroscopic model

The frequency dispersion properties of the macroscopic model come from changes with frequency of the voltages at the nodes. At zero frequency, the capacitors can be ignored and the resistors give rise to different voltages at the nodes. As the frequency increases, the capacitors allow the current to bypass the larger resistors. This will change the distribution of voltages at the nodes. Since the larger resistors are bypassed, the smaller resistors are now what limit the flow of current. The conductivity increases as the larger resistors are bypassed and smaller resistors become the limiting factor. This trend continues as more and more resistors are bypassed with increasing frequency.

The solution to equation 3.6 would entail the following. A voltage is applied between opposite sides of the circuit model to supply part of the boundary conditions. Periodic boundary condition can be applied to the other sides of the circuit. Using

equation 3.6, the voltage can be found at each point of the lattice. Since the voltage is known at each point in the lattice and the admittance is known between all lattice points, the total current moving through the circuit can be found. From the applied voltage and the total current, the total conductivity can be found as a function of frequency.

Instead of solving equation 3.6 as discussed above, one could try to find an analytic expression for the total impedance represented by the circuit model in figure 3.13. In general, however, the total impedance represented by figure 3.13 is an intractable problem. What can be done instead is to apply an approximating procedure to find the total impedance. The approximating procedure used is called the effective medium approximation.

In the effective medium approximation [14, 15, 16] all of the different admittances between two lattice points are replaced by an effective admittance. Consider a column of lattice points or nodes from figure 3.13 (the voltage source is attached to the boundaries parallel to the column considered). Each of these nodes will have a different voltage due to the different admittances. Now consider the average of the voltage nodes, V_m , along the column. In a circuit where all of the admittances are replaced by an effective admittance, the same average voltage will appear along the column of nodes. If one of the effective admittances perpendicular to the column is replaced by an admittance from the distribution $f(g)$, a new voltage, $V_m + V_x$, will appear at the node where the admittance is connected. The requirement that V_x disappear when

averaged over the distribution $f(g)$ leads to the condition

$$\int_0^\infty f(g) \frac{g - \sigma_{eff}}{g + (d-1)\sigma_{eff} + di\omega\epsilon_\infty\epsilon} dg = 0. \quad (3.7)$$

In equation 3.7, d is the dimension, $f(g)$ is the distribution for the conductance, and σ_{eff} is the effective conductance. As an example of the use of equation 3.7, take the conductances to be thermally activated, $g(E) = g_0 e^{E/kT}$, and consider a uniform distribution of activation energies with a maximum energy E_{max} . The result is [15, 16].

$$\sigma_{eff}(\omega) = \frac{\sigma_{eff}(\omega) + [(d-1)\sigma_{eff}(\omega) + di\omega\epsilon_0\epsilon_\infty]}{E_{max}/kT} \times \ln \left(\frac{(d-1)\sigma_{eff}(\omega) + di\omega\epsilon_\infty\epsilon_0 + g_0}{(d-1)\sigma_{eff}(\omega) + di\omega\epsilon_\infty\epsilon_0 + g_0 e^{-E_{max}/kT}} \right) \quad (3.8)$$

With certain assumptions concerning the frequencies and E_{max} , equation 3.8 can be written in the form

$$\frac{\sigma_{eff}(\omega)}{\sigma_{eff}(0)} \ln \left(\frac{\sigma_{eff}(\omega)}{\sigma_{eff}(0)} \right) = i \frac{\omega}{\omega_c} \quad (3.9)$$

where the DC conductivity is $\sigma_{eff}(0) = \frac{g_0}{d-1} e^{-E_{max}/kT}$ and $\omega_c = \frac{dkT\sigma_{eff}(0)}{\epsilon_\infty\epsilon_0 E_{max}}$.

Assuming that effective medium approximation is valid, equation 3.9 tells us that a random distribution of conductivities chosen from a uniform distribution of activation energies can be scaled onto the same master curve. Not only can conductivity curves at different temperatures be scaled, but conductivity curves with different E_{max} can be scaled also. Dyre [16] has shown that equation 3.9 is more general than the derivation from a uniform distribution of activation energies would suggest. In the limit, $T \rightarrow 0$, equation 3.9 should apply to any distribution. Dyre checked this result by solving equation 3.6 numerically for a two dimensional lattice, and found

good agreement between the numerical solutions and effective medium theory at low temperatures.

There are difficulties, however, in applying equation 3.9 to polymer electrolytes. One difficulty is in the frequency shift factor. The frequency shift factor for equation 3.9 is $\omega_c = \frac{dkT\sigma_{eff}(0)}{\epsilon_\infty\epsilon_0 E_{max}}$. For the C2000-LiTFSI polymer electrolyte, it was seen that the frequency shift factor did not depend on temperature but depended only on the DC conductivity. Another problem with polymer electrolytes unaccounted for by equation 3.9 was the lack of scaling with concentration. The conductivity spectrum of the different concentrations had slightly different shapes(see fig. 3.9). These different shapes prevent the concentrations from scaling onto a master curve which would have been independent of concentration and temperature. While equation 3.9 does demonstrate different scaling for different temperatures and different E_{max} , it can not be used to understand all aspects of polymer electrolyte scaling.

3.4.2 The symmetric hopping model

In the macroscopic model, macroscopic regions of a disordered solid are replaced by effective resistors which represents the conductivity of that region. The effects of any bound charge are taken into account by a capacitor in parallel with the resistor. Intuitively, however, one expects for a material such as an ionic glass that the disorder should be represented on the microscopic level. A model that represents disordered ionic conduction on the microscopic level is therefore desired. Hopping models are commonly used in models of conduction. A simple example of a hopping model is the

symmetric hopping model.

Consider a lattice of sites with a single particle in the lattice. Hopping models are often expressed in terms of a master equation for this lattice:

$$\frac{dP(i, t)}{dt} = \sum_k \Gamma(i, k)P(k, t) - \Gamma(k, i)P(i, t). \quad (3.10)$$

$P(i, t)$ is the probability that a particle is at site i at time t . The hopping rate from a site i to a site k is given by $\Gamma(i, k)$. The first term on the right hand side of equation 3.10 gives the probability flow into a site i while the second term gives the probability flow out of the site i . In general, $\Gamma(i, k)$ is not equal to $\Gamma(k, i)$. In the symmetric hopping model, however, $\Gamma(i, k)$ is taken to be equal to $\Gamma(k, i)$. Equation 3.10 then simplifies to

$$\frac{dP(i, t)}{dt} = \sum_k \Gamma(i, k)(P(k, t) - P(i, t)). \quad (3.11)$$

The hopping rates $\Gamma(i, k)$ can be considered as due to energy barriers between sites. The sites are situated at the same minimum energy while a distribution of energy barriers separate the sites. This situation is illustrated schematically in figure 3.14. The same minimum energy is a result of the symmetric requirement on $\Gamma(i, k)$. If the sites were at different energies, $\Gamma(i, k) = \Gamma(k, i)$ would not hold. The hopping rates are taken to be thermally activated, i.e. $\Gamma(i, k) \propto e^{E_{ij}/kT}$ where E_{ij} is the energy barrier between sites i and j .

Equations 3.10 and 3.11 give the probability of occupation of a site as a function of time. However what is measured experimentally is the conductivity as a function

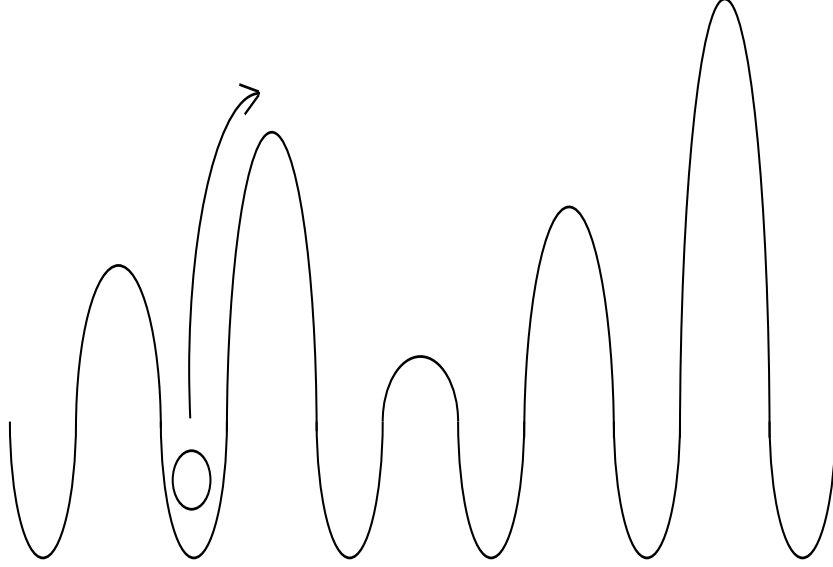


Figure 3.14: Schematic of symmetric barrier hopping

of frequency. A relation between the master equation approach and the frequency-dependent conductivity is required. This relation is supplied by linear response theory [17]. According to linear response theory, the frequency-dependent diffusion constant is given by

$$D(\omega) = \int_0^{\infty} e^{i\omega t} \langle v(0)v(t) \rangle dt. \quad (3.12)$$

The term $\langle v(0)v(t) \rangle$, in the linear response result, is the velocity autocorrelation function. It comes from considering an ensemble of systems each of which obey the same master equation. Velocities in a hopping model are not always clear since the hop itself is nearly instantaneous compared to the residence time at a site. The difficulty can be assuaged by formulating equation 3.12 in terms of the mean-squared displacement $\langle r^2(t) \rangle$. The conductivity is given by the frequency-dependent Nernst-

Einstein relation

$$\sigma(\omega) = \frac{Nq^2D(\omega)}{kT} \quad (3.13)$$

where N is the free charge concentration and q is the charge of the charge carriers.

As an simple example of the use of equation 3.12, consider the non-disordered situation where only nearest neighbor rates are non-zero and all barrier heights are equal. At any site a particle has an equal chance of hopping in any of the allowed directions. Once a particle hops in some direction to a new site, it immediately becomes decorrelated since at the new site there is again an equal chance of hopping in any of the allowed directions. The velocity autocorrelation function, $\langle v(0)v(t) \rangle$, is then, approximately, a delta function, $\delta(t)$. Inserting a delta function into 3.12 gives $D(\omega) = \text{const}$. Equation 3.13 then implies that conductivity is a constant independent of frequency. This contrast with the disordered solids discussed in this chapter where the conductivity is frequency independent at low frequencies but increases with frequency at higher frequencies.

In disordered solids the energy barriers will not all be the same, and this will lead to frequency dispersion seen at higher frequencies. To see how this comes about consider a particle sitting in its potential well. There are a number of different directions the particle can hop, but the highest probability hopping direction will be the one with the lowest energy barrier. Say the particle hops in the direction of the lowest energy barrier and arrives at a new site. What will be the particle's next hop? At the new site the most probable hop will again be in the direction of the lowest energy barrier. Since the particle just hopped over a low energy barrier, it is

possible that barrier just crossed is the lowest barrier at the new site as well. If this is the case, the particle will most likely hop back to the site from which it originated. This phenomenon is referred to as “bounce back”. The qualitative behavior of the autocorrelation function in which “bounce back” occurs is as follows. At very short times, before the second hop of the particle, the autocorrelation function is positive and close to its maximum. When the bounce back effect starts, the autocorrelation function decays rapidly and becomes negative (corresponding to $v(0)$ and $v(t)$ being in opposite directions). From the negative value the autocorrelation function will decay to zero as the particles become decorrelated from their initial hop. Since the autocorrelation function decays to zero at long times, the conductivity will be frequency independent at small frequencies. At short times there is a change from positive to negative values of the autocorrelation function. This short time behavior will be reflected in the high frequency behavior of the conductivity.

A more intuitive way to think about frequency dispersion in hopping models is in terms of which barriers can be crossed at a given frequency. Roughly speaking, at a given fixed frequency the barriers that can be crossed are those for which the hopping rate over the barrier is greater than the frequency. As the frequency is decreased larger and larger barriers will be encountered, and these larger barriers lead to a decrease in the conductivity. As the frequency is increased, the particle can only hop over smaller barriers. The particles are confined to hop in regions with small barriers that are surrounded by larger barriers. Since large barriers can be crossed at low frequencies and only small barriers can be crossed at high frequencies, the

conductivity will increase with increasing frequency.

As to the scaling properties of the symmetric hopping model, an analytic treatment of the symmetric hopping is even more unwieldy than the macroscopic model. However, Dyre [18] has done an approximate analytic calculation in the $T \rightarrow 0$ limit. The result turns out to be the same as equation 3.9. Numerical simulations were also performed for various distributions of barrier heights and compared with 3.9. Scaling was demonstrated for various distributions of barriers and different temperatures in the symmetric hopping model.

3.4.3 Site energy disorder and Coulomb interactions

While the symmetric hopping model does capture a number of features of frequency dispersion and conductivity scaling, a more realistic model would include site energy disorder and Coulombic interactions. If site energy disorder is applied, the particles are no longer trapped at the same potential depth. This excludes the symmetry, $\Gamma(i, j) = \Gamma(j, i)$, associated with the symmetric hopping model. Another, perhaps unrealistic, aspect of hopping models is that the charge carriers do not interact or that the interaction is dealt with effectively in the distribution of barriers. An explicit treatment of the interaction of the charge carriers along with the site energy disorder would be a more realistic model of disordered solids. An analytic treatment of this model is impossible. The main tool, therefore, used to investigate this model is Monte Carlo simulations. The hopping model with Coulomb interactions will be discussed again in a later chapter but some work related to scaling is presented below.

Porto et al. [19] performed monte carlo simulations on systems with site energy disorder. The site energy were chosen from a Gaussian distribution. While site exclusion was taken into account, Coulomb interactions were not included. Frequency dispersion with approximate power law behavior at high frequencies was seen in the simulations. However, scaling was somewhat poor at higher simulation temperatures. The scaling properties did improve at the lower temperatures.

Roling [20] performed monte carlo simulations on a symmetric hopping model with coulomb interactions. The scaled frequency used to investigate scaling properties was the experimentally verified, $f/\sigma_{dc}T$. For the symmetric hopping model without coulomb interactions, the scaled frequency $f/\sigma_{dc}T$ failed to scale different temperatures onto a master curve. Scaling could be regained, however, if the scaled frequency $f/\sigma_{dc}T^{1.3}$ was used. If Coulomb interactions are included, the temperature dependent conductivity were scaled by $f/\sigma_{dc}T$. Since $f/\sigma_{dc}T$ has been used experimentally, this suggests that Coulomb interactions might be important to the observed scaling behavior.

3.5 Summary

Transport in disordered solids have many striking similarities. These similarities include a power law behavior at high frequencies, the BNN relation, and scaling. These properties have been found to hold in a wide variety of materials such as amorphous semiconductors and ionic glasses. It is therefore surprising that very little work

has been in examining the frequency-dependent conductivity properties of polymer electrolytes. In polymer electrolytes, ionic transport certainly takes place in the disordered amorphous regions of the polymer. In some sense then it is not surprising that polymer electrolytes display some of same universal behavior as other disordered conductors. The reason that the parallels between polymer electrolytes and other disordered solids have not been drawn before is probably due to the perceived differences in the transport mechanism in materials such as ionic glasses/amorphous semiconductors and polymer electrolytes. In ionic glasses, the disorder inherent in the molten state of the glass is frozen in when the glass is made by quenching from the molten state. The available sites for ions are in fixed random positions in the glass. A distribution of barriers therefore seems a natural model for ionic transport in glasses. In amorphous semiconductors, the disorder comes from a distribution of tunneling rates between localized states in the semiconductor [21]. The situation is different in polymer electrolytes. In polymer electrolytes the polymeric environment of the ions is changing in time so that there is no fixed distribution of sites and ion movement is correlated with the polymer. Another difference between ionic glasses and polymer electrolytes is that in ionic glasses the temperature dependence of the DC conductivity usually follows the Arrhenius equation while the DC conductivity of polymer electrolytes is usually non-Arrhenian and follows a Vogel type equation. The perceived differences between polymer electrolytes and other disordered solids seem to have prevented the search for similarities. This chapter has showed that the similarities do exist which suggests that differences between transport in polymer

electrolytes and other disordered solids might not be as clear cut as first thought.

Bibliography

- [1] V. Di Noto, M. Vittadello, S. Lavina, M. Fauri, and S. Biscazzo. *J. Phys. Chem. B*, 105:4584, 2001.
- [2] V. Di Noto. *J. Phys. Chem. B*, 106:11139, 2002.
- [3] T. Furukawa, Y. Mukasa, T. Suzuki, and K. Kano. *J. Polym. Sci. B: Polym. Phys.*, 40:613, 2002.
- [4] J. C. Dyre and T. B. Schroder. *Rev. Mod. Phys.*, 72:873, 2000.
- [5] T. B. Schroder and J. C. Dyre. *Phys. Chem. Chem. Phys.*, 4:3173, 2002.
- [6] A. K. Jonscher. *Nature*, 267:673, 1977.
- [7] A. Ghosh and M. Sural. *Europhys. Lett.*, 47:688, 1999.
- [8] B. Roling, A. Happe, K. Funke, and M. D. Ingram. *Phys. Rev. Lett.*, 78:2160, 1997.
- [9] D. L. Sidebottom. *Phys. Rev. Lett.*, 82:3653, 1999.
- [10] D. L. Sidebottom and J. Zhang. *Phys. Rev. B*, 62:5503, 2000.

- [11] D. L. Sidebottom, B. Roling, and K. Funke. *Phys. Rev. B*, 63:24301, 2000.
- [12] T. B. Schroder and J. C. Dyre. *Phys. Rev. Lett.*, 84:310, 2000.
- [13] J. C. Dyre. *J. Appl. Phys.*, 64:2456, 1988.
- [14] S. Kirkpatrick. *Rev. Mod. Phys.*, 45:574, 1973.
- [15] I. I. Fishchuk. *Phys. Stat. Sol. (A)*, 93:675, 1986.
- [16] J. C. Dyre. *Phys. Rev. B*, 48:12511, 1993.
- [17] R. Kubo. *J. Phys. Soc. Jpn.*, 12:570, 1957.
- [18] J. C. Dyre. *Phys. Rev. B*, 49:11709, 1994.
- [19] M. Porto, P. Maass, M. Meyer, A. Bunde, and W. Dieterich. *Phys. Rev. B*, 61:6057, 2000.
- [20] B. Roling. *Phys. Chem. Chem. Phys.*, 3:5093, 2001.
- [21] S. R. Elliot. *Solid State Ionics*, 70/71:27, 1994.

Chapter 4

The Vogel Equation and Polymer Electrolytes

The last chapter pointed out a number of similarities between the frequency-dependent conductivity of polymer electrolytes and other disordered solids such as ionic glasses. These similarities are surprising since the ionic transport mechanism in polymer electrolytes is thought to be quite different than that in glasses. One reason the two mechanisms are thought to be so different is that in polymer electrolytes the temperature dependent DC conductivity usually follows the Vogel equation whereas in glasses the DC conductivity is usually described by the Arrhenius equation.

This chapter reviews the two standard arguments that lead to the Vogel equation. The first approach is the free volume arguments as presented by Cohen and Turnbull[1]. The free volume arguments are especially attractive because of their intuitive appeal. The second approach is the configurational entropy argument of Adam and Gibbs[2]. While both these approaches lead to the Vogel equation, they are quite different in terms of a microscopic picture.

After the review of the Vogel equation, the application of the Vogel equation

to polymer electrolytes is discussed. In particular, it is shown that under certain circumstances the Vogel equation fails to provide an adequate description of polymer electrolyte conductivity.

Finally, conductivity of ionic glasses and ionic crystals are shown that exhibit Vogel like behavior. This again demonstrates that ionic conduction in polymer electrolytes might not be so different from other ion conductors.

4.1 Approaches to the Vogel equation

4.1.1 Free volume theories

The free volume approaches are attractive because of their intuitive plausibility. For a particle to move from one point to another, there must be some unoccupied volume large enough to accommodate the particle in the direction of particle movement. This unoccupied volume is part of the free volume of a system of particles. Divide the total volume of a system of particles into two parts. One part is the volume occupied by the particles themselves. If, for example, the system of particles is a system of hard spheres the volume occupied by the particles is $V_{particles} = Nv_0$ where N is the number of particles and v_0 is the volume of one of the hard spheres. The free volume is the total volume minus the volume of the particles, $V_{free} = V_{total} - V_{particles}$. Dividing by the total number of particles, N , gives $v_f = v_t - v_0$ where v_f is the free volume per particle and v_t is the total volume per particle. The free volume per particle, v_f , is the average free volume per particle. The free volume associated with

an individual particle differs from particle to particle. In order for a particle to make a permanent displacement, there must be enough free volume associated with the particle for it to both move to a new location and for a different particle to move into its previous location. For this event to occur there must be some minimum, v^* , free volume associated with the particle. The free volume associated with a particle is not considered as a static property. The free volume associated with a particle is considered to be constantly redistributing. If at one point in time a particle does not have enough associated free volume for movement to occur, the particle might have enough associated free volume at a later point in time. This redistribution of free volume is thought to be unactivated or of having an activation energy much less than kT .

Using standard techniques from statistical mechanics, Cohen and Turnbull[1] derived the following equation for the distribution of free volume per particle.

$$p(v) = \frac{\gamma}{v_f} e^{-\gamma v/v_f} \quad (4.1)$$

The parameter γ is related to the overlap of free volume and is of the order unity, and again v_f is the average free volume per particle. The probability that the free volume associated with a particle is larger than v^* is

$$Prob[v > v^*] = \int_{v^*}^{\infty} p(v) dv = e^{-\gamma v^*/v_f}. \quad (4.2)$$

A property of the system of particles such as the diffusion constant which depends on the movement of the particles can then be written as

$$D = A e^{-\gamma v^*/v_f} \quad (4.3)$$

where A is a proportionality constant.

Equation 4.3 gives the diffusion constant in terms of the average free volume per particle, v_f . What is desired, however, is an equation in terms of temperature. Since knowledge of the exact temperature dependent behavior of v_f is lacking, the ansatz, $v_f = k\alpha(T - T_0)$, is made. The parameter, k , is a proportionality constant, α is the coefficient of thermal expansion, and T_0 is a temperature greater than zero at which the free volume disappears. Incorporating k , α , γ , and v^* into a new parameter, B , leads to the Vogel equation:

$$D = Ae^{\frac{-B}{T-T_0}}. \quad (4.4)$$

A free volume mechanism is probably the dominant picture of transport among polymer electrolyte researchers. In the free volume picture, the ions in the polymer electrolyte need a certain amount of free volume in order to move. The constant redistribution of the free volume is due to the movement of the polymer. As the polymer structure evolves in time, ions are able to diffuse through the polymer.

4.1.2 The configuration entropy approach

A very different approach to the Vogel equation developed by Adams and Gibbs is through the use of configurational entropy[2]. The entropy of a system is related to the number of degrees of freedom of the system. Consider first a crystal. In a crystal the degrees of freedom are mainly vibrational degrees of freedom. These vibrational degrees of freedom occur on a very small time scale and involve only short range motion of the particles. Consider now a viscous liquid close to the glass transition.

There will be a vibrational contribution to the entropy. However the heat capacity in the viscous liquid will be greater than the heat capacity of the corresponding crystal (assuming a crystal can be formed from the liquid). This additional heat capacity is largely due to the fact that in viscous liquids large scale structural changes can (slowly) occur. The different structural arrangements are different configurations, so the additional entropy in a viscous liquid is called configurational entropy. As the temperature drops the number of accessible configurations decreases so the configurational entropy also decreases. The slowness of the structural rearrangements and the decrease of configurational entropy are accounted for with the idea of cooperatively rearranging regions (CRRs). Unlike in a liquid or gas where individual particles are considered to be able to move largely independently of one another, in a cooperatively rearranging region a particle cannot move unless all particles in the region move nearly simultaneously. All of the particles must cooperate in the movement. As a simplifying assumption the different CRRs are considered to be independent so that rearrangement in one CRR does not depend on another CRR. As the temperature drops the CRR grows. As the CRRs get larger, the time between cooperative rearrangement gets longer and structural arrangements slow down. Eventually a temperature, T_2 , is reached where the configurational entropy is considered to be zero.

Instead of original Adam and Gibbs derivation, which is a bit opaque, a simpler derivation given in [3] is used. Divide a system of N particles into CRRs in which only two states are possible. Denote the number of such regions by N_c . The number of particles per region is then $n = N/N_c$. The total configurational entropy is $N_c k \ln 2$

since there are N_c regions each of which just has two states. The configurational entropy is also calculated by

$$S_{config}(T) = \int_{T_2}^T \frac{\Delta C_p(T)}{T} dT \quad (4.5)$$

Equation 4.5 is the standard thermodynamic equation for entropy with ΔC_p being the heat capacity of the viscous liquids minus the heat capacity of the crystal (the vibrational heat capacity). Experimentally it is found that ΔC_p is fairly constant at temperatures greater than the glass transition. With the experimental behavior of ΔC_p , for temperatures close to the glass transition, the configurational entropy is approximately given by

$$S_{config}(T) = \frac{\Delta C_p(T_g)}{T_g} (T - T_2). \quad (4.6)$$

Setting the above equation equal to $N_c k \ln 2$ gives n , the number of particles in a CRR, as function of temperature:

$$n(T) = \frac{NT_g k \ln 2}{\Delta C_p(T_g) (T - T_2)}. \quad (4.7)$$

It is now argued that the time it takes for rearrangements in a CRR depends on the volume of phase space that must be explored until an outlet to the new rearrangement can be found. This leads to

$$\tau \propto e^{\alpha n(T)} \quad (4.8)$$

where α is a new parameter. Finally comparing equations 4.7 and 4.8 leads, with the parameters of equations 4.7 and 4.8 incorporated into the Vogel parameter B, to the Vogel equation.

A configurational entropy approach to ionic transport in polymer electrolytes is less intuitive than the free volume mechanism, so it is far less used than the free volume mechanism in discussing ionic transport in polymer electrolytes.

4.2 Polymer Electrolytes and the Vogel equation

The two standard arguments leading to the Vogel equation have been presented in the previous section. As mentioned in the introduction, the Vogel equation has been successfully applied to a wide range of temperature dependent polymer electrolyte DC conductivity data. In this section some difficulties in applying the Vogel equation and the free volume interpretation of the Vogel equation are presented.

4.2.1 Partially crystalline polymer electrolytes

The first and most well known failure of the Vogel equation is to polymer electrolytes in which the polymer is partially crystalline. This situation is illustrated in figure 4.1. Figure 4.1 shows the PEO-LiTF system at a concentration of 10-1. The figure shows what appears to be two regions which are separated at the temperature at which PEO melts ($\sim 60^\circ$). Below the melting temperature of PEO, the conductivity appears to display Arrhenius behavior with a high activation energy. Above the melting temperature of PEO, the conductivity again appears to be Arrhenius like but with an activation energy less than the activation energy of the low temperature region. Obviously the Vogel equation with constant parameters A, B, and T_0 can not

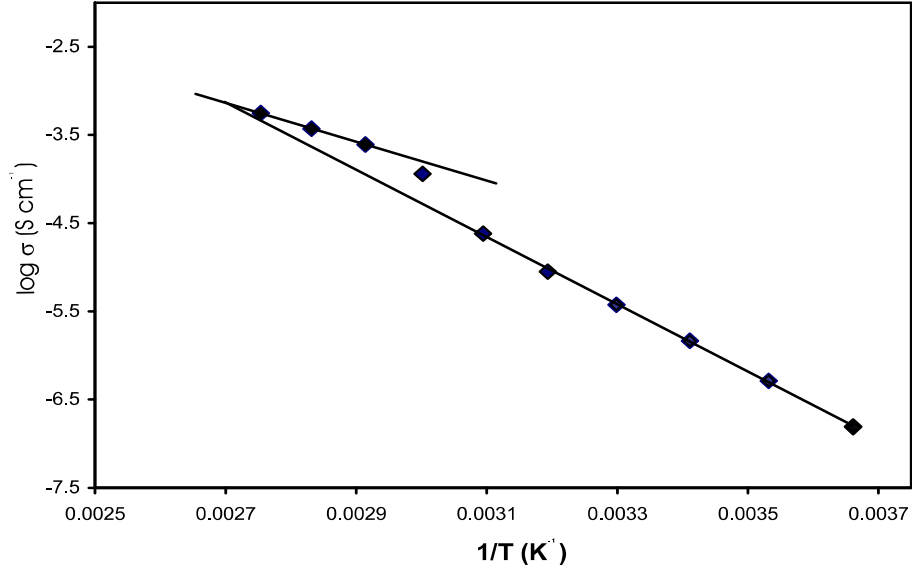


Figure 4.1: DC conductivity of PEO LiTF 10-1. The discontinuity in the conductivity occurs around the melting point of PEO.

be used to the fit the data.

One proposal for understanding the break in semi-crystalline polymer electrolytes was made by Lee and Crist[4]. They started by writing the mobility of an ion as

$$\mu \propto \exp \left(2.3 \frac{17.4(T - T_g)}{51.6 + (T - T_g)} \right) \quad (4.9)$$

where μ is the mobility of an ion and T_g is the glass transition temperature. The expression on the right hand side is the WLF equation which is similar to the Vogel equation. The numerical values in equation 4.9 have been found to work in a large number of polymer systems. According to Lee and Crist the break in the conductivity occurs because the glass transition temperature changes at the melting point. Below the melting point the concentration of salt in the amorphous regions is effectively greater because the salt is excluded from the polymer crystalline regions. When

the crystalline regions melt, the salt concentration effectively decreases. Since it is usually found the T_g depends on salt concentration[4], a change in the effective salt concentration will change T_g . With this theory Lee and Crist were able to reproduce the break in conductivity seen experimentally. In this theory the mechanism of ion transport is the same above and below the melting point. A change occurs because of an increase in polymer mobility due to a decrease in T_g . While this theory does reproduce the break, it does not quite reproduce the Arrhenius behavior seen in figure 4.1.

Instead of a single ion transport mechanism, consider the possibility that there are at least two mechanisms involved in ion transport. It is possible, for example, that in amorphous polymer electrolytes that a free volume/Vogel mechanism applies whereas in partially crystalline systems the Vogel mechanism along with an additional mechanism applies. The Vogel mechanism would be the dominant one at temperatures greater than the melting temperature. The unknown second mechanism would dominate at temperatures below the melting temperature. However, before speculating further, evidence that there are at least two mechanisms in partially crystalline polymer electrolytes is first presented.

How would two transport mechanisms be seen experimentally?. Consider again the resistor and capacitor in parallel. The imaginary part of the impedance of this resistor and capacitor circuit is

$$-ImZ(\omega) = \frac{\omega R^2 C}{1 + (\omega RC)^2}. \quad (4.10)$$

If $-Im Z(\omega)$ versus $\log \omega$ is plotted, the resulting graph would show a symmetric peak

centered at $\omega_0 = 1/RC$ with a maximum of $R/2$. If instead of a parallel RC circuit a Cole-Cole circuit element(see Experimental chapter) is considered, the peak would be symmetric but the maximum would be less than $R/2$. The Cole-Cole peak can be considered to be due to overlapping RC peaks. The RC peaks are not resolved so that the total peak is broader and flatter than the single RC peak. This is similar to a heterogeneously broadened peak in vibrational spectroscopy. Just because a broadened and flattened peak can be thought to be made up of overlapping peaks does not make it so. It would be desirable to have sufficient separation of the overlapping peaks so that an asymmetry or shoulder could be seen in the peak.

Figure 4.2 shows the negative of the imaginary part of the impedance of PEO LiTF 10-1 plotted versus the logarithm of the frequency for four different temperatures. The imaginary part of the impedance has been scaled by the DC resistance so that the curves at different temperatures can be easily compared. At 30°C, the peak is obviously asymmetric with a slight hint of a shoulder at higher frequencies. At 40°C, the asymmetry can be seen to be due to a second peak located at higher frequencies. At 50°C(close to the melting point of PEO), the higher frequency peak is comparable in height to the lower frequency peak. Finally at 60°C by which point the crystalline PEO regions have melted, only a single peak, which is consistent with the frequency trend of the higher frequency peak, can be seen. The lower frequency peak appears to have disappeared or to have become insignificant compared to the higher frequency peak.

As a further example of this two peak behavior figure 4.3 shows the same plot as

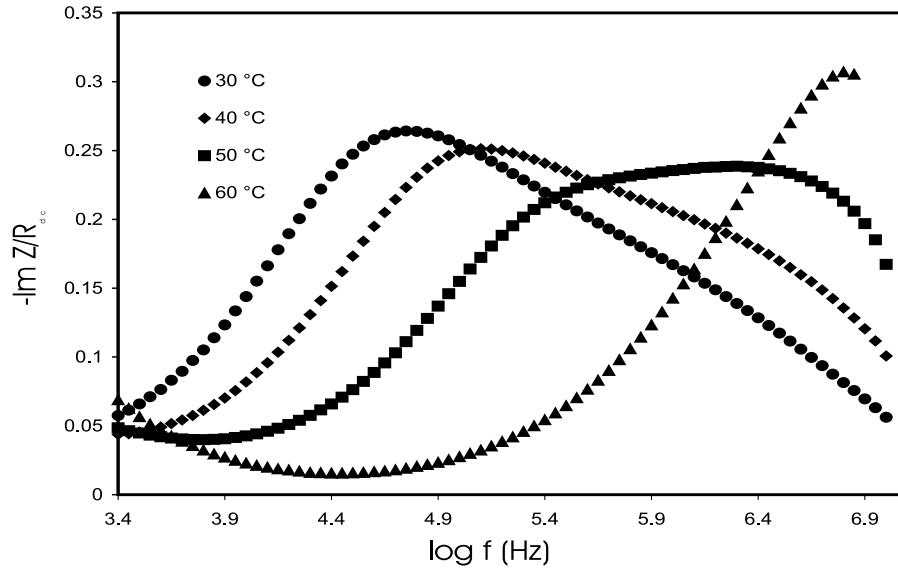


Figure 4.2: Imaginary part of the impedance of PEO LiTF 10-1 versus frequency. The impedance has been scaled by the DC resistance.

4.2 but with PEO LiBr 10-1 instead of PEO LiTF 10-1. Though the separation of the peaks is not as clear as in figure 4.2, the same general behavior is evident. Increasing from 40° to 50°C, a high frequency shoulder becomes more prominent. The 60°C curve nicely illustrates the remarks made earlier about overlapping peaks. In the 60°C curve no asymmetries or shoulders are evident. It would therefore be difficult to say whether the 60°C curve was made up of overlapping peaks or not. The 50°C and 70°C curves on either side of the 60°C peak strongly suggest that the 60°C peak is made up of at least two other peaks. By 70°C the high frequency peak is clearly larger and more important than the low frequency peak.

The thermal history of the sample has a large impact on whether or not two peaks can be seen in the semicrystalline PEO LiTF and LiBr systems. The films as cast from

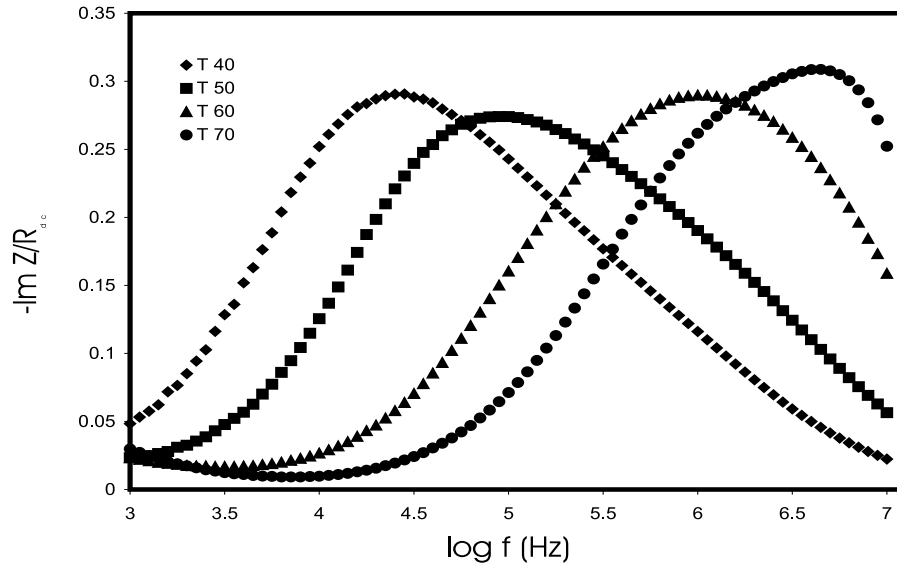


Figure 4.3: Imaginary part of the impedance of PEO LiBr 10-1 versus frequency. The impedance has been scaled by the DC resistance.

solution and prior to any heating are highly crystalline. At room temperature, the resistance is high and only one peak can be seen in the impedance. After heating the sample above the melting point of PEO and allowing the sample to cool back to room temperature, the resistance drops 1 to 2 orders of magnitude, and the two peaks can be seen in the impedance. The probable reason for the large drop in the resistance is that the polymer does not fully recrystallize to the extent it did before it was melted. Since the sample is not as crystalline the resistance is less. The reason that two peaks are not seen before melting is that the high frequency peak is overwhelmed by the low frequency peak. The high frequency peak can only be seen when the resistance of the low frequency peak drops and does not completely overwhelm the high frequency peak.

4.2.2 Amorphous polymer electrolytes

Figures 4.2 and 4.3 clearly demonstrate that two peaks can be seen in the impedance spectra of certain polymer electrolytes. These two peaks correspond to two contributions to the DC resistance. It is also evident from figures 4.2 and 4.3 that the temperature dependent behavior of these two peaks is quite different. These two peaks with different temperature dependent behavior can be ascribed to two different ionic transport mechanisms. Both of these mechanisms are necessary to understand the DC resistance and therefore the DC conductivity.

The DC conductivity of both PEO LiTF 10-1 and PEO LiBr 10-1 behave like the conductivity data of figure 4.1. Both PEO LiTF 10-1 and PEO LiBr 10-1 have partially crystalline regions. The question now becomes can two peaks be seen in amorphous polymer electrolytes that show Vogel like behavior? In the case of the C2000-LiTFSI system the answer is no. In general for amorphous polymer electrolytes the answer is probably no. However, similar to the PEO LiBr 10-1 at 60°C, just because overlapping peaks cannot be resolved does not mean that they are not there. In the case of figures 4.2 and 4.3, it was seen that there was a low frequency and a high frequency peak. The low frequency peak is dominant at lower temperatures whereas the high frequency peak becomes dominant at higher temperatures. This suggests that if a constant large frequency is examined that this large frequency will behave similarly to the high frequency peak.

Figure 4.4 shows the temperature dependent conductivity of C2000 LiTFSI 10-1 at a constant frequency of 1MHz. The DC conductivity is also shown for comparison.

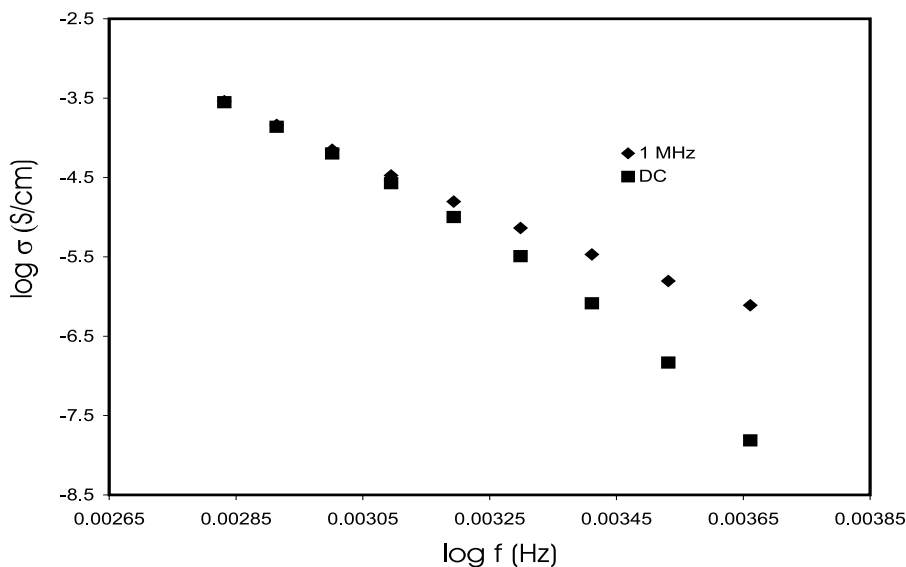


Figure 4.4: DC and 1MHz conductivity of C2000 LiTFSI 10-1.

Figure 4.5 shows the temperature dependent conductivity of C2000 LiTFSI 80-1 at a constant frequency of 1MHz. The DC conductivity is also included. The DC conductivity of both samples display Vogel like behavior. However, the 1MHz conductivity does not display Vogel like behavior. The 1MHz conductivity is more Arrhenius like than Vogel like. There is however some upturn in the 1MHz conductivity at the lower temperatures, so the 1 MHz conductivity is not quite a straight line. This upturn is more pronounced in the lower concentration 80-1 sample. What is especially important is that the 1MHz conductivity is nearly identical to the DC conductivity at high temperatures. This is what is expected if a high frequency peak is determining the 1MHz high frequency behavior, and a unresolved low frequency peak becomes insignificant at high temperatures compared to the high frequency peak.

Though certainly not as clear as in the partially crystalline polymer electrolytes

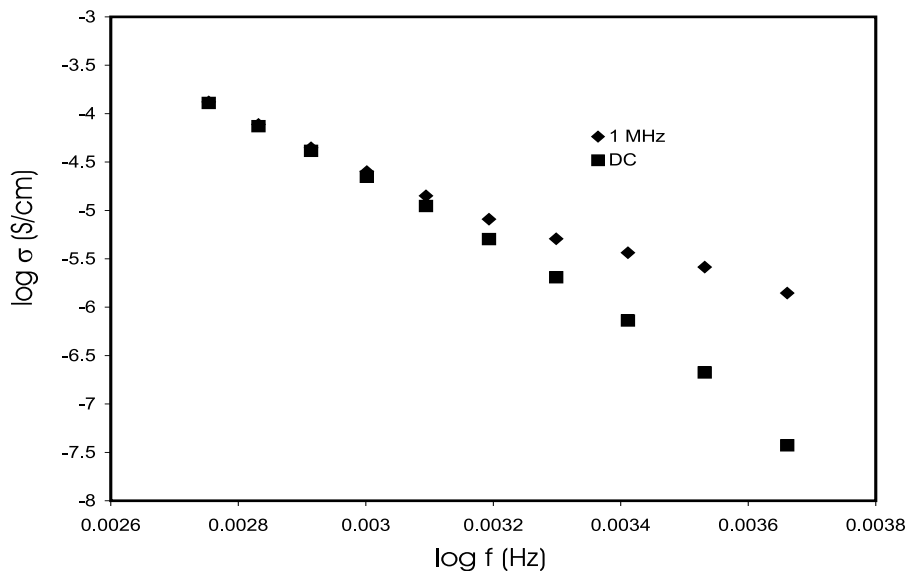


Figure 4.5: DC and 1MHz conductivity of C2000 LiTFSI 80-1.

shown in figures 4.2 and 4.3, there is evidence that at least two peaks, i.e. two transport mechanisms, are operating in amorphous polymer electrolytes. This conclusion would be very difficult to understand in terms of a free volume mechanism. In fact a free volume mechanism fails to provide much of any insight into the frequency-dependent conductivity properties of amorphous polymer electrolytes discussed in the previous chapter. Why, for example, should a free volume mechanism of ionic transport have similar frequency-dependent properties as ionic transport in ionic glasses? Hopping models of transport would supply some insight into the experimental results shown in figures 4.2, 4.3, 4.4, 4.5. For example the peaks shown in figure 4.2 could correspond to two different kinds of hop the particle has to make. By examining the isochronal conductivity at 1MHz as in figures 4.4 and 4.5, only one kind of hop is probed. The second kind of hop occurs on a time scale well outside of the time

scale probed by the constant frequency. Since only one kind of hop is probed, the 1 MHz conductivity does not follow the DC conductivity at lower temperatures. While hopping models would provide insight into the experimental results, there are difficulties toward their adoption. The main difficulty is that structural relaxation of the polymer and ionic transport occur on similar timescales. This is expected in a free volume mechanism, but it is harder to justify in terms of hopping models. This question will be returned to later.

4.2.3 Low temperature behavior of polymer electrolytes

The previous sections pointed out some of the difficulties if not outright failures in applying the Vogel equation to polymer electrolyte conductivity. While the failure of the Vogel equation for partially crystalline polymer electrolytes is well known, instances of the failure of the Vogel equation applied to amorphous polymer electrolytes are less well known. Chung et al.[5] have pointed out a failure at low temperatures.

Figure 4.6 shows DC conductivity data for PPO 4000-LiTF at various concentrations. The temperature range used is much larger than is typical for polymer electrolyte conductivity studies. Typically polymer electrolyte researchers content themselves with conductivity from room temperature to above. The reason for this is that this temperature range is the one important for applications. There are also a number of challenges associated with measuring the small conductivities at low temperatures. One of these challenges is that at small conductivities an incomplete arc is obtained in the plots of $-\text{Im } Z$ vs. $\text{Re } Z$. This makes extraction of a reliable

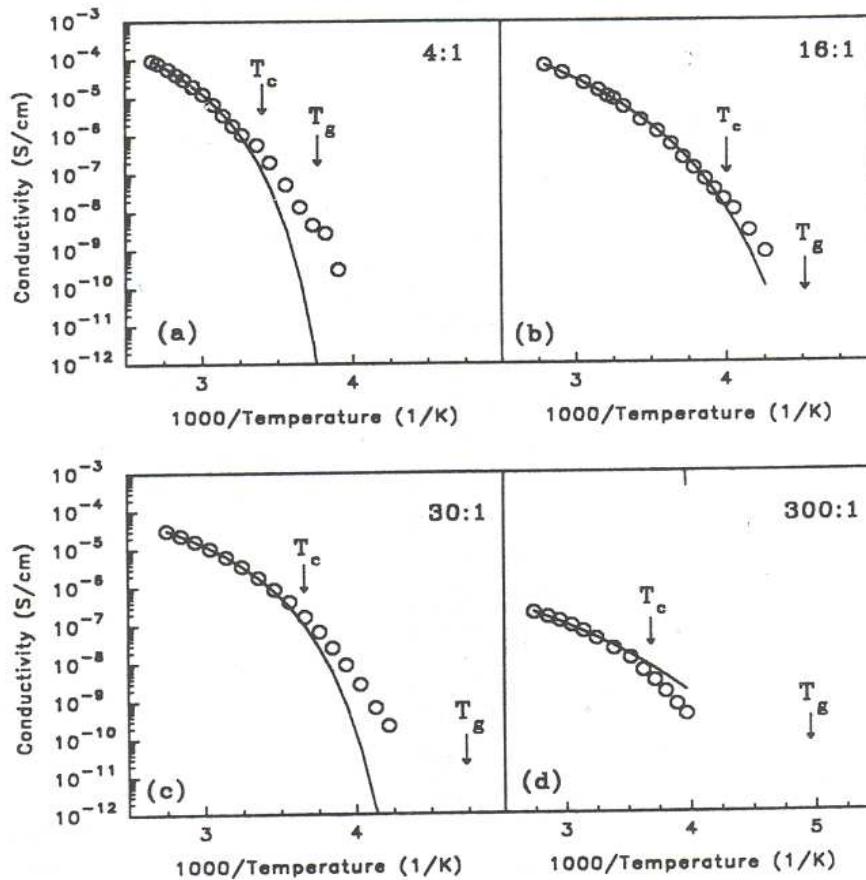


Figure 4.6: Wide temperature range plots of PPO LiTF system for various concentrations. Figure taken from ref. [5].

resistance from the plot difficult. Chung et al. measured conductivity down to temperatures below -20°C . They were able to fit the high temperature data to the Vogel equation (actually the VFT equation). As seen in figure 4.6, however, the Vogel fits failed at the lower temperatures. The low temperature conductivity was claimed to be Arrhenius like.

Chung et al.'s interpretation of this data is that at high temperatures the ions are coupled to polymer motion so that a free volume/Vogel description is appropri-

ate. At lower temperatures, the ions become decoupled from polymer motion, and a thermally activated mechanism results. According to the authors this change in mechanism occurs at a temperature T_C which is the critical temperature in mode-coupling theories.

An alternative interpretation consistent with two mechanisms of ion transport will be discussed in a later chapter.

It should be pointed out that the low temperature Arrhenius behavior is not seen in all polymer electrolytes. Other investigators [6, 7] reported non-Arrhenius behavior in amorphous samples at very low temperatures.

4.3 The Vogel equation and non-polymer electrolyte ionic conductors

One reason, that the ion transport mechanism in ionic glasses and polymer electrolytes is perceived to be different, is that in ionic glasses the conductivity is usually Arrhenius like whereas in polymer electrolytes the conductivity is usually Vogel-like. The Vogel-like behavior is considered to be due to the complex structural relaxations occurring in the polymer. In glasses the structure only undergoes short range vibrational motion, and the Arrhenius-like conductivity is thought to be related to large energy barriers that impede ion hopping.

Now consider the crystalline and glass fast ion conductors shown in figures 4.7 and 4.8. The conductivity is clearly non-Arrhenius, and is well fit by the Vogel equation.

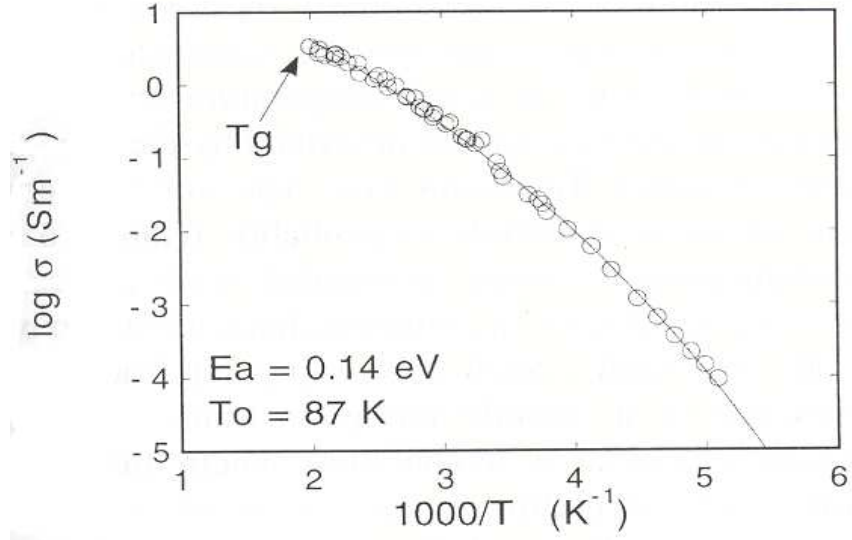


Figure 4.7: Conductivity of glass conductor, $0.5\text{Ag}_2\text{S} \cdot 0.5\text{GeS}_2$, displaying Vogel like behavior.

Figure taken from ref. [8].

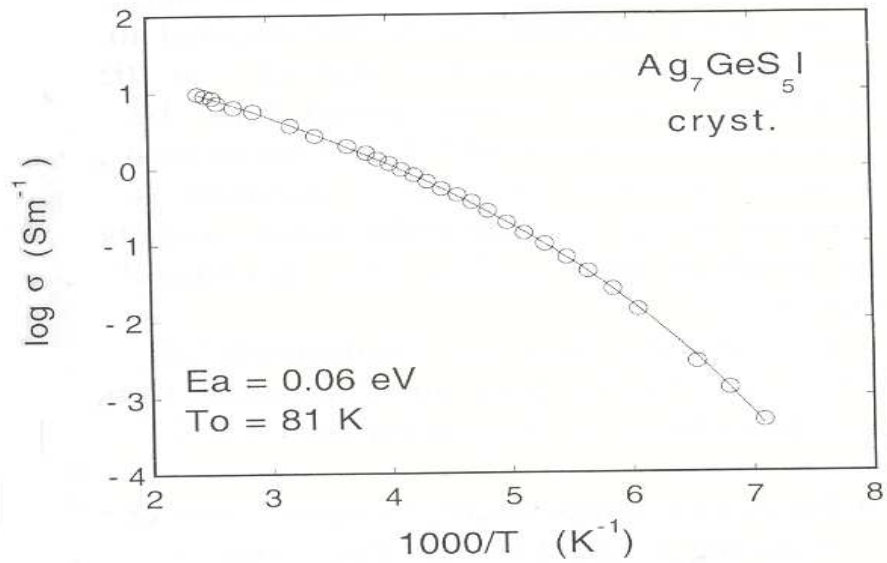


Figure 4.8: Conductivity of a crystal conductor displaying Vogel like behavior. Figure taken from

ref. [8].

The figures are taken from a paper by Ribes and co-workers[8] in which they argued for applicability of the Vogel equation based on configurational entropy. Whatever the physical basis for the non-Arrhenius behavior might be, the fact that Vogel like behavior is seen in crystals and glasses does raise some important questions in regards to polymer electrolytes. Is it possible, for example, that the source of the Vogel-like behavior in crystals and glasses be similar to the source of Vogel-like behavior in polymer electrolytes? This is an important question and should not be prejudiced by ideas of free volume. Note also that, since some glasses show Vogel-like behavior and since frequency-dependent conductivity of polymer electrolytes show glass like properties, it might be very difficult on qualitative grounds to distinguish between the conductivity of glasses and polymer electrolytes.

4.4 Summary

The two standard arguments, free volume and configurational entropy, leading to the Vogel equation were discussed. These arguments are not based on any fundamental theory, so their purpose is not to prove but to merely make the Vogel equation plausible. The Vogel equation must still be considered an empirical relation. A fundamental assumption of the free volume arguments is that there exists a temperature, T_0 , at which free volume disappears. The free volume then evolves with temperature as $v_f \propto T - T_0$. The configurational entropy approach uses the idea of cooperatively rearranging regions (CRRs). The CRRs grow as the temperature decreases. At some

temperature, T_0 , the configurational entropy goes to zero because the CRR consists of the entire sample. The configurational entropy approach also leads to a equation of the Vogel form. In terms of understanding polymer electrolyte conductivity, the free volume interpretation of the Vogel equation is commonly used.

A variety of experimental results involving the conductivity of polymer electrolytes were presented. The purpose of these results was to illustrate certain difficulties that the Vogel equation and its free volume interpretation encounter when applied to polymer electrolytes. It was seen that partially crystalline polymer electrolytes exhibit Arrhenius like behavior with different activation energies above and below the melting point of the polymer. It was also argued that in these partially crystalline polymer electrolytes that the transport mechanism can be divided into at least two different processes. These two processes were shown by plotting the imaginary part of the impedance versus frequency. Though similar plots of amorphous polymer electrolytes do not obviously display two processes, it was argued that this was due to overlapping peaks. Using the data of Chung et al. [5], it was seen that the Vogel equation fails to fit the DC conductivity of some amorphous polymer electrolytes at low temperatures. Instead of continuously curving over, a straight line Arrhenius like region is seen at low temperatures.

Finally, conductivity data for some ionic glasses show Vogel-like behavior. The question was asked whether the source of Vogel-like behavior in glasses could be similar to the source of Vogel-like behavior in polymer electrolytes. A common source would go a long way to explaining the similar frequency-dependent conductivity be-

havior seen in glasses and polymer electrolytes.

Bibliography

- [1] M. H. Cohen and D. Turnbull. *J. Chem. Phys.*, 31:1164, 1959.
- [2] G. Adam and J. H. Gibbs. *J. Chem. Phys.*, 43:139, 1965.
- [3] J. Jackle. *Rep. Prog. Phys.*, 49:171, 1986.
- [4] Y. L. Lee and B. Crist. *J. Appl. Phys.*, 60:2683, 1986.
- [5] S. H. Chung, K. Such, W. Wiczorek, and J. R. Stevens. *J. Polym. Sci. B*, 32:2733, 1984.
- [6] J. J. Fontanella. *J. Chem. Phys.*, 111:7103, 1999.
- [7] J. R. Dygas, B. Misztal-Faraj, Z. Florjanczyk, F. Krok, M. Marzantowicz, and E. Zygadlo-Monikowska. *Solid State Ionics*, 157:249–256, 2003.
- [8] M. Ribes, G. Taillades, and A. Pradel. *Solid State Ionics*, 105:159, 1998.

Chapter 5

Semi-Crystalline Polymer Electrolytes

The previous chapter pointed out a number of features of polymer electrolyte conductivity which the Vogel equation and its free volume interpretation failed to model. These features include: the two Arrhenius curves of partially crystalline polymer electrolytes, the two mechanisms seen in partially crystalline polymer electrolytes, the frequency-dependent properties of amorphous polymer electrolytes, and the low temperature conductivity of some amorphous polymer electrolytes.

A few schemes have been proposed to redress certain of the inadequacies of the Vogel equation. Fontanella and co-workers[1, 2, 3, 4] proposed the following Vogel-like equation as an alternative to the Vogel equation for fitting polymer electrolyte conductivity.

$$Ae^{\frac{-B}{(T-T_0)^\nu}} \quad (5.1)$$

The motivation for this equation comes from considering a defect diffusion model in which the defects interact and coalesce at T_0 . For the case $\nu = 3/2$, equation 5.1 is called the Bendler-Shlesinger equation[4]. A $\nu > 1$ means that there will be less

curvature as the temperature drops as compared to the Vogel equation. Equation 5.1 can therefore fit the low temperature conductivity of amorphous polymer electrolytes better than the Vogel equation. The cost of this better fit is an additional parameter. While equation 5.1 does account for the low temperature behavior of amorphous polymer electrolytes, it is of no obvious help in modelling partially crystalline polymer electrolytes.

As a preview of chapter 8 and to give the results of this chapter some plausible context, a hopping approach to viscous properties is briefly discussed. Various authors have discussed viscous properties in terms of hopping models (see chapter 8 for references). These models consider a quasi-particle hopping in a rough energy landscape. A property such as the viscosity would be determined by the distribution of barriers or traps seen by the quasi-particle and the hopping rate over the barrier or out of the traps. Simple versions of these models give

$$\frac{1}{\int_0^\infty e^{E/kT} g(E) dE} \quad (5.2)$$

for the mean hopping rate. The distribution of barriers or traps is given by $g(E)$ and the hopping rate is assumed to be thermally activated. It will be shown in chapter 8 how the Vogel equation can be understood within this hopping theory. In regards to the results of this chapter note that the simplest non-trivial distribution would involve two barriers.

5.1 Examination of the two mechanisms seen in partially crystalline polymer electrolytes

The use of the Vogel equation for polymer electrolyte conductivity resulted from the examination of the conductivity in amorphous polymer electrolytes. Instead of amorphous polymer electrolytes, the purpose of this section is a thorough examination of partially crystalline polymer electrolyte conductivity. As will be seen this leads to an equation other than the Vogel equation.

The previous chapter argued that there were at least two mechanisms operating in partially crystalline polymer electrolytes. These two mechanisms will now be investigated with non-linear curve fitting(see Experimental chapter). In performing non-linear curve fitting the first and most important step is to choose a equation to fit the experimental data. In impedance data, the equation is usually represented by a circuit model. The fit gives the parameters of the circuit model. Since no fundamental theory exists for polymer electrolytes, just which circuit model should be used is far from obvious.

An example of the data to be fit is shown as $-\text{Im } Z$ vs. $\text{Re } Z$ in figure 5.1. It is data for PEO LiTF 10-1 at 20°C. It is the same sample as the data shown in figure 4.2 but in a different representation and at a lower temperature. The curve in figure 5.1 is an asymmetric flattened semicircle. The experimental chapter discussed a number of possible fitting circuits. These included a resistor, a Cole-Cole element, and a Havriliak-Negami element each of which is in parallel with a capacitor. The resistor

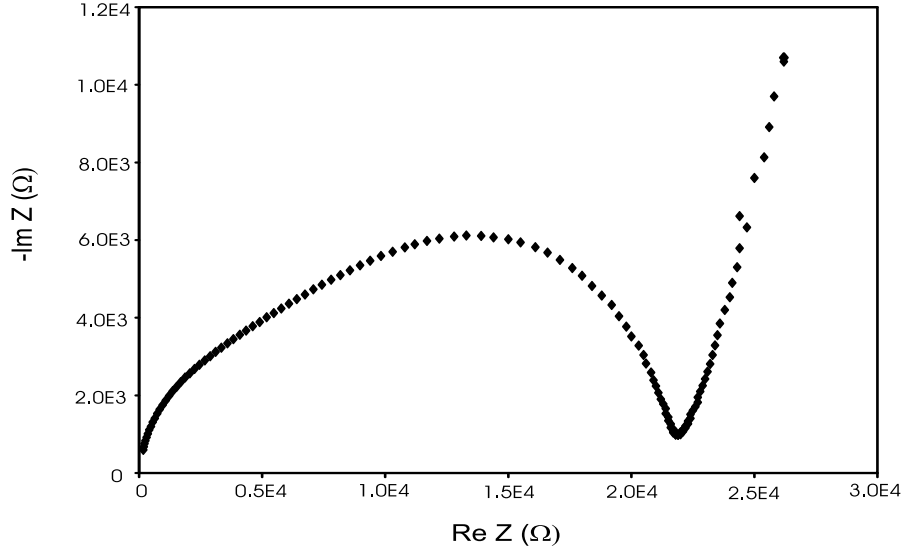


Figure 5.1: $-\text{Im } Z$ vs. $\text{Re } Z$ for PEO LiTF 10:1 at 20°C

does not give a flattened semicircle. The Cole-Cole element gives a flattened symmetric semicircle. The Havriliak-Negami element gives a flattened semicircle with some asymmetry. While the Havriliak-Negami element gives asymmetry, the Havriliak-Negami element by itself gives a poor fit at higher frequencies to the data represented by figure 5.1.

From figure 4.2 there is good reason to believe that this asymmetric flattened semicircle is due to at least two transport mechanisms. There is therefore reason to include two circuit elements in series. One circuit element represents the low frequency mechanism. The other circuit element represents the high frequency element. The two circuit elements are only necessary because there is decent resolution of the peaks seen in figure 4.2. If there was not sufficient resolution of the peaks a single Cole-Cole or Havriliak-Negami would probably be adequate for fitting.

The two circuit elements in series were chosen to be a Havriliak-Negami element and a resistor. The Havriliak-Negami element represents the low frequency peak, and the resistor represents the high frequency peak. The Havriliak-Negami element was chosen to see if the asymmetry could be accounted for solely by the Havriliak-Negami element. If the asymmetry could not be accounted for by the Havriliak-Negami element than the resistor would be non-zero. A resistor was chosen, instead of a Cole-Cole or a second Havriliak-Negami, simply to reduce the number of parameters the non-linear fitting program must use.

The circuit used in fitting the data represented by figure 5.1 is shown in figure 5.2. The circuit is composed of a resistor in series with a Havriliak-Negami element which are in turn in parallel with a capacitor. The capacitor represents the capacitance of the blocking electrodes with a polymer electrolyte as a dielectric. The circuit symbol marked CPE is a constant phase element. The CPE gives the slanted straight line seen in figure 5.1 and models the blocking effects of the electrodes. The slanted line corresponds to the low frequency conductivity dispersion seen in figure 3.1.

An example of the fits is shown in figure 5.3. Figure 5.3 shows the data in figure 5.1 (with some data points removed for clarity) along with the fit. As can be seen from the figure, the fit is rather good with the high frequency region being adequately modelled. The fitting was done for PEO LiTF 10-1 in the temperature range from 0°C to 40°C. At 50°C, the two mechanisms have about equal resistance, and the fits to the circuit model were poor. The 50°C resistors were therefore estimated from the $-\text{Im } Z$ vs. $\text{Re } Z$ plot. It was seen in figure 4.2 that the low frequency peak \ resistance

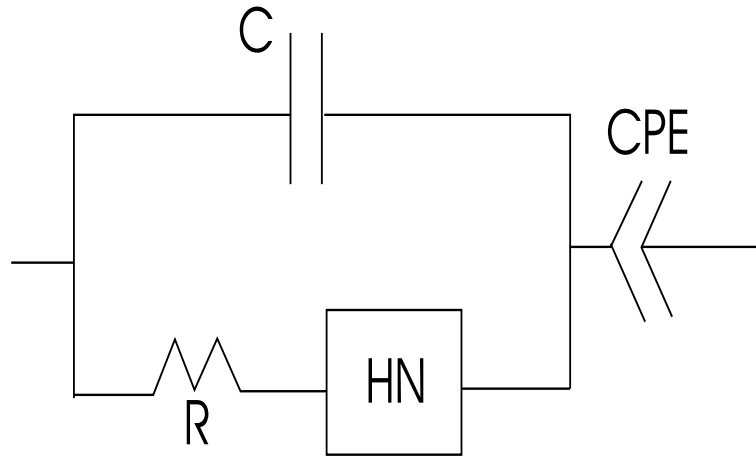


Figure 5.2: Circuit model used for fitting PEO LiTF impedance data

became insignificant compared to the high frequency peak resistance. Since there is only one significant mechanism operating above about 60°C, the resistance was simply read off the $-\text{Im } Z$ vs. $\text{Re } Z$ plot without fitting.

The primary interest in fitting the circuit to the experimental data is extracting the value of the resistor and the resistance associated with the Havriliak-Negami element (see Experimental section). In this way the value of the two resistors as a function of temperature can be had. The value of the two resistors as a function of temperature is shown in figure 5.4. The plot is in Arrhenius form with $\log \rho (=R A/l)$ on the y-axis and $1/T$ on the x-axis. The total resistance is also plotted. At low temperatures the total resistance is due almost completely to the low frequency resistance. However, the high frequency resistance can still be extracted at low temperatures. It is seen that this low temperature high frequency resistance is consistent with the total resistance above 60°C. In fact the high frequency resistance is approximately linear over the entire temperature range. The high frequency resistance is Arrhenius

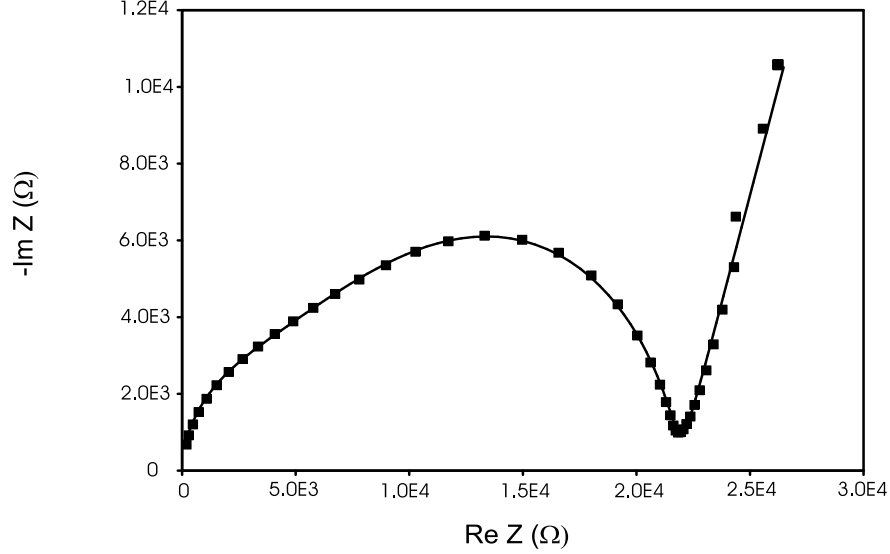


Figure 5.3: $-\text{Im } Z$ vs. $\text{Re } Z$ for PEO LiTF 10:1 at 20°C. The curve is the fit to the circuit model like. The low frequency resistance is also Arrhenius-like over its temperature range.

There are two resistors in series. Both of which appear Arrhenius like over some temperature range. This suggest the following equation for the total resistance.

$$R_{total} = R_{\beta}e^{\frac{E_{\beta}}{kT}} + R_{\alpha}e^{\frac{E_{\alpha}}{kT}} \quad (5.3)$$

The total conductivity is the inverse of equation 5.3.

$$\sigma_{total} = \frac{1}{\frac{e^{\frac{E_{\beta}}{kT}}}{\sigma_{\beta}} + \frac{e^{\frac{E_{\alpha}}{kT}}}{\sigma_{\alpha}}} \quad (5.4)$$

Equation 5.4 resulted from a careful investigation of partially crystalline polymer electrolytes. Most significantly equation 5.4 implies that the two Arrhenius regions seen above and below the melting point of the polymer are not due to a radical change in a single mechanism but are due to one of two mechanism dominating the total resistance. One mechanism dominates below the melting point of the polymer. A different mechanism dominates above the melting point.

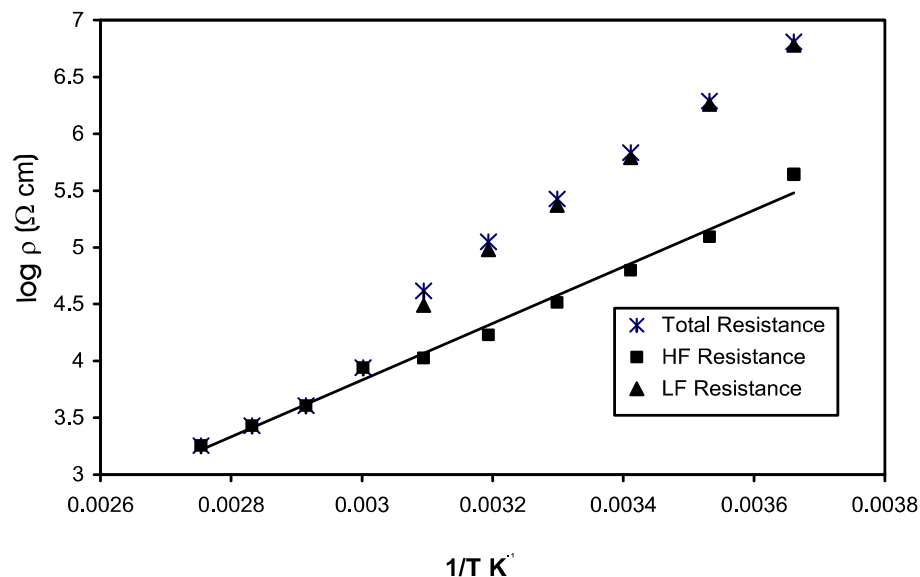


Figure 5.4: Results of circuit fit to PEO LiTF 10-1

5.2 Application of the two Arrhenius equation to the PEO LiTFSI system

In this section equation 5.4 is applied to the DC conductivity of the PEO LiTFSI system. The PEO LiTFSI system behaves very differently than the PEO LiTF system as the salt concentration is increased. The reason for this is that the large TFSI anion acts like a plasticizer. Plasticizers are added to crystalline polymers to make them softer and more flexible. They do this by preventing the polymer from crystallizing. Adding enough plasticizer will prevent any crystallization of the polymer. At low concentrations of LiTFSI, PEO is still largely crystalline. At high concentrations of LiTFSI (around 10-1), PEO (MW = 10⁵) is no longer crystalline but is a very viscous liquid. PEO LiTFSI 10-1 is, therefore, an amorphous polymer electrolyte. Differential

Table 5.1: Parameters from fit of PEO LiTFSI 10-1 to equation 5.4 and to Vogel equation

E_{β} (K)	σ_{β} (S/cm)	E_{α} (K)	σ_{α} (S/cm)
4248	267	12803	2.14E14
A (S/cm)	B (K)	T_0 (K)	
.554	827	211	

scanning calorimetry(DSC) also confirms that PEO LiTFSI 10-1 is amorphous [5]. The PEO LiTF system does not have an completely amorphous phase. This is because as the salt concentration is increased the polymer and salt form a crystalline complex. The existence of a partially crystalline and completely amorphous phase in the same polymer salt system is ideal for testing equation 5.4.

Figure 5.5 shows the DC conductivity for PEO LiTFSI for the concentrations 30-1, 20-1, and 10-1. The 30-1 and 20-1 concentrations are partially crystalline, so there is a discontinuous break in the conductivity around 60°C. The 10-1 concentration is amorphous, and there is no break in the conductivity. The 10-1 concentration exhibits non-Arrhenius behavior characteristic of amorphous polymer electrolytes. This non-Arrhenius behavior would traditionally be fit with the Vogel equation. As a test of equation 5.4, it is used to fit the 10-1 concentration. The result of the fit is shown in figure 5.6. The parameters extracted from the fit are shown in table 5.1. It can be seen that equation 5.4 can be used to fit conductivity data that would traditionally be fit with the Vogel equation.

Included in figure 5.6 are linear fits to the high temperature points and the low temperature points. These lines correspond approximately to the two different con-

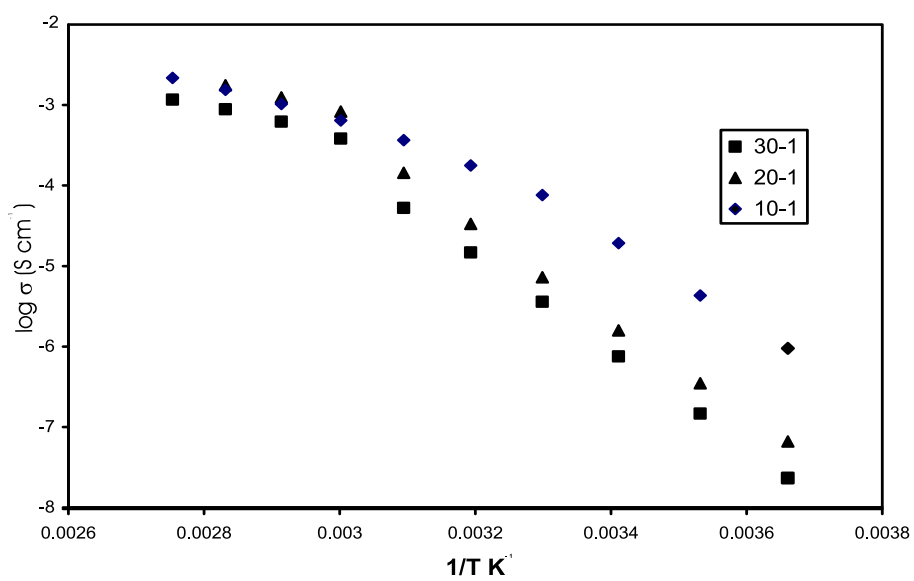


Figure 5.5: Arrhenius plots of the conductivity of PEO LiTFSI for the concentrations 30-1, 20-1, and 10-1.

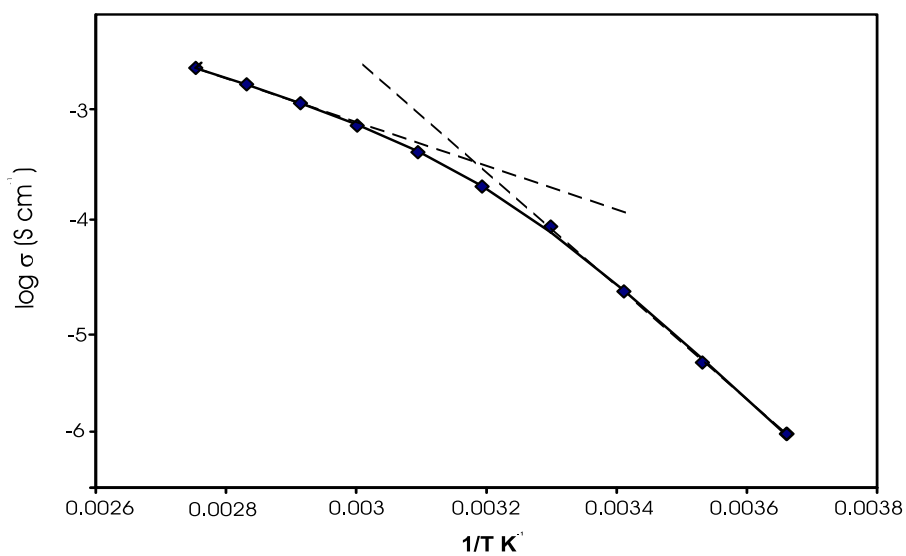


Figure 5.6: Fit of equation 5.4 to PEO LiTFSI 10-1

ductivities. Two resistors in series corresponds to two conductivities in parallel. When two conductivities are in parallel, the total conductivity is always smaller than the individual conductances. The bended region seen in figure 5.6 then corresponds to the region where the two conductivities are approximately equal. Note also that the low temperature behavior appears to be more Arrhenius-like than Vogel-like, consistent with the data in figure 4.6.

Equation 5.4 has been applied to the amorphous PEO LiTFSI 10-1 system. Equation 5.4 was suggested based on analyzing partially crystalline polymer electrolytes like PEO LiTFSI 20-1 and 30-1. How is equation 5.4 applied to the 20-1 and 30-1 concentrations seen in figure 5.5?

Consider again the simple model of a partially crystalline polymer electrolyte. The partially crystalline polymer electrolyte is made up of crystalline regions where no ion conduction takes place and amorphous regions where ion conduction occurs. The melting of the crystalline regions can have a number of possible effects on the polymer electrolyte. The simplest and probably most significant effect is that the melting of the polymer electrolyte results in a large increase in the number of possible conduction pathways through the polymer electrolyte. How would this increase in conduction pathways be expressed in terms of equations 5.3 and 5.4? A increase in the number of pathways could change the prefactors R_β and R_α . From figure 5.4 it is seen that the prefactor R_β (the high frequency resistance prefactor) does not change upon melting of the polymer. In figure 5.4, the low frequency resistance(labelled by subscript α in equation 5.3) becomes insignificant. This behavior can be accounted for by a large

decrease in R_α . It is therefore reasonable that a change in R_α be used to model the melting of the polymer.

The melting of the polymer results in a decrease in the parameter R_α . A decrease in the parameter R_α means an increase in the parameter σ_α in equation 5.4. The parameter σ_α would have two values corresponding to the regions above and below the melting temperature of the polymer. Below the melting point σ_α would have the value $\sigma_\alpha^{T < 60^\circ}$. Above the melting point σ_α would be $\sigma_\alpha^{T > 60^\circ}$. These ideas are now used to simulate the data in figure 5.5. In figure 5.7, the top curve uses equation 5.4 and the parameters from table 5.1 to model PEO TFSI 10-1. For the lower two curves, $\sigma_\alpha^{T > 60^\circ}$ is set equal to σ_α from table 5.1. The parameter, $\sigma_\alpha^{T < 60^\circ}$, is set equal to $\sigma_\alpha^{T > 60^\circ} / 5$ and $\sigma_\alpha^{T > 60^\circ} / 10$ for the middle curve and lower curve respectively. By changing σ_α , it is seen that the two Arrhenius region behavior of partially crystalline polymer electrolytes is reproduced. Figure 5.7 reproduces the qualitative features of the experimental data in figure 5.5. A even closer correspondance to figure 5.5 could be obtained by tweaking the values of σ_β .

When there are no crystalline polymer regions, equation 5.4 can reproduce the Vogel-like behavior seen in PEO LiTFSI 10-1. When there are crystalline regions, by changing σ_α the two Arrhenius regions seen in partially crystalline polymer electrolytes can also be reproduced. It is physically plausible that σ_α changes since on melting more conduction pathways are available in the polymer electrolyte. The ability of equation 5.4 to model the behavior of both amorphous polymer electrolytes and partially crystalline polymer electrolytes must be considered an advantage of equation

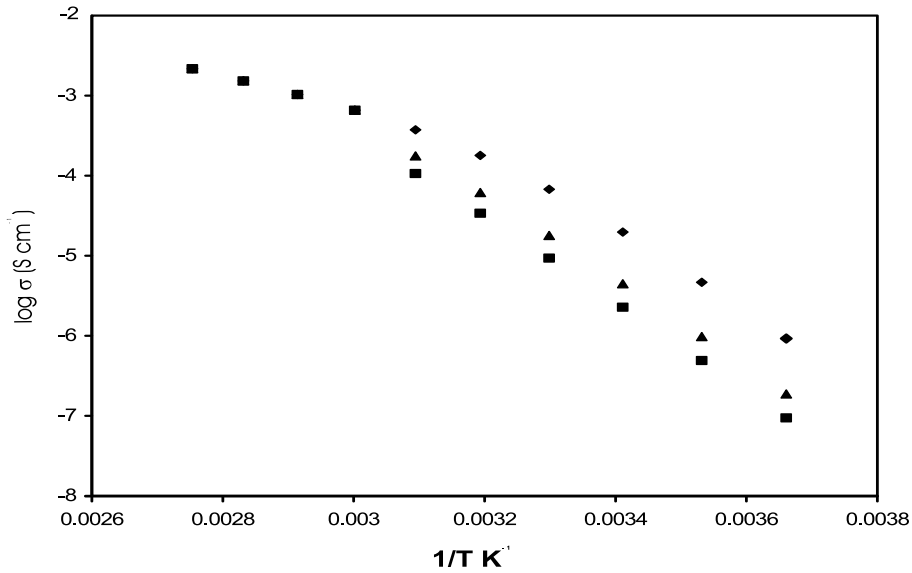


Figure 5.7: Conductivity data simulated using equation 5.4

5.4 over the Vogel equation.

5.3 New parameters for the two Arrhenius equation

Equation 5.4 has the advantage that it can reproduce both amorphous and partially crystalline polymer electrolyte behavior. However, in performing the fits as represented by the parameters in table 5.1, it is noticed that there are some peculiar numbers. Specifically, the σ_α value is around 10^{14}Scm^{-1} . This is a rather large value. It is not surprising that some other mechanism acts as a choke to prevent the conductivity from approaching 10^{14}Scm^{-1} as the temperature increases. Perhaps, however, the parameterization in equation 5.4 is not the most relevant physically. A different

Table 5.2: Parameters from fit of equation 5.4 to C2000 LiTFSI

C2000 LiTFSI	E_β (K)	$\ln\sigma_\beta$ (S/cm)	E_α (K)	$\ln\sigma_\alpha$ (S/cm)
10-1	9065	17.3	18765	50.6
20-1	7456	12.3	14434	35.7
40-1	6304	8.23	12605	29.1
60-1	5946	7.41	13242	31.5
80-1	6180	7.95	14197	35.0

parameterization could yield more physically relevant and reasonable parameters.

In order to justify a new parameterization, experimental evidence is needed. Figure 5.8 shows the DC conductivity for C2000 LiTFSI at various concentrations. The concentrations shown in the plot are for 10-1, 20-1, and 80-1. Data was also taken for the 40-1 and 60-1 concentrations but is not shown in order to reduce the clutter of the plot. C2000 is a amorphous polymer so the conductivity behavior is Vogel-like. As was shown in the previous section, equation 5.4 can be used to fit polymer electrolyte conductivity data that displays Vogel-like behavior. This was done, and the results are shown in table 5.2. It is again seen that the σ_α parameters are rather large.

Notice in table 5.2 that $\sigma_\alpha \setminus \sigma_\beta$ seems to increase with increasing $E_\alpha \setminus E_\beta$. In order to explore this correlation further, $\ln \sigma_\alpha \setminus \sigma_\beta$ is plotted versus the energies $E_\alpha \setminus E_\beta$ in figure 5.9. Also included in the plot are error bars for the parameters. Remarkably the plot is linear. Even more remarkable, the plot is linear over about 15 orders of magnitude of $\sigma_\alpha \setminus \sigma_\beta$. One should be concerned with the large error bars for the points between about 12000 K and 15000 K. Since the error bars overlap for those

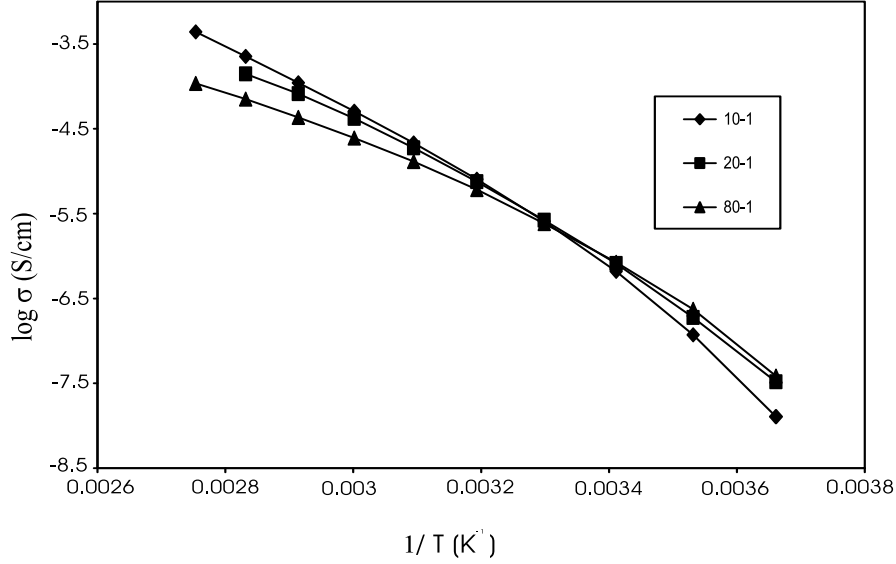


Figure 5.8: Conductivity for C2000 LiTFSI

four points, the data value for those four points is probably no greater than a single point. Even so there are data points above and below those four points that lend confidence to the linear fit between $\ln \sigma_\alpha \setminus \sigma_\beta$ and $E_\alpha \setminus E_\beta$.

What figure 5.9 reveals is that there is a linear relation between the log of the prefactor and the activation energy, i.e. $\ln \sigma \propto E$. This is known as the compensation effect. The compensation effect has been observed in a wide variety of experiments (see next chapter for references). It will be discussed in some detail in the next chapter. For now the experimentally observed relation, $\ln \sigma \propto E$, is used to rewrite the parameters of equation 5.4.

From figure 5.9 it is seen that $\ln \sigma_\alpha$ versus E_α and $\ln \sigma_\beta$ versus E_β lie on the same line. This can be expressed mathematically as

$$\ln \sigma_\alpha = aE_\alpha + b$$

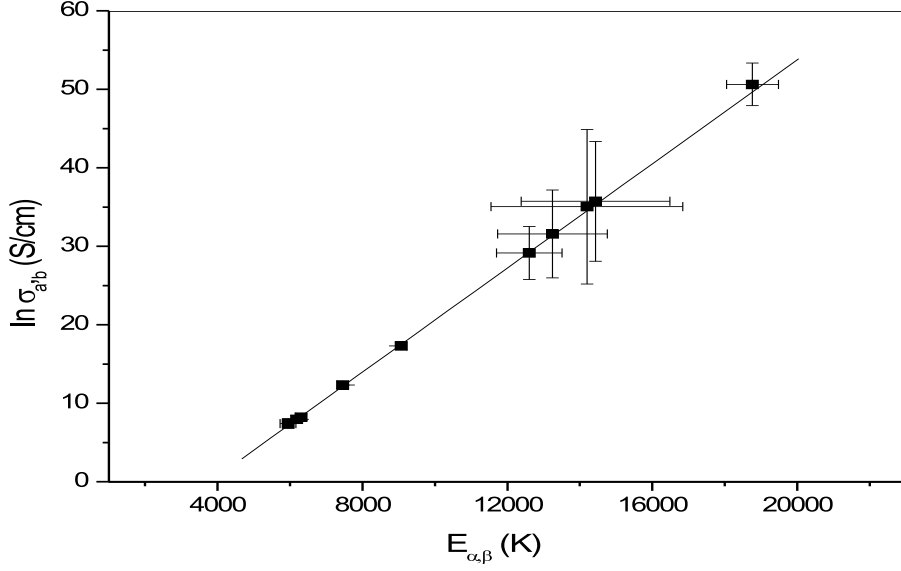


Figure 5.9: Plot of data points from table 5.2

$$\ln \sigma_{\beta} = aE_{\beta} + b. \quad (5.5)$$

Solving for a , the slope, and b , the intercept, gives

$$\begin{aligned} a &= \frac{\ln(\sigma_{\beta}/\sigma_{\alpha})}{E_{\beta} - E_{\alpha}} \\ b &= \frac{-E_{\alpha} \ln \sigma_{\beta} + E_{\beta} \ln \sigma_{\alpha}}{E_{\beta} - E_{\alpha}}. \end{aligned} \quad (5.6)$$

The slope, a , has units of inverse energy. Define a new parameter, T_e , as $kT_e = 1/a$.

Similarly the intercept, b , is written in terms of a new parameter σ_0 as $2\sigma_0 = e^b$.

The new parameters, T_e and σ_0 , take the place of the old parameters, σ_{α} and σ_{β} .

Write the slope, a , and the intercept, b , in terms of T_e and σ_0 . Inserting this result

into equation 5.5 and then inserting equation 5.5 into equation 5.4 gives the new

parameterization of equation 5.4:

$$\sigma(T) = \frac{2\sigma_0}{e^{E_{\beta}(\frac{1}{kT} - \frac{1}{kT_e})} + e^{E_{\alpha}(\frac{1}{kT} - \frac{1}{kT_e})}}. \quad (5.7)$$

Using the data from tables 5.1 and 5.2, the parameters, σ_0 and T_e , can be calculated for PEO LiTFSI 10-1 and C2000 LiTFSI. Using equations 5.6 and table 5.1, T_e for PEO LiTFSI 10-1 is found to be approximately 312 K, and σ_0 is found to be 1.64E-4 (S/cm). By finding the slope and intercept in figure 5.9, one finds $T_e = 297K$ and $\sigma_0 = 1.19E-6$ (S/cm) for C2000 LiTFSI.

Some insight into the parameters, T_e and σ_0 , can be had by examining figure 5.6. The two dotted lines in figure 5.6 represent the conductivities $\sigma_\alpha e^{-E_\alpha/kT}$ and $\sigma_\beta e^{-E_\beta/kT}$. The two dotted lines cross at some temperature T_{equal} . Setting the conductivities equal to one another and solving for T_{equal} gives $T_{equal} = T_e$. The new parameter, T_e , is the temperature at which the two conductivities are equal. If the temperature in equation 5.7 is set equal to T_e , the conductivity, $\sigma(T_e)$, is equal to the new parameter, σ_0 . The new parameter, σ_0 , is the value of the conductivity at the temperature, T_e . In figure 5.8, the temperature, T_e , is the point in the figure where all three curves (actually five curves since two are not shown) meet, approximately, at a point. The conductivity at that point is σ_0 . The above interpretation of T_e is basically a graphical interpretation. Possible physical interpretations of T_e will be discussed in the chapter on the compensation effect.

The new parameterization solves the problem of the large σ_α values seen in tables 5.1 and 5.2. The large values are seen to be due to an exponential dependence on the activation energy, $\sigma_\alpha = \sigma_0 e^{E_\alpha/kT_e}$.

While the change from the parameterization, $\{\sigma_\alpha, \sigma_\beta, E_\alpha, E_\beta\}$, to the parameterization, $\{\sigma_0, T_e, E_\alpha, E_\beta\}$, can be made, it is necessary to ask if it is relevant to do so.

The parameters, σ_0 and T_e , were used above for the PEO LiTFSI 10-1 amorphous polymer electrolyte. The PEO LiTFSI 10-1 is a single curve, and it would be hard justify the use of $\{\sigma_0, T_e\}$ over $\{\sigma_\alpha, \sigma_\beta\}$ if only that single curve were available. However for the C2000 LiTFSI system, five curves, depending on concentration are available. If the $\{\sigma_\alpha, \sigma_\beta, E_\alpha, E_\beta\}$ parameterization is used, a total of 20 parameters would be need to described the five curves(4(parameters/curve) * 5(curves) = 20). If the Vogel equation were used to described the family of curves a total of 15(3 * 5) parameters would be needed. If the $\{\sigma_0, T_e, E_\alpha, E_\beta\}$ parameters are used, only 12 parameters are need since σ_0 and T_e apply to each of the five curves. The parameterization, $\{\sigma_0, T_e, E_\alpha, E_\beta\}$, is certainly warranted for C2000 LiTFSI.

Further evidence of the compensation effect is desirable so that greater confidence can be had in applying equation 5.7 to wider range of polymer electrolyte systems. For this purpose the work of Quartarone et al.[6] is discussed. Quartarone et al. investigated the conductivity of PEO mixed with the filler lithium triborate ($Li_2O \bullet 3B_2O_3$). The system does not involve a salt, but there is lithium conduction due to lithiums supplied by the filler. The PEO is still partially crystalline, so two Arrhenius regions are expected in the conductivity. Figure 5.10 shows indeed that two Arrhenius regions are seen in the conductivity. The different conductivity curves seen in figure 5.10 depend on the weight percent of the filler used. As shown in figure 5.10 straight line fits were used to extract a prefactor and activation energy for the two regions and for the different concentrations.

The results of the fitting are shown in figure 5.11. It is again seen that there is a

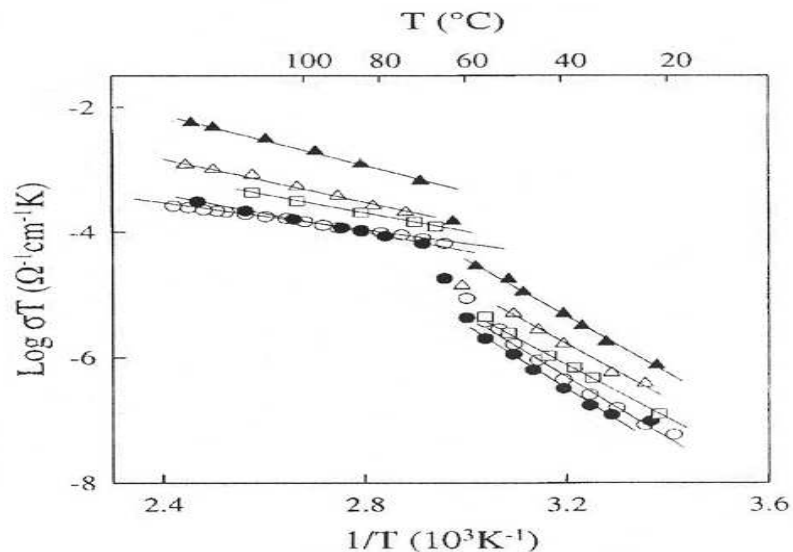


Figure 5.10: Conductivity of PEO with lithium triborate filler. Figure taken from reference [6].

linear relationship between the natural logarithm of the prefactors and the activation energies. Quartarone et al. argued that since there exists a linear slope in figure 5.11 that the transport mechanism above and below the melting point of the polymer was the same. This chapter has shown, however, that this is not necessarily the case. The inverse of the slope gives a value of 445 K for T_e . This is much larger than the result, $T_e = 312K$, arrived at for the amorphous PEO LiTFSI 10-1 system. This large value of T_e is (in the author's view) due to a failure to take into account the melting of the crystalline polymer. From equation 5.6, T_e can be found with

$$kT_e = \frac{E_\alpha - E_\beta}{\ln(\sigma_\alpha/\sigma_\beta)}. \quad (5.8)$$

As discussed before because of the crystallinity of the PEO, σ_α will be smaller than it would be if the polymer were amorphous. This smaller value of σ_α will yield a larger value of T_e when placed in equation 5.8. The value, $T_e = 312K$, is probably more

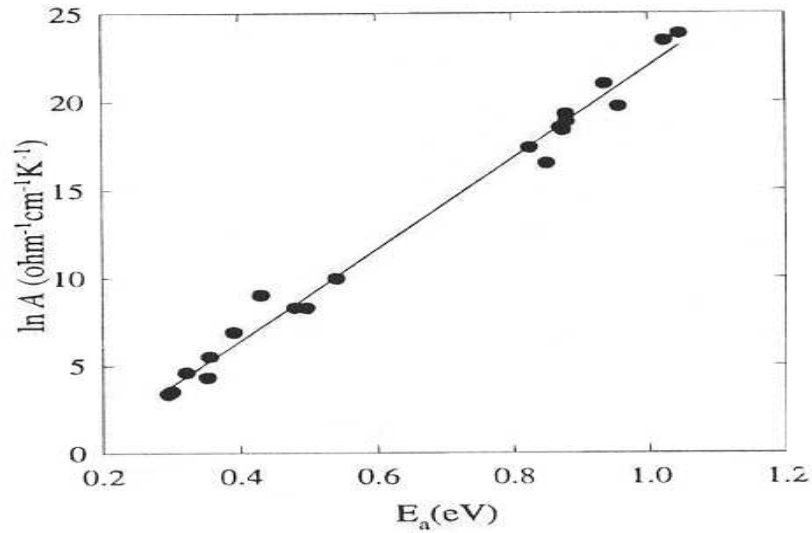


Figure 5.11: Plot \ln prefactors vs. activation energies for data from figure 5.8. Figure taken from reference [6].

physically relevant than the value, $T_e = 445K$. Even though a compensation-like effect is seen in figure 5.11, caution should be exercised especially when dealing with the discontinuous conductivity data of figure 5.10.

An additional example of the compensation effect in polymer electrolytes is the work of Wieczorek et al.[7]. This work is an extension of the work of Chung et al.[8] discussed in the previous chapter. The polymer electrolyte system investigated was OMPEO LiClO_4 with various fillers. Wieczorek et al. fitted the low temperature Arrhenius region seen by Chung et al.. They too saw a linear relation between the logarithm of the prefactors and the activation energy. The values measured for T_e were between 260 K and 310 K. This range agrees with 312 K measured for PEO LiTFSI 10-1 and the 297 K measured for C2000 LiTFSI. Since Wieczorek et al. believed that

the high temperature region followed the Vogel equation, they did not check to see if the high temperature region also followed the compensation effect.

5.4 Summary

The previous chapter discussed a number of problems in the application of the Vogel equation to polymer electrolyte conductivity. Do equations 5.4 and 5.7 improve the situation? One problem with the Vogel equation was that it cannot be used to understand the two Arrhenius regions seen in partially crystalline polymer electrolytes. In partially crystalline polymer electrolytes, there is a activated region below the melting point of the polymer with a large activation energy. Above the melting point of the polymer, there is an activated region with a smaller activation energy. With equation 5.4, these two regions are interpreted as being due to two different activated processes that are always operating in the polymer electrolyte. Both of these processes are modelled by the Arrhenius equation. The discontinuity seen in partially crystalline conductivity is modelled by an abrupt change in the parameter σ_α when the crystalline regions melt.

Besides offering insight into partially crystalline polymer electrolytes, equation 5.4 was also able to fit amorphous polymer electrolyte conductivity. Amorphous PEO LiTFSI 10-1 was successfully fitted with equation 5.4. Figure 5.7 demonstrates how equation 5.4 can reproduce amorphous and partially crystalline polymer electrolyte conductivity.

Chung et al.[8] pointed out that at low temperatures some amorphous polymer electrolytes exhibit Arrhenius-like conductivity. This is what would be predicted based on equation 5.4. Chung et al. also proposed a change in mechanism from a Vogel mechanism at high temperature to a Arrhenius mechanism at low temperatures. With equation 5.4 no change in mechanism occurs. Instead there are two series mechanisms occurring in the polymer electrolyte. One mechanism dominates at high temperature, and the second mechanism dominates at low temperatures. The temperature range, where the two mechanisms are about equal in importance, gives the curved behavior characteristic of amorphous polymer electrolytes.

Equations 5.4 and 5.7 supply insight into semi-crystalline polymer electrolytes and polymer electrolytes that exhibit Arrhenius behavior at low temperatures. However, as was mentioned some polymer electrolyte show non-Arrhenius behavior at low temperatures. In chapter 8, a generalization of equations 5.4 and 5.7 to handle non-Arrhenius behavior at low temperatures will be presented. This generalization will be consistent with a hopping picture of ion transport. The next chapter discusses the compensation effect. This will supply some ideas as to the possible meaning of T_e . The chapter after that discusses possible physical sources for the barriers E_β and E_α .

Bibliography

- [1] J. J. Fontanella. *J. Chem. Phys.*, 111:7103, 1999.
- [2] M. C. Wintersgill, J. J. Fontanella, P. E. Stallworth, S. A. Newman, S. H. Chung, and S. G. Greenbaum. *Solid State Ionics*, 135:155, 2000.
- [3] J. T. Bendler, J. J. Fontanella, M. F. Shlesinger, and M. C. Wintersgill. *Electrochim. Acta*, 46:1615, 2001.
- [4] J. T. Bendler, J. J. Fontanella, and M. F. Shlesinger. *Phys. Rev. Lett.*, 87:195503, 2001.
- [5] A. Vallee, S. Besner, and J. Prudhomme. *Electrochim. Acta*, 37:1579, 1992.
- [6] E. Quartarone, P. Mustarelli, C. Tomasi, and A. Magistris. *J. Phys. Chem. B*, 102:9610, 1998.
- [7] W. Wiczorek, S. H. Chung, and J. R. Stevens. *J. Poly. Sci. B*, 34:2911, 1996.
- [8] S. H. Chung, K. Such, W. Wiczorek, and J. R. Stevens. *J. Poly. Sci. B*, 32:2733, 1994.

Chapter 6

The Compensation Effect

In the previous chapter, equation 5.4 was proposed as a possible alternative to the Vogel equation for fitting polymer electrolyte conductivity. Applying equation 5.4 to the C2000 LiTFSI system, it was seen that there was a relation between the prefactors of equation 5.4 and the activation energies. This relation is called the compensation effect. The compensation effect leads to equation 5.7 and to the new parameters T_e and σ_0 . The purpose of this chapter is to review the compensation effect and to gain insight into the physical meaning of T_e .

6.1 Introduction to the compensation effect

The Arrhenius equation is written as

$$rate = Ae^{-E/kT}. \quad (6.1)$$

Experimentally it is often found that

$$\ln A \propto E. \quad (6.2)$$

This means that the prefactor, A , can be written as $A = x_0 e^{E/kT_e}$ (writing the proportionality constant between $\ln A$ and E as $1/kT_e$ is for later convenience). The inverse of T_e is the proportionality factor between the logarithm of the prefactor and the activation energy. This relation between the logarithm of the prefactor and the activation energy is known as the compensation effect. In the context of charge hopping it is also known as the Meyer-Neldel rule.

A slightly different way to express the compensation effect is to write the Arrhenius equation in terms of the Gibbs free energies:

$$rate = x_0 e^{-\Delta G/kT}. \quad (6.3)$$

Thermodynamics says that Gibbs free energies can be written as $\Delta G = \Delta H - T\Delta S$, where ΔH is the enthalpy and ΔS is the entropy. Inserting this expression into the above equation gives

$$rate = x_0 e^{\Delta S/k} e^{-\Delta H/kT}. \quad (6.4)$$

The effective prefactor of equation 6.4 is $x_0 e^{\Delta S/k}$. The compensation effect will hold if the entropy is proportional to the enthalpy, i.e. $\Delta S = \Delta H/T_e + const..$ When expressed in terms of entropy and enthalpy the compensation effect is sometimes called enthalpy-entropy compensation.

The compensation effect has been seen in a diverse number of fields including chemical reactions, ionic conductors, physical aging in polymers, and biological death rates (see Introduction sections of Yelon et al.[1] and Peacock-Lopez and Suhl[2] for references). A number of theories have been proposed to account for the compensation

effect. Some of the theories are now reviewed.

6.2 Heat bath excitations and the compensation effect

6.2.1 The theory of Peacock-Lopez and Suhl

A very general approach to the compensation effect has been made by Peacock-Lopez and Suhl[2]. In this approach an energy barrier much larger than kT is considered. In order to surmount this barrier a large number of excitations from the heat bath must be assembled and absorbed. The number of ways these excitations can be assembled leads to the compensation effect.

The transition rate for a process from an initial state, i , to a final state, f , can be written as

$$\frac{2\pi}{\hbar} \sum_{f,i} |\langle f|T|i\rangle|^2 \frac{e^{-\beta E_i}}{Z} \delta(E_f - E_i). \quad (6.5)$$

The initial state relates to a particle trapped in a well, and the final state relates to a particle that has escaped from the well. Z is the partition function of the system when the particle is in the well. The partition function also includes the thermal excitations of the system. The matrix element for the transition from the initial state to the final state is given by $\langle f|T|i\rangle$.

The total energy of the initial state is given by E_i . This total energy includes the energy of the particle in the well, E_i^0 , and the energy of the excitations. Likewise

the total energy of the final state is given by E_f . It too includes the energy of the particle out of the well along with the energy of the excitations. The total energies are written as

$$\begin{aligned} E_i &= E_i^0 + \sum_k (m_k + n_k) \epsilon_k \\ E_f &= E_f^0 + \sum_k m_k \epsilon_k. \end{aligned} \quad (6.6)$$

The set $\{m_k\}$ gives the number of excitations in a state labelled by k . Likewise, ϵ_k gives the energy of an excitation labelled by k . The kets, $|i\rangle$ and $|f\rangle$, can also be written in terms of the particle energies and excitation occupation numbers.

$$\begin{aligned} |i\rangle &= |E_i^0, \{n_k + m_k\}\rangle \\ |f\rangle &= |E_f^0, \{m_k\}\rangle \end{aligned} \quad (6.7)$$

In the initial state, there are additional excitations, $\{n_k\}$, present. These excitations are absorbed to produce the final state. The difference between the total final energy, E_f , and the total initial energy, E_i is

$$E_f - E_i = E_f^0 - E_i^0 - \sum_k n_k \epsilon_k. \quad (6.8)$$

According to equation 6.5, the total energy difference must be zero; therefore, $\epsilon \equiv E_f^0 - E_i^0 = \sum_k n_k \epsilon_k$.

With certain assumptions[2], equation 6.5 becomes

$$\frac{2\pi}{\hbar} \sum_i \int_{\epsilon_b - E_i^0}^{\epsilon_c} d\epsilon e^{-\beta\epsilon} R_f(E_i^0 + \epsilon) \sum_{\{n_k\}} |T(E_i^0, n, \epsilon)|^2 \frac{e^{-\beta E_i^0}}{Z_r} \delta(\epsilon - \sum_k n_k \epsilon_k) \quad (6.9)$$

where ϵ_b is the barrier height, $n = \sum_k n_k$, and ϵ_c is an upper energy cutoff. $R_f(E)$ is the density of states at the final state. The sum over the occupation number, $\{n_k\}$,

can be broken up as

$$\sum_{\{n_k\}} = \sum_n \sum_{\sum_k n_k = n} . \quad (6.10)$$

Inserting the above form of the summation into equation 6.9, the following term is encountered:

$$\sum_{\sum_k n_k = n} \delta(\epsilon - \sum_k \epsilon_k n_k) = \rho_n(\epsilon). \quad (6.11)$$

Equation 6.11 is the density of states for n excitations having a total energy of ϵ . With the identification of $\rho_n(\epsilon)$ in equation 6.9, it is seen that if there are a large number of ways that n excitations can be assembled to give $\epsilon > \epsilon_b$, i.e. if $\rho_n(\epsilon)$ is large, there will be an enhancement of the transition rate.

The Laplace transform of $\rho_n(\epsilon)$ is $[\tilde{\rho}(p)]^n$ where $\tilde{\rho}(p)$ is the Laplace transform of the single particle density of states, $\rho(\epsilon)$.

$$\tilde{\rho}(p) = \int_0^\infty e^{-p\epsilon} \rho(\epsilon) d\epsilon \quad (6.12)$$

Considering only a single level, E_i^0 , instead of a distribution of levels and choosing the energy scale by setting $E_i^0 = 0$, the transition rate equation simplifies to

$$\frac{1}{i\hbar} \int_{\epsilon_b}^{\epsilon_c} d\epsilon e^{-\beta\epsilon} R_f(\epsilon) \int_{c-i\infty}^{c+i\infty} dp e^{p\epsilon} \sum_{n=1}^{\infty} |T(n, \epsilon)|^2 [\tilde{\rho}(p)]^n \quad (6.13)$$

The real number, c , is chosen to be to the right of the singularities of the integrand.

After arriving at equation 6.13, Peakcock-Lopez and Suhl then considered the term $\sum_{n=1}^{\infty} |T(n, \epsilon)|^2 [\tilde{\rho}(p)]^n$. Specifically, what are the poles corresponding to this term? Peakcock-Lopez and Suhl argue that when performing the contour integral the poles of the term $\sum_{n=1}^{\infty} |T(n, \epsilon)|^2 [\tilde{\rho}(p)]^n$ will be dominated by the right most pole

which lies on the radius of convergence of the sum. This pole lies on the real axis and is located at $p = \beta_e$. Assuming that the pole is a simple pole and that the density of states, $R_f(\epsilon)$, is fairly constant, the transition rate equation 6.13 is for $\beta > \beta_e$ approximately

$$R \sim e^{(\beta_e - \beta)\epsilon_b}. \quad (6.14)$$

The compensation effect is evident in equation 6.14. Equation 6.14 applies for $\beta > \beta_e$. It was seen in the previous chapter that the compensation effect can also apply for $\beta < \beta_e$. In considering $\beta < \beta_e$, Peacock-Lopez and Suhl also derived a rate equation resembling equation 6.14 but with ϵ_b replaced by the cutoff energy ϵ_c . This change in the activation energy for $\beta < \beta_e$ resembles the case for polymer electrolytes where there was also a change in the activation energy for $\beta < \beta_e$ (see equation 5.7).

The above derivation of the compensation effect started by considering a general equation for the transition from one state to another. These two states could correspond to a particle in a well and a particle outside a well. In order to conserve energy, a number of excitations were absorbed so that the particle could escape the well. Intuitively, the more ways there are to assemble the excitations from the bath the faster the transition can take place. By taking this assembling of excitations into account, one is lead to an approximate analytic result that resembles the compensation effect.

6.2.2 The theory of Yelon and co-workers

The above argument due to Peacock-Lopez and Suhl is quite general but also quite mathematical. A simpler argument in the same spirit as the above argument has

been given by Yelon et al.[1].

Consider a number of excitations of energy E_e in the vicinity of a particle in a deep well. Denote the number of nearby excitations by N and with equation 6.4 the well depth is given by ΔH . The number of excitations needed for the particle to escape the well is $n = \Delta H/E_e$. The entropy change associated with leaving the well is related to the number of pathways the particle can take to escape the well. The number of pathways is related to the number of ways n excitations can be assembled from the total available excitations, N . The entropy change is therefore given by

$$\Delta S/k = \ln \frac{N!}{n!(N-n)!} \quad (6.15)$$

Using Stirling's formula and assuming $n \ll N$, the above equation simplifies to

$$\Delta S/k \approx n \ln \frac{N}{n} \approx \frac{\Delta H}{E_e} \ln N. \quad (6.16)$$

From equation 6.4, the compensation effect can be established if the entropy is shown to be proportional to the enthalpy. This is just what equation 6.16 does.

Part of the goal of this chapter is to gain insight into the physical meaning of the parameter T_e from equation 5.7. From the Peacock-Lopez and Suhl arguments, the meaning of $\beta_e = 1/kT_e$ is somewhat elusive. Based on the Peacock-Lopez and Suhl arguments one might guess that β_e is related to some average excitation energy, but this guess would be based more on intuition than on the mathematical development. Equation 6.16 makes the connection between T_e and the energy of excitation more explicit. From equation 6.16, kT_e is equal to $E_e/\ln N$. This relation is not very useful since N , the number of excitations near the escaping particle, is unknown. While the

Yelon et al. argument is more easily understood and intuitive, the Peacock-Lopez and Suhl argument is more rigorous and therefore a more satisfying explanation of the compensation effect.

It is often noticed that systems with high activation energies often show the compensation effect. However, systems with low activation energies do not show the compensation effect. The picture of assembling excitation makes clear why this could be the case. With high energy barriers many excitations must be assembled and absorbed to overcome the barrier. The many ways in which these excitations can be assembled leads to the compensation effect. With low energy barriers where only one or a few excitations are necessary, there is little enhancement to the prefactor from assembling the excitations. Since there is little effect on the prefactor the compensation effect is not evident for low energy barriers.

6.2.3 The theory of Linert

In a series of related chemical reactions, it is often seen that the rate constants of the different reactions cross at a single point when plotted as $\ln k$ vs. $1/kT$. The temperature of this point has been termed the isokinetic temperature, T_{iso} . For the purposes of this study T_{iso} is the same as T_e . Linert[3, 4, 5] has given the following equation as a condition for the isokinetic temperature.

$$\left. \frac{\partial \ln k(\eta)}{\partial \eta} \right|_{1/k_B T_{iso}} = 0 \quad (6.17)$$

In equation 6.17, η is a parameter that indexes the members of the related chemical reaction series, and k is the reaction rate.

Linert's treatment of the isokinetic temperature relies on theoretical treatments used in the study of unimolecular reactions. The work of McCoy and Carbonell[6, 7] on unimolecular reactions is presented. Following that Linert's arguments leading to the compensation effect are discussed.

Consider a potential energy well. This potential energy well has a large number of energy levels. The potential energy well is coupled to a heat bath, so the diagonal density matrix elements, σ_n , can change with time. The time dependence of the diagonal density matrix elements can be written in terms of a master equation.

$$\frac{d\sigma_n}{dt} = R_{n,n-1}\sigma_{n-1} - R_{n-1,n}\sigma_n - R_{n+1,n}\sigma_n + R_{n,n+1}\sigma_{n+1} \quad (6.18)$$

$R_{n,m}$ is the transition probability from level m to level n . Equation 6.18 assumes that only nearest neighbor transition probabilities are non-zero.

The energy level spacing is written as $\omega_{nm} = (\epsilon_n - \epsilon_m)/\hbar$. By assuming that the energy level spacing is much smaller than kT , McCoy and Carbonell[7] rewrote equation 6.18 in terms of a partial differential equation.

$$\frac{\partial\sigma}{\partial t} = \frac{\partial}{\partial s} \left(R(s) \frac{\partial\sigma}{\partial s} \right) + \frac{1}{kT} \hbar \frac{\partial}{\partial s} (R(s)\omega(s)\sigma) \quad (6.19)$$

The energy levels are now indexed by the continuous variable s , and the energy associated with the level s can be found with

$$\epsilon(s) = \hbar \int_0^s \omega(s') ds'. \quad (6.20)$$

The steady state solution ($\partial\sigma/\partial t = 0$) of equation 6.19 is the Boltzmann distribution. In order to discuss reaction rates, however, it is necessary to introduce some additional complications to equation 6.19. The potential energy well is considered to have some maximum level, s_N . If during the random walk the system reaches the level s_N , the system escapes the potential energy well and the reaction takes place. The boundary condition for this situation is $\sigma(s_N) = 0$. Another complication is the addition of a source term, $g(s)$, to equation 6.19. Since the boundary condition allows for the reactants to leave the system, there must be flux of reactants into the well to ensure steady state conditions. The reaction rate is given by the flux of reactants leaving the system divided by the number of reactants in the system. Under steady state conditions, the flux into the system must be equal to the flux out of the system. The forward reaction rate can therefore be written as

$$k_f = \frac{j(s_N)}{x_R} \quad (6.21)$$

where flux into the system is

$$j(s_N) = \int_0^{s_N} g(s) ds \quad (6.22)$$

and the number of reactants in the well is

$$x_R = \int_0^{s_N} \sigma(s) ds. \quad (6.23)$$

Equation 6.19 (with the source term included) can be solved under steady state conditions. Inserting the resulting expression for $\sigma(s)$ into equation 6.21 gives

$$k_f = j(s_N) \left\{ \int_0^{s_N} ds \exp \left(-\frac{1}{kT} \hbar \int_0^s \omega(s') ds' \right) \right\}$$

$$\times \int_s^{s_N} \frac{ds'}{R(s')} \exp\left(\frac{1}{kT} \hbar \int_0^{s'} \omega(s'') ds''\right) j(s') \}^{-1}. \quad (6.24)$$

If it is assumed that the barrier energy is much greater than the thermal energy, i.e.

$\hbar\omega s_N/kT \gg 1$, then the reaction rate simplifies dramatically to

$$k_f \approx R(s_N) \left(\frac{\hbar\omega}{kT}\right)^2 e^{-\frac{s_N \hbar\omega}{kT}} \quad (6.25)$$

where it is assumed that $\omega(s) = \omega$.

Starting from equation 6.25, Linert considered the appropriate form for $R(s_N)$ when the system couples to the heat bath. It is expected that the energy levels in the heat bath are much more closely spaced than in the reactant well. Denote the energy level spacing in the heat bath by ν . If energy is transferred resonantly from the heat bath to the reactant well, then one has the condition

$$m\nu = l\omega \quad (6.26)$$

where m and l denote levels in the heat bath and reactant well respectively. Linert argues that the transition probability for the energy transfer from the heat bath to reactant well is[3]

$$le^{l\omega/\nu}. \quad (6.27)$$

The transition probabilities in the reactant well should depend on the energy transfer from the heat bath. This implies that $R(s_N) \propto l \exp(s_N \omega/\nu)$. Inserting this $R(s_N)$ into equation 6.25 yields

$$k_f = A_0 s_N \left(\frac{\hbar\omega}{kT}\right)^2 e^{s_N \left(\frac{\omega}{\nu} - \frac{\hbar\omega}{kT}\right)} \quad (6.28)$$

where A_0 is a proportionality constant.

Linert then uses equation 6.17 with s_N as index parameter to derive the result

$$\frac{1}{kT_{iso}} = \frac{1}{s_N \hbar \omega} + \frac{1}{h\nu}. \quad (6.29)$$

Since $s_N \hbar \omega \gg \hbar \nu$, $kT_{iso}(T_e)$ is approximately equal to $h\nu$.

Linert has interpreted ν as some characteristic vibration of the medium in which the reaction takes place. A correlation between medium vibrations and experimentally measured values of T_{iso} is shown in figure 6.1. The x-axis corresponds to vibrational peaks seen in the IR spectra of the solvents listed in the figure. The y-axis corresponds to T_{iso} values measured for a related series of reactions in a particular solvent. The figure shows that there is a strong correlation between IR peaks and T_{iso} as suggested by Linert's theory. Examples of far IR spectra for polymer electrolytes will be presented in the next chapter.

6.2.4 The compensation effect and the melting temperature

An example of the compensation effect having to do with the diffusion of metals is now discussed. The temperature dependence of diffusion in metals is found to be of the Arrhenius form

$$D = D_0 e^{-E/kT}. \quad (6.30)$$

In his study of the prefactor D_0 , G.J. Dienes listed a number of different equations that had been proposed for D_0 [8]. However, on examining the prefactors and activation energies of a number of different metals, Dienes proposed the following relation for

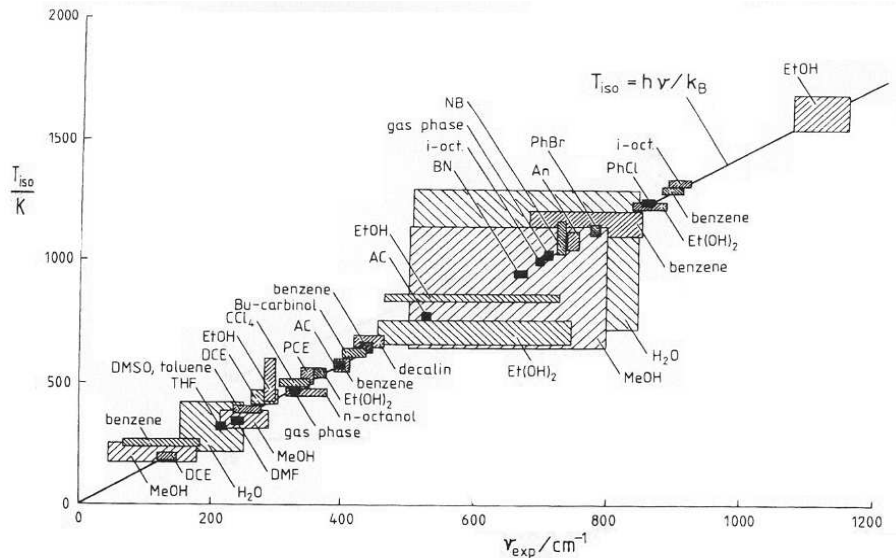


Figure 6.1: Plot of T_{iso} versus IR peaks seen in solvent. Figure taken from reference [4]

the prefactor.

$$D_0 \propto e^{E/kT_m} \quad (6.31)$$

This says that diffusion of metals obey the compensation effect. Interestingly, the compensation effect temperature, T_m , is the melting temperature of the metal.

Dienes explained the presence of T_m in the compensation effect as follows[8]. Normally a metal atom can not diffuse because it is trapped by its neighbors. Therefore instead of considering just the diffusing atom, consider a region containing the diffusing atom and its neighbors. This is similar to the cooperatively rearranging region idea used when discussing configuration entropy. For the diffusing metal atom to move the neighboring metal atoms must move also. Before the metal atoms move they will probably have some crystal-like order. As the metal atoms move simultaneously this crystal like structure will be destroyed. Therefore this cooperative rearrangement of

the metal atoms can be thought of as localized melting of the region. This localized melting allows the diffusing atom to move. Consider the thermodynamics of melting. This is done by considering the free energy.

$$\Delta G = \Delta H - T\Delta S \quad (6.32)$$

At the melting temperature, ΔG equals zero. Therefore at the melting point $\Delta S = \Delta H/T_m$. If the thermodynamics of melting of the sample is similar to the thermodynamics of melting of a localized region, the presence of T_m in the compensation effect can be understood.

Similar conclusions to the above have been made by Khait et al.[9]. They considered diffusion in silicon and germanium. It was seen that there is a linear relation between the logarithm of the diffusion prefactor and the activation energy. Using Khait's theory of short-lived large energy fluctuations(SLEFs), the proportionality constant between the logarithm of the diffusion prefactor and the activation energy was predicted to be the inverse of the melting temperature. This prediction agreed with experiment. The SLEFs provide large thermal energies to overcome barriers but are short lived, $10^{-13} - 10^{-12}s$.

Dienes's result has also been discussed by Almond and West in regards to solid ionic conductors[10].

This discussion of localized melting is, perhaps, not so different from the discussion of excitations. The cause of localized melting at a temperature below the melting point is due to thermal fluctuations in the system. These thermal fluctuations are due to the distribution of excitations in the system. If there are a large enough number of

excitations in a localized region, localized melting can occur. In discussing excitations and the compensation effect, a single particle in a well picture was used. Perhaps this is a overly restrictive picture. A picture in which the particle in the well actually represents a localized region might be more useful. In this picture the particle in the well might represent a region where there is crystal like order and no long range movement. The particle out of the well would then represent a region in a disordered liquid like state. Long range movement can occur in the liquid like state.

The compensation temperature, T_e , was found in the last chapter for PEO LiTFSI 10-1 and C2000 LiTFSI. For C2000 LiTFSI, T_e was found to be about 296 K. For PEO LiTFSI 10-1, T_e was found to be about 312 K. Similar to PPO, C2000 does not crystallize, so $T_e = 296$ K can not be compared to the melting temperature. PEO does crystallize. The melting point of PEO is usually between 50-60°C. Polymers usually have a wide temperature range over which they melt, so it can be difficult to pinpoint a melting temperature. Even so, the 50-60°C temperature range is higher than the $T_e = 312$ K found for PEO LiTFSI 10-1. This does not necessarily mean that T_e is unrelated to melting of the polymer. As stated before, transport occurs in the amorphous regions of the polymer electrolyte. Any ordered crystalline like regions in the amorphous region will be small and surrounded by disordered regions. In a material such as a metal or semiconductor, the local regions are surrounded by other crystalline regions. In a metal or semiconductor, the thermal fluctuations necessary to melt the localized region will probably be characterized by the melting temperature. The fluctuations/excitations necessary to melt the small crystalline like

regions surrounded by the disordered regions in the amorphous polymer phase will likely be characterized by a temperature different than the melting temperature. A T_e less than the melting temperature for a polymer is therefore not unreasonable. Since T_e does not match the melting temperature the term disordering or fluidizing will be used rather than melting. It is also reasonable that the T_e for PEO LiTFSI 10-1 is larger than the T_e for C2000 LiTFSI. Most likely if C2000 did crystallize, its melting temperature would be less than the melting temperature of PEO. It would therefore be expected that T_e for C2000 would be less than the T_e for PEO.

6.3 The compensation effect and polymers

The compensation effect has been seen in a number of mechanical and dielectric experiments on polymers[11]. For example, Lawson[12] found that the change in enthalpy divided by the change in entropy was fairly constant for the diffusion of various gases in polymers. The compensation effect is also often observed in thermally stimulated depolarization current(TSDC) experiments performed on polymers[13, 14, 15]. A TSDC experiment is similar to a dielectric experiment and therefore involves microscopic motion of the polymer. High frequency mechanical measurements on polymers have also indicated a constant ratio between enthalpy and entropy[16]. Crine [17] has reviewed one theoretical approach(discussed below) that has been used to understand the compensation effect in polymers and has suggested an equation for T_e in terms of the mechanical properties of the polymer.

Using simple thermodynamics, Lawson[18] argued that the activation entropy could be related to an activation volume approximately as follows.

$$\Delta S = \Delta V \frac{\alpha}{\beta} \quad (6.33)$$

In equation 6.33, α is the coefficient of thermal expansion and β is the isothermal compressibility.

$$\beta = \frac{1}{V} \left(\frac{\partial V}{\partial P} \right)_T \quad (6.34)$$

It was later argued by Keyes[19] that there exists a relation between the activation enthalpy and the activation volume. This relation is

$$\Delta H = \Delta V / K\beta \quad (6.35)$$

where K is a constant. Combining equations 6.33 and 6.35 gives

$$\Delta S = K\alpha\Delta H. \quad (6.36)$$

Equation 6.36 expresses a linear relation between ΔH and ΔS as required by the compensation effect. From equation 6.36, T_e would be given by $1/K\alpha$.

As a check of equation 6.33 for polymer electrolytes, it is necessary to perform pressure dependent measurements on the conductivity. With pressure dependent conductivity data, the activation volume can be found with

$$\left(\frac{\partial \ln \sigma}{\partial P} \right)_T = -\frac{\Delta V}{RT}. \quad (6.37)$$

Because of the experimental difficulties involved, pressure dependent measurements on polymer electrolytes are rarely done. When pressure dependent measurements

are done, they are usually done with amorphous polymers such as PPO. Stoeva et al.[20] have performed pressure dependent measurements on partially crystalline PEO LiClO₄ 20-1. For the activation energy of the partially crystalline region, Stoeva et al. found $\Delta H \approx 141kJ/mol$. For the activation volume, they found $\Delta V \approx 36cm^3/mol$. Inserting ΔH and ΔV into equation 6.33 and using $K = 2.2$ (see below), β is calculated to be $1.16E-10 m^2/N$ which is the correct order of magnitude for the isothermal compressibility of a polymer.

Originally the parameter K had to be determined experimentally. Crine[17], however, proposed that K is given approximately by the Rao acoustical parameter, n_R . Crine checked this relation for a variety of polymers and found some agreement.

The Rao acoustical parameter is given by

$$n_R = \left(\frac{\partial \ln u}{\partial \ln \rho} \right)_P \quad (6.38)$$

where u is the speed of sound and ρ is the density. Using the relation $u = (B_s/\rho)^{1/2}$, Warfield and Hartmann[21] derived the following alternate expression for n_R .

$$n_R = \frac{1}{2} \left[\left(\frac{1}{\alpha B_s} \frac{\partial B_s}{\partial T} \right)_P - 1 \right] \quad (6.39)$$

In the above, B_s is the bulk modulus of the sample. This result is interesting because, in the same paper in which Warfield and Hartmann found equation 6.39, Warfield and Hartmann measured the bulk modulus of PEO above and below its melting point. This allowed them to calculate the Rao acoustical parameter for PEO above and below its melting point. Below the melting temperature of PEO, the value for the Rao acoustical parameter was found to be $n_R(\text{solid}) = 23$. Above the melting

temperature of PEO, the value of the Rao acoustical parameter was found to be $n_R(\text{melt}) = 2.2$.

With the above values of the Rao acoustical parameter and the relation $T_e = 1/\alpha n_R$, T_e can be calculated for PEO. The thermal expansion coefficients for PEO are $\alpha(\text{solid}) = 3.3\text{E-}4/\text{K}$ and $\alpha(\text{melt}) = 14\text{E-}4/\text{K}$. Inserting the values for α and n_R into $1/\alpha n_R$, one finds $T_e(\text{solid}) = 132 \text{ K}$ and $T_e(\text{melt}) = 324 \text{ K}$.

Recall now how ions are transported in PEO. Ion transport does not occur in the crystalline/solid regions of PEO. Ion transport occurs in the amorphous regions of PEO. This amorphous region should have properties similar to the melt. Therefore, $T_e(\text{melt}) = 324 \text{ K}$ might have some relevance to ion transport. Equation 5.7 includes a parameter $T_e(\text{cond})$ relevant to conductivity. Equation 5.7 was used to fit the amorphous polymer electrolyte PEO LiTFSI 10-1. This fitting gave the result $T_e(\text{cond}) = 312 \text{ K}$. It is seen that $T_e(\text{cond}) = 312 \text{ K}$, which comes from impedance measurements, compares well with $T_e(\text{melt}) = 324 \text{ K}$, which comes from mechanical measurements.

It is remarkable that an electrical measurement should compare well with a mechanical measurement. Why should this be so? The mechanically measured T_e is based on the measurement of the Rao acoustical parameter. The Rao acoustical parameters in turn depends on the speed of sound in the sample. The speed of sound in turn depends on the characteristic vibrations of the sample. If these characteristic vibrations served as the source of the excitations discussed in the previous section, then a connection is made between $T_e(\text{cond})$ and $T_e(\text{melt})$. If $T_e(\text{cond})$ and $T_e(\text{melt})$ do arise from the same source then a similar value would not be unexpected. The fact

that polymer electrolytes have similar times scales for conductivity and mechanical relaxation is also more readily understood if there is a similar set of excitations.

6.4 Summary

A number of theoretical treatments of the compensation effect were presented. Many of these treatments relied on the idea of absorbing energy from the heat bath. The compensation parameter T_e can then be related to some characteristic excitation of the heat bath. Other treatments related T_e to a melting or disordering temperature. A localized disordering would allow a trapped particle to move in a liquid like environment. It was argued that the localized disordering picture might not be inconsistent with the excitation picture if the excitations are the cause of the melting.

The compensation effect has also been seen in experiments on polymers. One theoretical interpretation of these experiments relates the activation enthalpy and the activation entropy through an activation volume. The proportionality factor between the activation enthalpy and activation entropy is $T_e = 1/n_R\alpha$ where n_R is the Rao acoustical constant and α is the thermal expansion coefficient. Mechanical measurements on melted PEO give $T_e = 324K$. Interestingly this value compares well with the compensation temperature measured by conductivity.

Even though there are theoretical arguments to support it, the compensation effect is still a controversial topic. For example, it is difficult to measure ΔH and ΔS independently. If ΔH and ΔS are not measured independently a false statistical

correlation can result[22]. Sauer has argued against the physical significance of the compensation effect seen in TSDC experiments[23], and Widenhorn et al.[24] have argued that the compensation effect seen CCD currents is due to an improper analysis. While these cautions must be kept in mind, thorough statistical analysis indicates that in many cases the compensation effect is probably real and physically significant[4, 22].

Bibliography

- [1] A. Yelon, B. Movaghar, and H. M. Branz. *Phys. Rev. B*, 46:12244, 1992.
- [2] E. Peacock-Lopez and H. Suhl. *Phys. Rev. B*, 26:3774, 1982.
- [3] W. Linert. *Chemical Physics*, 116:381, 1987.
- [4] W. Linert and R. F. Jameson. *Chem. Soc. Rev.*, 18:477, 1989.
- [5] W. Linert. *Chem. Soc. Rev.*, 23:429, 1994.
- [6] B. J. McCoy and R. G. Carbonell. *J. Chem. Phys.*, 66:4564, 1977.
- [7] B. J. McCoy and R. G. Carbonell. *Chemical Physics*, 20:227, 1977.
- [8] G. J. Dienes. *J. Appl. Phys.*, 21:1189, 1950.
- [9] Y. L. Khait, R. Beserman, D. Shaw, and K. Dettmer. *Phys. Rev. B*, 50:14893, 1994.
- [10] D. P. Almond and A. R. West. *Solid State Ionics*, 23:27, 1987.
- [11] J. Rault. *J. Non-Cryst. Solids*, 235-237:737, 1998.

- [12] A. W. Lawson. *J. Chem. Phys.*, 32:131, 1960.
- [13] G. Teyssedre and C. Lacabanne. *J. Phys. D: Appl. Phys.*, 28:1478, 1995.
- [14] E. Dudognon, A. Bernes, and C. Lacabanne. *Macromol.*, 34:3988, 2001.
- [15] N. M. Alves, J. F. Mano, and J. L. Gomez Ribelles. *Polymer*, 43:3627, 2002.
- [16] R. K. Eby. *J. Chem. Phys.*, 37:2785, 1962.
- [17] J. Crine. *J. Macromol. Sci.-Phys.*, B23:201, 1984.
- [18] A. W. Lawson. *J. Phys. Chem. Solids*, 3:250, 1957.
- [19] R. W. Keyes. *J. Chem. Phys.*, 29:467, 1958.
- [20] Z. Stoeva, C. T. Imrie, and M. D. Ingram. *Phys. Chem. Chem. Phys.*, 5:395, 2003.
- [21] R. W. Warfield and B. Hartmann. *J. Appl. Phys.*, 44:708, 1973.
- [22] L. Liu and Q. Guo. *Chem. Rev.*, 101:673, 2001.
- [23] B. B. Sauer and J. J. Moura Ramos. *Polymer*, 38:4065, 1997.
- [24] R. Widenhorn, A. Rest, and E. Bodegom. *J. Appl. Phys.*, 91:6524, 2002.

Chapter 7

A microscopic picture of polymer electrolyte conductivity

Chapters 4 and 5 argued that the Vogel equation was unable to satisfactorily capture certain empirical aspects of polymer electrolyte conductivity. Equation 7.1 was proposed as an alternative to the Vogel equation.

$$\sigma(T) = \frac{1}{\sigma_{\beta} e^{\frac{E_{\beta}}{kT}} + \sigma_{\alpha} e^{\frac{E_{\alpha}}{kT}}} \quad (7.1)$$

Equation 7.1 is able to reproduce a wider range of polymer electrolyte conductivity phenomenology such as partially crystalline polymer electrolytes as well as amorphous polymer electrolytes. The compensation effect was seen in applying equation 7.1 to a family of amorphous polymer electrolytes. Incorporating the compensation effect into equation 7.1 yields

$$\sigma(T) = \frac{2\sigma_0}{e^{E_{\beta}(\frac{1}{kT} - \frac{1}{kT_e})} + e^{E_{\alpha}(\frac{1}{kT} - \frac{1}{kT_e})}}. \quad (7.2)$$

The compensation effect was discussed in chapter 6, and different theories for the physical meaning of T_e were presented. While theories of the compensation effect are diverse, there are certain common threads. Many of the theories relate T_e to a heat

bath excitations or a local disordering/fluidizing.

In this chapter a microscopic interpretation of equation 7.2 is discussed. Microscopic pictures must be proposed cautiously. For example, in the early days of polymer electrolyte research, conductivity was thought to occur in the crystalline regions. The cations were thought to travel through the center of the polymer crystal helices. This seems to be a reasonable idea when one notices that the crystalline polymer PEO has a greater conductivity than the amorphous polymer PPO. It was later shown that the conductivity takes place primarily in the amorphous regions. It is necessary, however, to give equation 7.2 some plausible physical basis. Therefore, a microscopic picture is proposed but should be considered tentative. While some comment is made in regard to the C2000 based systems, the microscopic picture presented in this chapter applies mainly to PEO based systems.

7.1 Microscopic pictures of ion transport

The introductory chapter on polymer electrolytes emphasized the importance of ion-ion interactions and ion-polymer interactions. Ion-polymer interactions are necessary to dissolve the salt in the first place, and ion-ion interactions are clearly seen in vibrational spectra and in the dependence of conductivity on concentration. It would seem reasonable then that ion-polymer and ion-ion interactions should play a role in the conductivity. Before discussing a model consistent with equation 7.1, a simple hydrodynamic model commonly used to discuss ion transport in liquid electrolytes

and dynamic bond percolation, which is often used as a model of polymer electrolyte ion transport, are briefly presented.

7.1.1 hydrodynamic model

A simple model which is often used to discuss conductivity in liquid electrolytes assumes that the ion can be treated as a macroscopic object in a continuum medium so that Stokes law can be applied. The inadequencies of this model were presented long ago[1], but it remains popular because of its simplicity and because it seems to account adequately for steady state behavior.

The forces on the ion are the electric field and a dissipative force due to the viscosity of the medium. The equation of motion is

$$m \frac{dv}{dt} = qE - 6\pi r_s \eta v \quad (7.3)$$

where m is the ion mass, q is the ion charge, r_s is the ion radius, and η is the viscosity of the medium. In a constant electric field at steady state ($dv/dt = 0$), the mobility of the ion is

$$\mu = \frac{v}{qE} = \frac{1}{6\pi r_s \eta}. \quad (7.4)$$

The conductivity is then simply $\sigma = qn\mu$ where n is the ion density. Equation 7.4 says that the conductivity is inversely proportional to the viscosity of the medium. This result is known as Walden's law and is found to hold to some extent in polymer electrolytes.

Equations 7.3 and 7.4 can account reasonably well for the DC conductivity but

fails to account for the AC conductivity. By inserting $E = E_0 e^{i\omega t}$ and $v = \mathbf{v} e^{i\omega t}$ into equation 7.3, the complex velocity, \mathbf{v} , is found to be

$$\mathbf{v} = \frac{qE_0}{6\pi r_s \eta + im\omega}. \quad (7.5)$$

The real part of the conductivity is

$$\sigma = qn \operatorname{Re}(\mu) = \frac{qn}{6\pi r_s \eta} \frac{1}{1 + \left(\frac{m\omega}{6\pi r_s \eta}\right)^2}. \quad (7.6)$$

Equation 7.6 predicts that the conductivity is roughly constant up to a frequency of approximately $\omega \sim \frac{6\pi r_s \eta}{m}$ after which the conductivity decreases rapidly. This prediction contrasts dramatically to the experimental data shown in chapter 3 in which the conductivity increases with increasing frequency.

7.1.2 Dynamic Bond Percolation

Druger et al.[2, 3, 4, 5] have given a microscopic model based on dynamically renewing environments. Dynamically renewing environments are akin to free volume ideas, but the Druger et al. picture is a much more detailed microscopic picture than free volume. The first model of a dynamically renewing environment was a percolation model in which the bonds between sites were randomly redistributed after a renewal time τ_{ren} . This model was called the dynamic bond percolation(DBP) model. In standard percolation theory, a grid of sites is specified, and a fraction of the bonds between nearest neighbor sites are available for conduction. One of the major goals of standard percolation theory is to determine the minimum fraction of sites that must be available for conduction from one side of the grid to another. This minimum

fraction is called the percolation threshold. In DBP, the fraction of available bonds is well below the percolation threshold. A particle that is moving from site to site will be trapped in a small cluster of sites. However, after a time τ_{ren} the bonds will redistribute and the travelling particle might be able to move to a new cluster of sites. With DBP a particle can diffuse from one side of the grid to another even though the fraction of bonds is below the percolation threshold. There are two characteristic times in dynamic bond percolation. One is the previously mention renewal time τ_{ren} , and the other is the hopping time, τ_{hop} , from site to site along a available bond. If $\tau_{hop} \ll \tau_{ren}$, the diffusion of the particle will be limited by the renewal time. If the renewal time follows the Vogel equation as a function of temperature, then the diffusion of the particle will follow the Vogel equation. The dynamic bond percolation model has been generalized[4], and many important mathematical results have been derived. However, similar to the free volume theories, the dynamic bond percolation theory and its generalizations do not shed light on the role of ion-ion and ion-polymer interactions in conductivity or do so only indirectly[6].

7.1.3 Requirements of a microscopic interpretation based on partially crystalline polymer electrolytes

The reasoning that lead to equation 7.1 is reviewed for possible physical insight. Partially crystalline polymer electrolytes were instrumental to equation 7.1. It was noticed that in partially crystalline PEO LiTF 10-1 there are two peaks in the $-\text{Im } \mathbf{Z}$ vs. $\log f$ plots. These two peaks correspond to two resistors in series. The fact that

the two resistors are in series is significant. It was also argued that at the melting point of the polymer the regions that were formerly crystalline are now available for conduction. In figure 5.4, it is seen that while one of the resistors changes dramatically when the polymer melts the other resistor does not change when the polymer melts. It was argued that the change in the resistor can be accounted for by a change in the prefactor of the resistor. Denote the resistor that changes on melting as the α -resistor or α -process, and denote the resistor that does not change on melting as the β -resistor or β -process. It is obvious the the β -process cannot be a free volume/Vogel-like process. The conductivity associated with a free volume type process would change when the polymer melted. The β -process does not change. The fact that the β -process does not change when the polymer melts suggests that it is localized and associated with short range movement. The α -process changes upon melting so it is possible that it could be related to free volume. The α -process, however, appears Arrhenius like over the temperature range of this study. To summarize, some requirements for a microscopic interpretation of equations 7.1 and 7.2 are that there be two processes in series and that one process should not depend heavily on the number of conduction pathways while the other process should depend on the number of pathways. Neither of the two processes appear to be a free volume/Vogel-like processes.

7.1.4 Models of transport in non-polymer electrolyte ionic conductors

There is a distinct lack of microscopic models dealing with polymer electrolyte conductivity. There are a number of models available dealing with ionic conductors such as ionic conducting glasses and ionic conducting crystals. Connections between these models and polymer electrolytes have not been drawn. This is because ionic conduction in glasses/crystals is thought to be completely different from and unrelated to ionic conduction in polymer electrolytes. In the chapter on frequency-dependent conductivity, it was demonstrated that the frequency-dependent conductivity of polymer electrolytes show remarkable similarities to the frequency-dependent conductivity of ionic glasses. The frequency-dependent conductivity contains far more information on the microscopic mechanism of ionic conduction than the DC conductivity. It might therefore be worthwhile to investigate models of ionic transport in glasses and crystals for insights into ionic transport in polymer electrolytes.

A coulomb lattice gas with site energy disorder is a model of a disordered conductor that has been developed by P. Maass, A. Bunde, M. Meyer, W. Dieterich and co-workers[7, 8, 9, 10, 11]. This theory was mentioned briefly when the scaling properties of ionic conductors were discussed. The theory is based mainly on monte carlo computer simulations[12].

Start with a grid of points such as a three dimensional square lattice. Each point of the square lattice is assigned a site energy, ϵ_l , taken from some distribution $f(\epsilon)$.

A natural choice for the distribution $f(\epsilon)$ is a Gaussian distribution with variance σ_ϵ^2 and average zero. Charged particles are placed on some fraction of the sites. A site, l , can be occupied ($n_l = 1$) or unoccupied ($n_l = 0$). The interactions between the charged particles are taken to be coulombic in nature. The energy for a given configuration of charges, $\{n_l\}$, is

$$E = \frac{1}{2} \sum_{l \neq l'} \frac{e^2}{|\mathbf{r}_l - \mathbf{r}_{l'}|} n_l n_{l'} + \sum_l \epsilon_l n_l \quad (7.7)$$

where \mathbf{r}_l is the position of site l . While calculating the energy of a given configuration using equation 7.7 is straightforward in principle, in practice equation 7.7 is too inefficient for numerical calculations. In performing numerical calculations on a computer, periodic boundary conditions are usually used. The use of periodic boundary conditions simplifies the necessary programming and effectively makes the lattice infinite in size. The problem that arises is that the sum over the inverse distance in equation 7.7 converges too slowly. The solution is to use the Ewald summation technique[12] to calculate the coulombic energy contribution.

In order for the coulomb lattice gas with site disorder to model a disordered ionic conductor, there must be some way for the ions to move. Ion movement is accomplished through a Monte Carlo simulation. An ion is chosen at random from the lattice. One of the nearest neighbor sites is chosen around the ion. If the nearest neighbor site is already occupied the hop attempt fails. If the nearest neighbor site is not occupied the hop attempt may succeed or may fail. The criteria for the success or failure of a hop to an empty nearest neighbor position is determined by the Metropolis algorithm. In the Metropolis algorithm, the energy of a configuration is calculated.

An ion is then moved to a nearest neighbor position, and the energy of this new configuration is calculated. If the energy of the new configuration is less than the energy of the old configuration the move is accepted. If the new configuration is higher in energy than the old configuration, the move is accepted with probability $e^{-\Delta E/kT}$ where ΔE is the energy difference between the new and old configurations. The probability for a move to be accepted given that the nearest neighbor site is unoccupied is $\min[1, e^{-\Delta E/kT}]$. Using the Metropolis algorithm ensures that the configurations that are accepted correspond to equilibrium configurations.

Following a period of equilibration, a starting equilibrium configuration is chosen. This starting configuration provides the initial positions of the ions. The system is then evolved using the Metropolis algorithm. As the system evolves from the starting configuration the mean squared distance can be calculated. The mean squared distance is given by

$$\langle r^2(t) \rangle = \frac{1}{N} \sum_i^N |\mathbf{r}_i(t) - \mathbf{r}_i(0)|^2 \quad (7.8)$$

where N is the number of ions, $\mathbf{r}_i(0)$ is the starting positions of the ions, and $\mathbf{r}_i(t)$ is the positions of the ions after time t . Time in a monte carlo simulation corresponds roughly to the number of monte carlo steps, i.e. jump attempts. Once the mean squared distance is found the long time diffusion constant can be found with

$$D = \lim_{t \rightarrow \infty} \frac{\langle r^2(t) \rangle}{6t}. \quad (7.9)$$

Finally with the diffusion constant the DC conductivity can be calculated with the

Nernst-Einstein equation:

$$\sigma_{DC} = \frac{Nq^2D}{kT}. \quad (7.10)$$

The above simulation procedure has been applied to ionic glasses and ionic crystals in order to understand the non-Arrhenius behavior occasionally seen in those systems. For example, Kincs and Martin[13] have shown that the conductivity, of the fast ion conductor $zAgI + (1 - z)[0.525Ag_2S + 0.475(B_2S_3 : SiS_2)]$, demonstrates non-Arrhenius behavior at temperatures close to but below the glass transition temperature. Maass et al.[10] used monte carlo simulations to study the non-Arrhenius behavior. The results are shown in figure 7.1. Figure 7.1(a) shows the simulation results. The different lines in figure 7.1(a) correspond to different values of σ_ϵ . The standard deviation, σ_ϵ , can be thought of as the amount of disorder in the system. A large σ_ϵ corresponds to a large amount of disorder, and a small σ_ϵ corresponds to a small amount of disorder. The open diamonds in figure 7.1(a) corresponds to the largest value of σ_ϵ ; the open triangles correspond to the next largest and so on. The filled squares corresponds to $\sigma_\epsilon = 0$. For $\sigma_\epsilon = 0$ all site energies ϵ_l are zero since the average of Gaussian distribution is set to zero. The dotted line that fits the filled squares corresponds to a temperature dependent diffusion constant in which only ion-ion interactions are operating. For $\sigma_\epsilon \neq 0$, the conductivity is less than the $\sigma_\epsilon = 0$ case. This is because the introduction of disorder introduces an activation energy higher than the activation energy associated with the ion-ion interactions. There are therefore two activation energies. A low temperature activation energy is associated with disorder, and a high temperature activation energy is associated with ion-ion

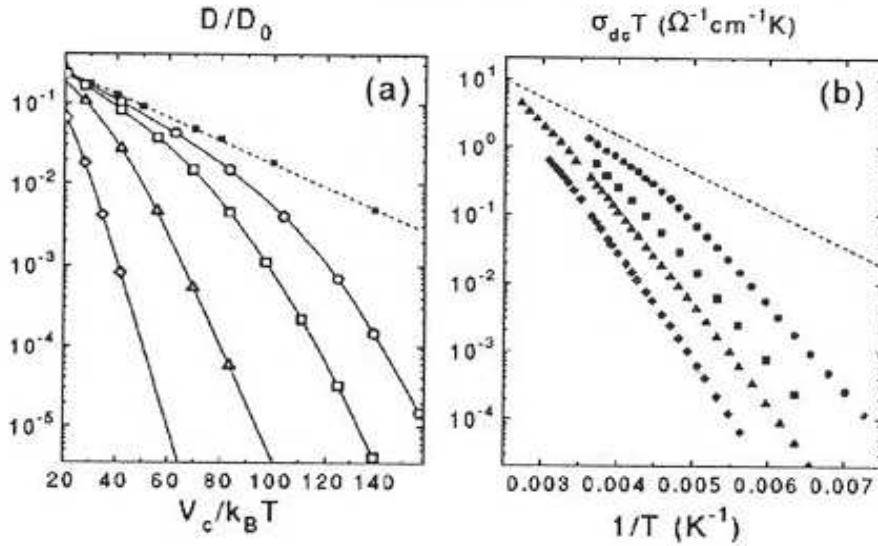


Figure 7.1: (a) Monte Carlo simulation of system with site disorder and ion-ion interactions. (b) Experimental data on ionic glass conductors showing non-Arrhenius conductivity. Figure taken from reference [10]

interactions. As can be seen in figure 7.1(a) the higher the disorder the larger the low temperature activation energy. As the temperature becomes higher and higher in the disordered systems, the conductivity bends over and appears to reach a saturation limit given by the ion-ion interactions. The ion-ion interactions set an upper bound for the conductivity. Figure 7.1(b) shows the experimental data of Kins and Martin. It is seen that at the higher temperatures the conductivities do appear to bend over as they near the dotted line. The dotted line is the estimated upper bound due to ion-ion interactions. To summarize, site disorder can lead to a high activation energy, but as the temperature increases ion-ion interactions can limit the conductivity resulting in non-Arrhenius behavior.

The Coulomb gas model was also used to understand the frequency-dependent dispersion properties of the conductivity and diffusion constant. It was shown that both Coulomb interactions without disorder in the site energies and site energy disorder without Coulomb interactions can produce mild dispersion in the conductivity. However, the presence of both site disorder and Coulomb interactions are necessary to produce the strong dispersion seen experimentally[7].

Another model that takes into account ion-ion interactions is the Jump Relaxation Model due to K. Funke[14]. This model is briefly described. Consider an ion along with its neighboring ions. This ion is at a potential minimum with respect to its neighboring ions. Along with being in a potential minimum with respect to the other ions, the ion is also in a potential minimum of the lattice. When the ion hops to a new potential of the lattice, the ion is no longer in a potential minimum with respect to the neighboring ions. This situation can be resolved in one of two ways: (1) the ions can hop back to its previous position or (2) the neighboring ions can move to accommodate the new position of the ion. The first case is more likely but is undesirable since if all ions hopped back to their old location after making a hop to a new location there could be no long range ion movement, i.e. no DC conductivity. The second case is less likely but allows for DC conductivity. The Jump Relaxation Model introduces a function $g(t)$ to describe the ionic environment around the hopping ion. If $g(t)$ decays significantly before the ion hops back to its previous location, the new location is now the new potential minimum with respect to the neighboring ions, and the hop is considered successful. Another function, $W(t)$, related to $g(t)$ is introduced to

described the decay of the velocity autocorrelation function. The Jump Relaxation Model has been used successfully to model the frequency-dependent conductivity properties of ionic glasses and crystals[14]. These frequency-dependent properties are also seen in polymer electrolytes.

The two models discussed above both emphasize the importance of ion-ion interactions in ionic glasses and crystals. This suggests that ion-ion interactions might also be important in ionically conducting polymer electrolytes.

7.1.5 Polymer electrolytes

A microscopic interpretation of equation 7.2 is now offered. This entails a physical mechanism that would lead to two resistors in series. The presence of the compensation effect in equation 7.2 is also elucidated.

The β and α resistors

The requirements for the β -resistor and the α -resistor were previously laid out. One requirement was that the α -resistor and the β -resistor be in series. The previous section discussed the importance of site energies and ion-ion interactions. Consider an ion that is hopping in the presence of ion-ion interactions only. This situation can be modeled by a resistor with a Arrhenius temperature dependence. Consider now an ion that is hopping in the presence of site energies only. Again this situation can be modeled with a resistor with a Arrhenius temperature dependence. How would an ion hopping in the presence of both site energies and ion-ion interactions be modeled?

Long range movement of the ion would entail overcoming the resistance of both the ion-ion interactions and the site energy. Since both resistances must be overcome, this would seem to entail two resistors in series as the appropriate model. Ion-ion interactions and site energy might provide a physical basis for the two resistors in series.

Another requirement besides that the resistors be in series is that the α -resistor changes as the polymer crystalline regions melt and more pathways become available. The β -resistor does not change as the polymer melts. Consider an ion hopping among the different sites and imagine what would happen if a large fraction of those sites were removed. The prefactor for the resistor modelling this situation depends on the number of nearest neighbor sites around the ion. If a large fraction of sites are removed the resistance will increase. If the removed sites suddenly reappear, the resistance will decrease because there are now more nearest neighbor sites. This decrease in resistance as the sites reappear is similar to the change in the α -resistor as the polymer melts. The situation in regards to the ion-ion interactions is a bit more complicated. It might be imagined that as the polymer melts that ions rearrange themselves so that there is a large change in the β -resistor. On the other hand if the ion-ion effects are mainly due to local interactions of the ions, the melting of the polymer might not have a large effect on the β -resistor.

Site energy and ion-ion interactions appear to satisfy the two criteria mentioned above for the physical processes associated with the β and α resistors.

What is a “site”?

The use of the term site energy with regard to polymer electrolytes might be a little deceptive. When using the word “site”, a lattice of fixed sites might be mentally pictured. This would be a mistake for polymer electrolytes. The polymer is not fixed but is undergoing various complicated motions. As the polymer moves, the “sites” disappear, reform, or otherwise change. The sites are not fixed. A slightly more general notion of site energy must be used for discussing polymer electrolytes.

Figure 7.2 shows a cartoon of a polymer electrolyte. The beads making up the polymer are not necessarily atoms but could represent monomeric units. The cartoon shows three beads coordinated to a lithium cation. The way to think of the site energy is not just the energy well due to the cation coordination to the polymer but instead consider the energy associated with the structure in the dotted box. This structure includes the lithium and the polymer localized around the lithium. The site energy depends on these local structures (LS) present in the polymer electrolyte. Different LS will have different energies. In order for cation transport to take place this LS must be disordered or fluidized. This involves disordering the polymer backbone around the cation and breaking one or more coordinative bonds. The language, disordering and fluidizing, is used in analogy with the language used in the chapter on the compensation effect. Figure 7.3 shows a LS in an energy well and a transition state at the top of the well that features a disordered polymer backbone and fewer coordinative bonds. The transition state shown in figure 7.3 shows one coordinative bond. The figure is of course a cartoon and does not reflect the actual number of

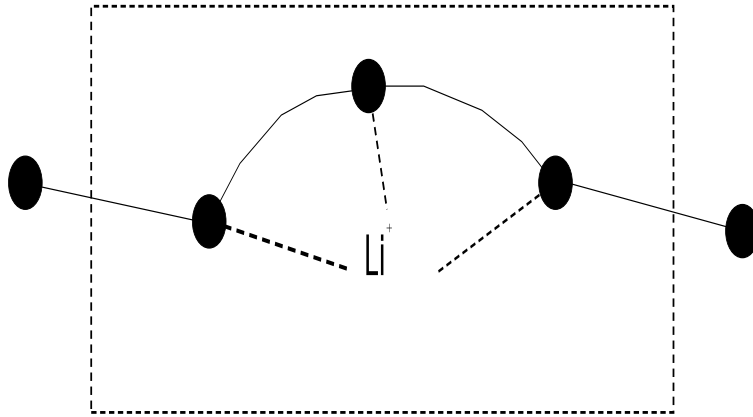


Figure 7.2: Cartoon showing a local structure present in a polymer electrolyte

coordinative bonds associated with a transition state.

From table 5.1 the activation energy for the PEO LiTFSI 10-1 α -resistor was 12803 K or 1.1 eV. This suggests that the energy difference between the LS and the transition state is around 1.1 eV. The energy difference between a LS and a transition state can be estimated with ab initio calculations. These calculations have been performed by Johansson [15]. Johansson calculated the energy difference between a state where a lithium ion was coordinated to three ether oxygens and a state where one of the dihedral angles was rotated so that the lithium was coordinated to two ether oxygens. The energy difference was found to be 1 eV. While the calculations agree well with PEO LiTFSI 10-1, from table 5.2 the C2000 LiTFSI 10-1 α -resistor activation energy is 18756 K or 1.62 eV. This perhaps indicates a more complicated LS and a more complicated transition state than the PEO LiTFSI 10-1.

In polymer electrolytes a site is not a fixed position where the cation can hop into or out of. Instead a small region surrounding the cation must be considered. The

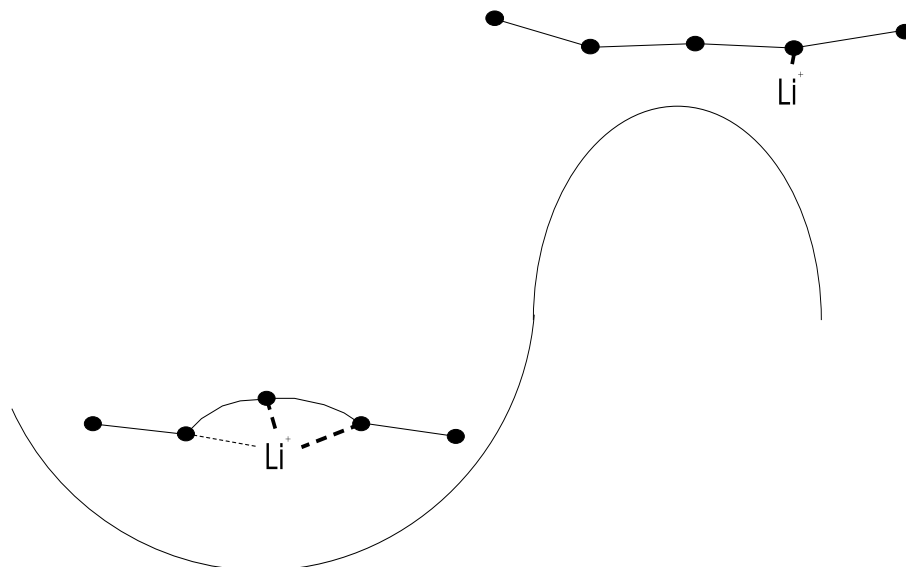


Figure 7.3: Cartoon showing a local structure in a well and a disordered structure that has escaped from the well.

energy of this local structure gives the site energy. The transition state of this site is a disordering or fluidizing of this local structure.

Ion-ion interactions

In going from the local structure to the disordered transition state one or more coordinative bonds are broken. This results in a change in enthalpy (ΔH). Also in going from the local structure to the disordered/fluidized transition state there is change in entropy (ΔS). It seems intuitively plausible that large ΔH 's would lead to large ΔS 's and small ΔH 's would lead to small ΔS 's. Theories leading to a linear relation between ΔH and ΔS were discussed in the previous chapter on the compensation effect. As the temperature is increased, the entropy penalty for forming a LS increases. This means that as the temperature is increased the time it takes for a local region

to fluidize decreases. Since local regions are fluidizing rapidly, it seems plausible that the disordering step will no longer be the limiting factor of the conductivity. It is proposed that the limiting factor at high temperatures is the ion-ion interactions.

The importance of ion-ion interactions can not be doubted. As discussed in the introduction, pairs and larger aggregates are seen in the vibrational spectra of polymer electrolytes. Even when free ions are seen, local charge neutrality requires the opposite ion to be nearby. Ratner and Nitzan have emphasized the importance of ion-ion interactions in polymer electrolytes and have referred to polymer electrolytes at high salt concentrations as “Coulomb fluids” [16]. Molecular dynamics and Monte Carlo simulations have also demonstrated the significance of ion-ion interactions [17, 18].

It is difficult to estimate the magnitude of the ion-ion interaction effects, so it is hard to say what a reasonable value for activation energy due to ion-ion interaction might be. If the β -resistor is indeed related to ion-ion interactions, from table 5.1 the barriers due to ion-ion interactions in PEO LiTFSI 10-1 are around .36 eV.

Ion-ion interactions are proposed as the physical basis of the β -resistors for three reasons: (1) ion-ion interactions provide a mechanism in which the β -resistor would not necessarily change dramatically on melting of the polymer, (2) computer simulations incorporating ion-ion interactions show conductivity plots similar to those expected from equation 7.1, and (3) experiments have demonstrated the importance of ion-ion interactions in polymer electrolytes. While it would be desirable to have estimates for the dissociation of pairs into free ions and the dissociation of aggregates into smaller pieces, it would be surprising if these processes did not have significant

impact on the conductivity.

C2000 based polymer electrolytes

So far it has been implied that the ion-ion interaction contribution to the total resistance and the ion-polymer contribution to the total resistance can be cleanly separated into the β -resistor and the α -resistor. This may be the case for PEO based systems, but the C2000/PPO based systems might be more complicated. For example, one of the reasons for assigning the β -resistor to ion-ion interactions is that the β -resistor is continuous when semi-crystalline PEO melts. Since C2000/PPO based systems are amorphous, it is not known whether the β -resistor would be continuous or discontinuous.

In the C2000 LiTFSI 10-1 E_β is around .78 eV. From table 5.2, the E_β 's at all concentrations are larger in C2000 LiTFSI than in PEO LiTFSI 10-1. This can be understood to some extent by the fact that C2000/PPO is a poorer solvent than PEO. Since C2000 is a poorer solvent higher salt aggregation is expected, and higher salt aggregation would lead to greater ion-ion interactions and therefore larger values of E_β . Another possibility is that ion-ion interactions and ion-polymer interactions both contribute to the β -resistor and the α -resistor. There also might be a more complicated distribution of local structures and transition states which would cause more complicated behavior. The effect of a broad distribution of local structures will be considered in the next chapter.

7.1.6 The microscopic basis of the compensation effect

Theories on the compensation effect were discussed in the previous chapter. Many of the theories made use of the idea of collecting excitations from the heat bath in order to overcome large energy barriers. In particular Linert correlated experimentally measured values of $T_{iso}(T_e)$ with peaks seen in the IR spectra of the systems investigated (see figure 6.1). In this section the far IR spectra of polymer electrolytes are investigated to see if vibrational peaks in the far IR can be correlated with the values of T_e found from fitting the conductivity.

The values of T_e have been reported in units of Kelvin. Vibrational spectra are usually expressed in inverse centimeters. The conversion between Kelvin and wavenumbers is

$$wavenumber(cm^{-1}) = \frac{k_B T_e}{100hc} \quad (7.11)$$

where k_B is Boltzmann's constant, h is Planck's constant, and c is the speed of light. The value of T_e found for PEO LiTFSI 10-1 is 312 K which gives a wavenumber value of about 217 cm^{-1} . The of T_e found for C2000 LiTFSI is 296 K which gives a wavenumber value of about 206 cm^{-1} .

Figure 7.4 shows the far IR spectra of PEO at room temperature. As shown in the figure there is a peak in the far IR spectra of PEO that agrees well with the T_e found for PEO LiTFSI 10-1. Recall that PEO is largely crystalline below its melting temperature. The structure of crystalline PEO is known (see figure 1.3) so it is therefore possible to calculate the normal vibrations of crystalline PEO. These

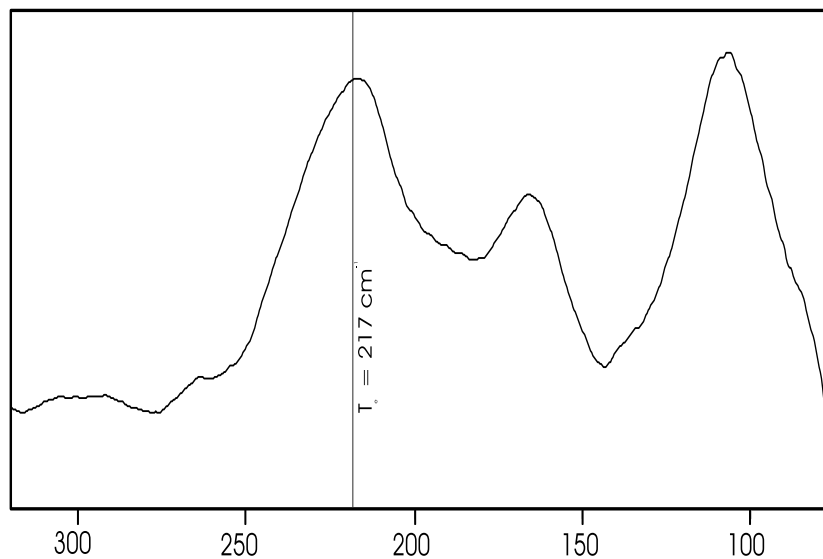


Figure 7.4: Far IR of semicrystalline PEO

calculations were performed by Yoshihara et al.[19]. The vibrational peak at 217 cm^{-1} has been assigned by Yoshihara et al. to a doubly degenerate E_1 mode. The mode is made up a complex mixture of polymer backbone bending vibrations and torsions. This vibration can be imagined as opening the polymer helix which is encircling the cation. This opening of the helix would provide the disordering necessary to allow the cation to move.

Whereas PEO is largely crsyttalline at room temperature, PEO LiTFSI 10-1 and C2000 LiTFSI are amorphous. Being amorphous, there are now a large range of conformations possible along the polymer backbone. This leads to much broader peaks. Figure 7.5 shows PEO LiTFSI 10-1, C2000 LiTFSI 10-1, and C2000 LiTF 10-1. The C2000 LiTFSI 10-1 and the PEO LiTFSI 10-1 are almost identical in the region shown. There are two prominent peaks seen in the C2000 LiTFSI 10-1 and

PEO LiTFSI 10-1 at 224 cm^{-1} , and 206 cm^{-1} . The two peaks are sitting on a broad distribution of polymer backbone modes. This causes the two peaks to be on the slope seen in the C2000 LiTFSI 10-1 and the PEO LiTFSI 10-1. In pure C2000(not shown) only the broad distribution of conformation is present and only the slope without the two peaks at 224 cm^{-1} and 206 cm^{-1} is evident. On addition of the LiTFSI, the lithium cations locally order the polymer backbone which leads to the presence of the two peaks on top of the broad distribution. In crystalline PEO there is a doubly degenerate peak at 217 cm^{-1} . If the crystalline structure of PEO is perturbed, this doubly degenerate peak will split into two peaks. One of the peaks will be at a higher frequency than the 217 cm^{-1} peak and the other peak will be a lower frequency than the 217 cm^{-1} peak. This seems to fit what is seen in figure 7.5. The cations will locally order the polymer backbone, but the locally ordered conformations are not exactly the same as in crystalline PEO. This therefore leads to the two peaks. The values of T_e found from the fits to the conductivity are also shown in figure 7.5. In PEO LiTFSI 10-1, the value of T_e is 217 cm^{-1} . As seen in figure 7.4, this is the location of the unsplit crystalline PEO peak. For C2000 LiTFSI 10-1, T_e is 206 cm^{-1} . This is the location of low frequency split peak. Also shown in figure 7.5 is C2000 LiTF 10-1. The splitting in C2000 LiTF 10-1 is not as great as with LiTFSI. Unlike in C2000 LiTFSI, the value of T_e (221 cm^{-1}) for C2000 LiTF 10-1 appears to correspond to the high frequency peak rather than the low frequency peak.

As to why the different values of T_e correlate to different peaks and not the same peak is not known. What is significant, however, is, that the peaks the T_e 's do

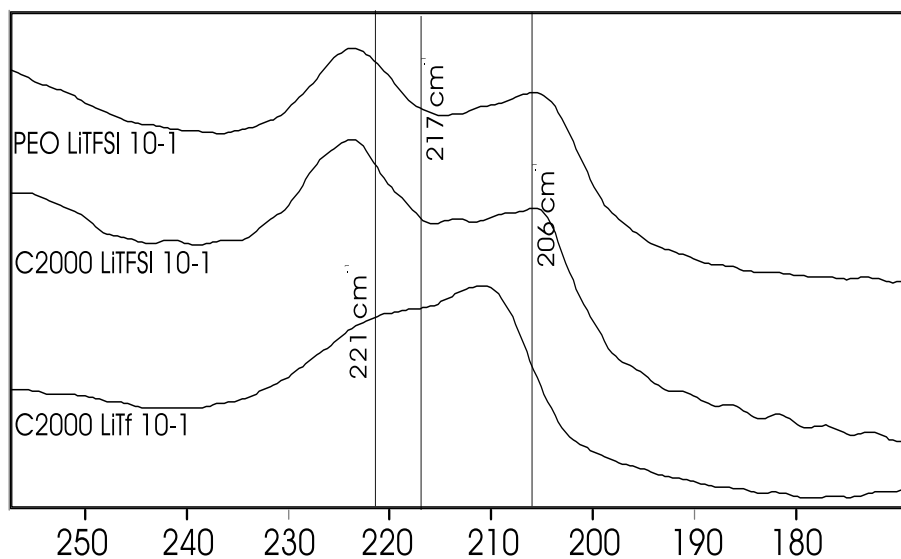


Figure 7.5: Far IR of polymer electrolytes showing correlation with the values of T_e obtained from curve fitting.

correlate with, correspond to vibrations that disorder the polymer backbone. These results correspond nicely with the theories of the compensation effect which ascribe T_e to some excitation of the system.

7.2 Summary

This chapter proposes a possible microscopic interpretation for the α and β resistors. Models of solid ionic conductors, in which site energies and ion-ion interactions play a role, were discussed. Site energies and ion-ion interactions would be modeled by two resistors in series and so provide a possible physical basis for the α and β resistors. For PEO systems, the β resistor was assigned to ion-ion interactions, and the α resistor was assigned to site energies for reasons discussed in the chapter. It was

argued that a “site” in polymer electrolytes was not the position of the lithium cation. Instead a “site” includes not only the lithium cation but the lithium cation and the surrounding polymer that is coordinating the cation. To hop out of the “site” entails both breaking coordinative bonds and disordering the polymer backbone. As the temperature is increased, any locally ordered site is quickly disordered due to entropy. The site energies no longer limit the conductivity. Ion-ion interactions become the limiting factor for conductivity. The situation for PPO/C2000 systems might be more complicated so that a clean separation into ion-ion interactions and ion-polymer interactions might not apply. Finally, peaks are seen in far IR spectra that do correlate with values of T_e found from the conductivity.

Bibliography

- [1] M. J. Polissar. *J. Chem. Phys.*, 6:833, 1938.
- [2] S. D. Druger, A. Nitzan, and M. A. Ratner. *J. Chem. Phys.*, 79:3133, 1983.
- [3] S. D. Druger, M. A. Ratner, and A. Nitzan. *Phys. Rev. B*, 31:3939, 1985.
- [4] S. D. Druger and M. A. Ratner. *Phys. Rev. B*, 38:12589, 1988.
- [5] A. Nitzan and M. A. Ratner. *J. Phys. Chem.*, 98:1765, 1994.
- [6] M. Lonergan, M. A. Ratner, and D. F. Shriver. *Electrochim. Acta*, 40:2041, 1995.
- [7] P. Maass, J. Petersen, A. Bunde, W. Dieterich, and H. E. Roman. *Phys. Rev. Lett.*, 66:52, 1991.
- [8] J. Petersen and W. Dieterich. *Phil. Mag. B*, 65:231, 1992.
- [9] P. Maass, M. Meyer, and A. Bunde. *Phys. Rev. B*, 51:8164, 1995.
- [10] P. Maass, M. Meyer, A. Bunde, and W. Dieterich. *Phys. Rev. Lett.*, 77:1528, 1996.
- [11] M. Meyer, P. Maass, and A. Bunde. *J. Chem. Phys.*, 109:2316, 1998.

- [12] Daan Frenkel and Berend Smit. *Understanding Molecular Simulation*. Academic Press, New York, 2001.
- [13] J. Kincs and S. W. Martin. *Phys. Rev. Lett.*, 76:70, 1996.
- [14] K. Funke. *Prog. Solid State Chem.*, 22:111, 1993.
- [15] P. Johansson. *Polymer*, 42:4367, 2001.
- [16] M. Ratner and A. Nitzan. *Faraday Discuss. Chem. Soc.*, 88:19, 1989.
- [17] V. Payne, M. Lonergan, M. Forsyth, M. Ratner, D. Shriver, S. de Leeuw, and J. Perram. *Solid State Ionics*, 81:171, 1995.
- [18] M. Lonergan, J. Perram, M. Ratner, and D. F. Shriver. *J. Chem. Phys.*, 98:4937, 1993.
- [19] T. Yoshihara, H. Tadokoro, and S. Murahashi. *J. Chem. Phys.*, 41:2902, 1964.

Chapter 8

Generalization and glass phenomenology

One of the main results of the study of glass forming substances is that the Vogel equation is often found to apply over some temperature range. Previous chapters argued that for polymer electrolytes the two Arrhenius equation provides better insight into the ionic transport mechanism. Can the two Arrhenius equation be applied to other systems showing Vogel-like behavior? In general the answer is no. The Vogel equation continually curves as the temperature is lowered on an Arrhenius plot. The two Arrhenius equation will eventually become linear on an Arrhenius plot as the temperature is lowered. The two Arrhenius equation might show curving behavior over 3-4 orders of magnitude whereas experimental data for the viscosity of glass forming substances might show curving behavior over 10-12 orders of magnitude. The two Arrhenius equation can not fit data that curves over 10-12 orders of magnitude, so the Vogel equation does a much better job of fitting such data.

In this chapter it will be shown that the Vogel equation can be understood within a distribution of activation energies picture. The reasons for doing so are as fol-

lows: It was seen that a distribution of hopping barriers can be used to understand the frequency-dependent conductivity of polymer electrolytes. If the hopping models reflect the actual physics of the frequency-dependent conductivity then the non-Arrhenius DC conductivity should also be understood in terms of a distribution of hopping barriers. Also, a distribution of hopping barriers is the logical extension to the two Arrhenius equation. If the two Arrhenius equation accurately represents the physics over a limited temperature range, then a distribution of barriers might reflect the physics over a larger temperature range.

8.1 Generalization to a Distribution of Activation Energies

The two Arrhenius equation with the compensation effect is repeated below:

$$x(T) = \frac{2x_0}{e^{E_\beta(\frac{1}{kT} - \frac{1}{kT_e})} + e^{E_\alpha(\frac{1}{kT} - \frac{1}{kT_e})}}. \quad (8.1)$$

The form of equation 8.1 suggests the following generalization:

$$x(T) = \frac{x_0}{\int_0^\infty e^{E(\frac{1}{T} - \frac{1}{T_e})} g(E) dE}. \quad (8.2)$$

Equation 8.2 has written equation 8.1 in terms of an arbitrary distribution of activation energies(DAE)(from now on Boltzmann's constant will be incorporated into E so that energies will be in Kelvin). The distribution of activation energies is given by $g(E)$. The distribution $g(E)$ is taken to be normalized. In order to recover equation

8.1 from equation 8.2, the distribution would obviously be

$$g(E) = \frac{1}{2}\delta(E - E_\alpha) + \frac{1}{2}\delta(E - E_\beta). \quad (8.3)$$

As a further simple example, consider a uniform distribution.

$$g(E) = \begin{cases} 1/(E_1 - E_2) & E_1 \leq E \leq E_2 \\ 0 & \text{otherwise} \end{cases}$$

Inserting the uniform distribution into equation 8.2 gives

$$x(T) = x_0(E_2 - E_1) \frac{\frac{1}{T} - \frac{1}{T_e}}{e^{E_2(\frac{1}{T} - \frac{1}{T_e})} - e^{E_1(\frac{1}{T} - \frac{1}{T_e})}}. \quad (8.4)$$

Equations similar to equation 8.2 have been used to understand the conductivity of glass ionic conductors [1, 2] and the phenomenological properties of glass-forming substances(see below).

The question now becomes what is the relation between a DAE and the Vogel equation. In particular, is there a $g(E)$ that gives the Vogel equation, i.e. does the following equation hold?

$$\frac{1}{x_0} \int_0^\infty e^{E(\beta - \beta_e)} g(E) dE = \frac{1}{A} e^{\frac{B}{T - T_0}} \quad (8.5)$$

Before giving a definite yes or no answer to the above equation, assuming $g(E)$ does exist, relations can be established between the parameters of the Vogel equation and $g(E)$. The distribution that gives the Vogel equation will be denoted by $g_V(E)$. Requiring that $g_V(E)$ be normalized and setting $\beta(= 1/T) = \beta_e(= 1/T_e)$ gives $x_0/A = e^{-B/T_e - T_0}$. Equation 8.5 becomes

$$\int_0^\infty e^{E(\beta - \beta_e)} g_V(E) dE = e^{\frac{B}{T - T_0} - \frac{B}{T_e - T_0}}. \quad (8.6)$$

The moments of the distribution $g_V(E)$ can be calculated with

$$\langle E^n \rangle = \int_0^\infty E^n g_V(E) dE = \frac{d^n}{d\beta^n} \int_0^\infty e^{E(\beta-\beta_e)} g_V(E) dE \Big|_{\beta=\beta_e} = \frac{d^n}{d\beta^n} e^{\frac{B}{T-T_0} - \frac{B}{T_e-T_0}} \Big|_{\beta=\beta_e}. \quad (8.7)$$

All the moments of the distribution can be found in this way. The requirement that $\langle E^n \rangle \geq 0$ means that all derivatives of the Vogel equation must be non-negative. This is indeed the case for $T > T_0$ ($\beta T_0 < 1$) as can be seen by writing the exponent of the Vogel equation as

$$\frac{B}{T-T_0} = \frac{\beta B}{1-\beta T_0} = B\beta(1 + \beta T_0 + (\beta T_0)^2 + \dots). \quad (8.8)$$

The first and second moments of the distribution $g_V(E)$ are

$$\langle E \rangle = B \left(\frac{T_e}{T_e - T_0} \right)^2 \quad (8.9)$$

$$\langle E^2 \rangle = \frac{B^2 + 2BT_0(1 - T_0/T_e)}{(1 - T_0/T_e)^4}. \quad (8.10)$$

Solving for B from equation 8.9 and inserting it into equation 8.10, the following equation for T_0 can be derived:

$$\frac{1}{T_0} = \frac{2\langle E \rangle}{\sigma_E^2} + \frac{1}{T_e} \quad (8.11)$$

where $\sigma_E^2 = \langle E^2 \rangle - \langle E \rangle^2$. All three parameters of the Vogel equation, A, B, and T_0 , have been related to x_0 , T_e , and the statistical properties of the distribution $g_V(E)$.

While having the relations between the parameters is nice, the most direct way of proving $g_V(E)$ exists is to actually find it.

Equation 8.6 resembles a Laplace transform. In fact, $g_V(E)$ can be found by a inverse Laplace transform of Vogel equation. The details of this procedure are given

in a mathematical appendix at the end of the chapter. Performing the inverse Laplace transform gives

$$g_V(E) = e^{-B/(T_e - T_0)} \sum_{n=0}^{\infty} \frac{1}{n!} \left(\frac{-B}{T_0} \right)^n e^{E(1/T_e - 1/T_0)} \sum_{k=0}^n \binom{n}{k} \frac{1}{(k-1)!} E^{k-1} \left(\frac{-1}{T_0} \right)^k. \quad (8.12)$$

where

$$\binom{n}{k} = \frac{n!}{k!(n-k)!}. \quad (8.13)$$

The above equation gives $g_V(E)$ in terms of the Vogel parameters B and T_0 . Using equations 8.9 and 8.11 to write $g_V(E)$ in terms of $\langle E \rangle$ and σ_E^2 gives

$$g_V(E) = e^{\frac{-\langle E \rangle}{T_e} \left(\frac{2\langle E \rangle}{\sigma_E^2} \right) \left(\frac{2\langle E \rangle}{\sigma_E^2} + \frac{1}{T_e} \right)^{-1}} \sum_{n=0}^{\infty} \frac{1}{n!} \left(-\langle E \rangle \left(\frac{2\langle E \rangle}{\sigma_E^2} \right)^2 \left(\frac{2\langle E \rangle}{\sigma_E^2} + \frac{1}{T_e} \right)^{-1} \right)^n \\ \times e^{-E \left(\frac{2\langle E \rangle}{\sigma_E^2} \right)} \sum_{k=0}^n \binom{n}{k} \frac{1}{(k-1)!} E^{k-1} \left(\frac{-2\langle E \rangle}{\sigma_E^2} - \frac{1}{T_e} \right)^k. \quad (8.14)$$

The compensation temperature T_e appears in equation 8.14. It would be hard to justify physically the presence of T_e in the distribution of activation energies. Fortunately, the presence of T_e is just an artifact of the method of derivation of $g_V(E)$. The distribution $g_V(E)$ is independent of T_e . This can be shown by calculating the characteristic function of $g_V(E)$.

The characteristic function of some distribution $g(E)$ is defined as

$$\phi(p) = \int e^{ipE} g(E) dE. \quad (8.15)$$

For $g_V(E)$, $\phi_V(p)$ is (see end of chapter appendix)

$$\phi_V(p) = \exp \left(\langle E \rangle \frac{ip}{1 - \frac{\sigma_E^2}{2\langle E \rangle} ip} \right) \quad (8.16)$$

which is indeed independent of T_e .

Comparing the L.H.S. of equation 8.6 and the R.H.S. of equation 8.15, the two equations are equivalent if the identification $ip \Leftrightarrow 1/T - 1/T_e$ is made. The L.H.S. of equation 8.6 with $g_V(E)$ is by construction equivalent to the Vogel equation. Replacing ip in equation 8.16 by $1/T - 1/T_e$ gives

$$\frac{x(T)}{x_0} = \exp\left(\frac{\langle E \rangle \left(\frac{1}{T} - \frac{1}{T_e}\right)}{1 - \frac{\sigma_E^2}{2\langle E \rangle} \left(\frac{1}{T} - \frac{1}{T_e}\right)}\right). \quad (8.17)$$

Equation 8.17 is an alternate parameterization of the Vogel equation. The new parameterization reflects the fact that the Vogel equation can be arrived at from a distribution of activation energies.

One of the characteristic features of the Vogel equation is the parameter T_0 . When $T = T_0$ the Vogel equation blows up. If on the other hand $T_0 \rightarrow 0$, the Vogel equation becomes equivalent to the Arrhenius equation. How can this behavior be understood in terms of a distribution of activation energies?

How is the singular behavior reflected in the distribution of activation energies?

Equation 8.14 is of the form

$$g_V(E) = e^{-E\left(\frac{2\langle E \rangle}{\sigma_E^2}\right)} f(E) \quad (8.18)$$

where $f(E)$ is a non-normalizable function. If the temperature is such that in equation 8.2 $e^{E(1/T-1/T_e)}$ cancels $e^{-E(2\langle E \rangle/\sigma_E^2)}$, then one is left with the integral from zero to infinity of a non-normalizable function. Therefore the resulting expression diverges like the Vogel equation at $T = T_0$. The temperature at which the DAE diverges is given by equation 8.11. The singular behavior of the Vogel equation can be reproduced

by a DAE with a distribution function consisting of a decaying exponential times a non-normalizeable function. The singularity due to a exponential decay of activation energies has been emphasized by Monthus and Bouchaud [3].

As $T_0 \rightarrow 0$, the Vogel equation becomes equivalent to the Arrhenius equation. How does the DAE approach interpret this behavior? From equation 8.11 as $T_0 \rightarrow 0$, $2\langle E \rangle / \sigma_E^2$ goes to infinity. Since the ratio of the mean to the variance is increasing, the distribution becomes narrower and more strongly peaked. The effect of increasing $2\langle E \rangle / \sigma_E^2$ on the distribution $g_V(E)$ can best be seen with the characteristic function. Equation 8.19 shows a sequence of approximations for the characteristic function of $g_V(E)$ valid as $2\langle E \rangle / \sigma_E^2$ becomes larger and larger.

$$\exp\left(\langle E \rangle \frac{ip}{1 - \frac{\sigma_E^2}{2\langle E \rangle} ip}\right) \rightarrow \exp\left(ip\langle E \rangle - \frac{p^2\sigma_E^2}{2}\right) \rightarrow e^{ip\langle E \rangle} \quad (8.19)$$

The right-most equation is the characteristic function for a delta function and applies for $T_0 = 0$. A delta function in equation 8.2 just yields the Arrhenius equation as expected. The middle equation is more interesting; it is the characteristic function for the Gaussian distribution. Note that the approximation that leads to the characteristic function of the Gaussian is $\frac{\sigma_E^2}{2\langle E \rangle} ip \ll 1$ which is true if $2\langle E \rangle / \sigma_E^2 \rightarrow \infty$. It is also true if $ip \ll 2\langle E \rangle / \sigma_E^2$. Previously the identification $ip \Leftrightarrow 1/T - 1/T_e$ was made. The Gaussian is a valid approximation to $g_V(E)$ if

$$\frac{1}{T} - \frac{1}{T_e} \ll \frac{2\langle E \rangle}{\sigma_E^2} \Rightarrow T \gg T_0 \quad (8.20)$$

where equation 8.11 has been used. This says that unless one has data near T_0 it would be difficult to distinguish between the Vogel equation and a Gaussian DAE.

Figure 8.1 shows $g_V(E)$ for $\sigma_E^2 = 8.64E6$ and for various values of $\langle E \rangle$. The largest $\langle E \rangle / \sigma_E^2$ ratio is for $\langle E \rangle = 12200$ K. According to the discussion of preceding paragraphs a large $\langle E \rangle / \sigma_E^2$ ratio should lead to a distribution that approximates the Gaussian distribution. Indeed the plot for $\langle E \rangle = 12200$ K does resemble a Gaussian distribution. The curve for $\langle E \rangle = 12200$ K shows some asymmetric non-Gaussian behavior at large values of E. This is expected. In order for there to be singular behavior at $T_0 \neq 0$, the distribution must eventually decay as a exponential. A Gaussian decays much faster than an exponential, so there must be non-Gaussian behavior at high energies. This non-Gaussian behavior at high energies is more evident in the $\langle E \rangle = 7200$ K plot. While the $\langle E \rangle = 7200$ K plot still in some ways resembles a Gaussian, the exponential-like decay leads to a strong asymmetry in the distribution. As $\langle E \rangle$ continues to decrease the distribution ceases to resemble a Gaussian in any way. In fact, the curve for $\langle E \rangle = 2200$ K resembles a decaying exponential.

It is remarkable that $g_V(E)$ displays both decaying exponential behavior or Gaussian behavior depending on the mean and variance of the distribution. The fact that the decaying exponentials and Gaussians are physically plausible distributions gives support to the contention that the Vogel equation is related to a distribution of activation energies. It would be desirable, however, to have a microscopic model that lead to $g_V(E)$ instead of deducing $g_V(E)$ from the empirical Vogel equation. This, unfortunately, must be left as future work.

Various $g_V(E)$ plots were shown in figure 8.1. As formulated in this chapter, $g_V(E)$ does not depend on temperature. The temperature dependence of $x(T)$ in

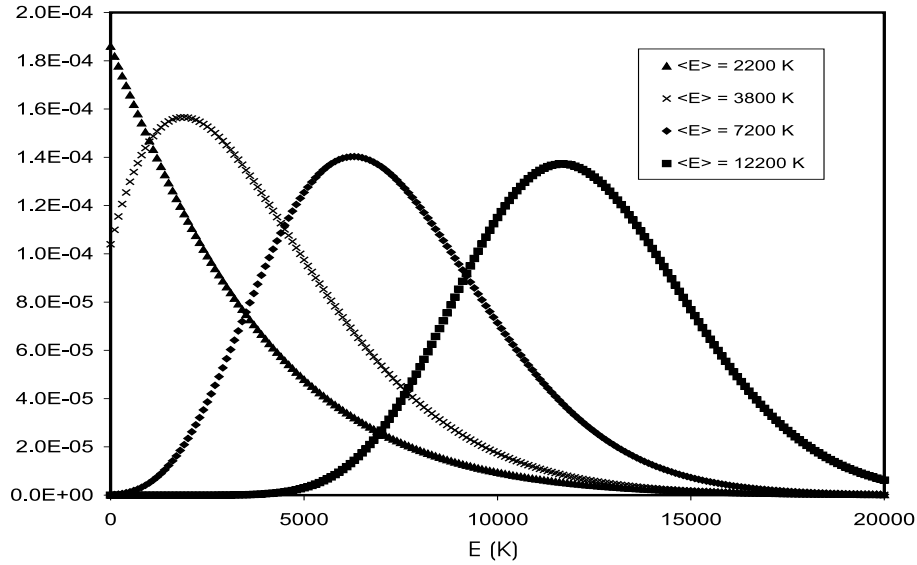


Figure 8.1: Plot of $g_V(E)$ for $\sigma_E^2 = 8.64E6$ and different values of $\langle E \rangle$.

equation 8.2 comes about from the term $e^{E(1/T-1/T_e)}$ in the integral. How exactly $e^{E(1/T-1/T_e)}$ causes the temperature dependence of $x(T)$ is illustrated in figure 8.2. Figure 8.2 shows $e^{E(1/T-1/T_e)}$ for three different values of T . Also shown in the figure is the $\langle E \rangle = 7200\text{ K}$ distribution from figure 8.1 (the distribution has been scaled so that it can be seen on the same plot as the exponentials). For $T < T_e$, $e^{E(1/T-1/T_e)}$ increases exponentially with E . For $T > T_e$, $e^{E(1/T-1/T_e)}$ decreases exponentially with increasing E . For $T = T_e$, $e^{E(1/T-1/T_e)}$ is equal to one. For $T < T_e$, $e^{E(1/T-1/T_e)}$ is increasing exponentially, and large values of the activation energy will be emphasized. As T continues to decrease larger and larger values of the activation energy will be emphasized. $x(T)$ will curve as the temperature is lowered since large values of the activation energy contribute more. For $T = T_e$, all values of the distribution contribute equally to $x(T)$. For $T > T_e$, $e^{E(1/T-1/T_e)}$ is decreasing exponentially, and

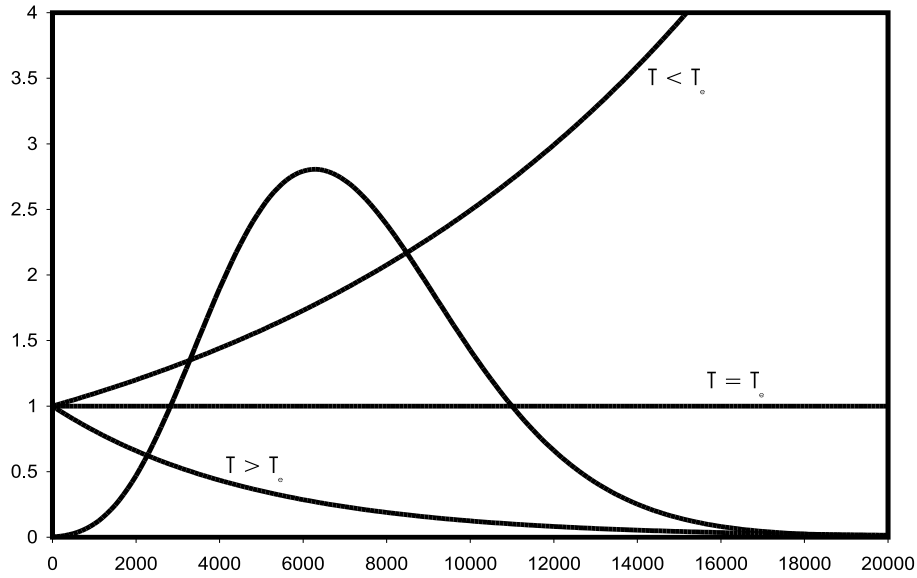


Figure 8.2: $e^{E(1/T-1/T_g)}$ plotted for different values of T . Also shown is a $g_V(E)$ from figure 8.1.

smaller values from the distribution of activation energies will be emphasized. Different temperatures emphasize different parts of the distribution. Low temperatures emphasize high activation energies, and high temperatures emphasize low activation energies. This results in non-Arrhenius behavior observed in plots of $\log x(T)$ vs. $1/T$.

8.2 Some theories of glass phenomenology

The chief experimental results involving glasses are (1) the dramatic non-Arrhenius increases in viscosity as the the glass transition temperature is approached and (2) the non-exponential decay of relaxation processes above but close to the glass transition temperature. An example of an experiment in which a relaxation process in observed might involve a rapid drop in temperature of say 1 K and then subsequently observing

the volume at constant pressure. The non-Arrhenius increases in viscosity are often fit using the Vogel equation. The non-exponential decay of a relaxation process is often fit by the stretched exponential shown below.

$$e^{-(t/\tau)^\phi} \tag{8.21}$$

Theories about glasses should be able to account for these phenomenological aspects. Some review papers on glass phenomenology are references [4, 5, 6, 7, 8].

Previously the theory of free volume was presented in relation to the Vogel equation. Free volume theory does not explicitly involve activated processes. In free volume theories flow or molecular movement depends largely on density. At higher densities there is less free volume available for movement so flow should be reduced. At lower densities more volume is available for movement so flow should be enhanced. Under free volume theories density should be the determining factor for molecular movement. Temperature should play a lesser role in movement. On the other hand if activated processes are responsible for molecular movement then temperature should be the dominant factor and density should have a lesser role. Ferrer et al.[9, 10] investigated the density dependent viscosity and temperature dependent viscosity for various glass-forming liquids. The data presented by them showed a strong dependence on temperature and a weak dependence on density. Ferrer et al. concluded that “it is the temperature and not the density that is the dominant control variable”[9] for their data. Similar statements about the relative importance of density and temperature to the conductivity of polymer electrolytes have also been made[11].

Goldstein [12] also objected to the free volume picture and proposed a picture

of molecular flow based on potential energy barriers. In a potential energy picture, the potential energy landscape is considered. The potential energy landscape can be thought of a $3N+1$ dimensional plot of the potential energy $U(\mathbf{r}_1, \mathbf{r}_2, \dots, \mathbf{r}_N)$. A schematic diagram of the potential energy landscape in one dimension is given in figure 8.3. The potential energy landscape is made up basins of various depths. Some of the basins correspond to amorphous structures whereas some of the basins correspond to crystal structures. The structures corresponding to an amorphous state have been termed inherent structures[13, 8]. One can also speak of local inherent structures to denote the inherent structures of small regions. A supercooled liquid is explained as a system which has not been able to find the basin corresponding to the crystalline structure. A supercooled liquid only explores basins corresponding to amorphous structures. At the glass transition, the system is stuck in basically one basin on the observational timescale; it is therefore a solid.

Equation 8.2 is closer in spirit to the potential energy landscape picture than the Vogel equation with the parameters A , B , T_0 . Various authors[14, 3, 15] have used equations similar to equation 8.2 to understand glass properties in terms of a distribution of energy barriers. The following picture of $g(E)$ is typically used[16, 15]. The distribution $g(E)$ is related to the various local inherent structures that can form. The different local structures have different energy depths. In order to change from one local inherent structure to another local inherent structure, the local inherent structure “hops” to a fluidized state. In this fluidized state the atoms or molecules that make up the localized region rearrange and randomly form a new local inherent

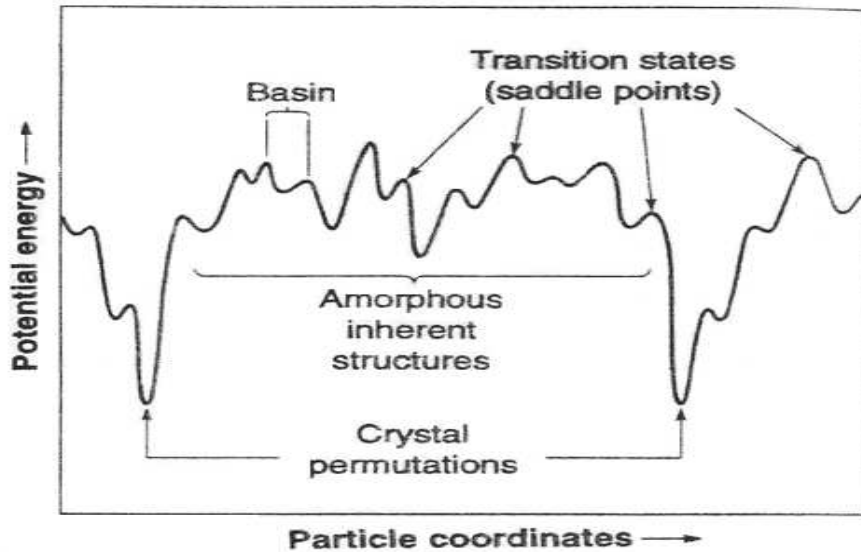


Figure 8.3: Schematic picture of an potential energy landscape. Figure taken from ref. [13]

structure. The probability, that a new local inherent structure with a energy E forms, is given by $g(E)$. The picture therefore is of a small locally ordered region “hopping” to a disordered state and then “falling” back to a different ordered state. This picture is not unlike that used in the previous chapter to describe polymer electrolyte conductivity.

Equation 8.2 assumes that the Arrhenius equation is the proper expression for the transition rate over a energy barrier. If the temperature is low and the barriers are high, the Arrhenius equation is probably appropriate. If on the other hand the temperature is high and the barriers are low, the Arrhenius equation might not be appropriate. The many particle system is represented as a point on the surface of the potential energy landscape. At low temperatures the point can be thought of as oscillating in some potential minimum basin. These oscillations around the minimum

of the basin correspond to the vibrations of the solid. The particle spends most of its time in the minimum of the basin. Occasionally, the point escapes the minimum of the basin, quickly traverses a saddle point, and ends up in a new potential energy basin. This is the situation where equation 8.2 might hold. At high temperatures, the point of the surface may not spend much time oscillating at the bottom of a potential basin. The point will simply pass through the basin over a saddle point and through another basin. The point is moving continuously over the potential energy surface instead of pausing for long periods of time in a potential basin. In this situation, a diffusive description might be more appropriate. Goldstein has given some criteria for the change from a barrier picture to a diffusive picture[12].

The other canonical feature of the glass phenomenology is the stretched exponential seen in relaxations. Formally, the stretched exponential can be written as a distribution of relaxation times[17, 18]:

$$\int_0^{\infty} h(\tau)e^{-t/\tau}d\tau = e^{-(t/\tau\beta)^\phi}. \quad (8.22)$$

Assuming relaxation times are activated, i.e. $\tau = \tau_0 e^{E/T}$, the distribution of relaxation times can be rewritten in terms of a distribution of activation energies. Monthus and Bouchaud [3] and Svare et al.[19] have considered the relaxation function resulting from a distribution of activation energies. Using a Gaussian distribution of activation energies, relaxation functions were produced that resemble stretched exponential relaxation functions.

A distribution of activation energies seem to capture many of the phenomenological aspects of the glass-forming materials. Though equation 8.2(without the compen-

sation temperature) has been considered by previous researchers, to the best of the author's knowledge no one previously has investigated the distribution that yields the Vogel equation.

8.3 Some comments on polymer electrolytes

In light of the discussion of this chapter, some statements can be made that would lead to a slight modification of equation 8.1. Equation 8.1 was proposed for polymer electrolyte conductivity, specifically PEO based polymer electrolytes. Equation 8.1 is equivalent to equation 8.2 with a two delta function distribution. The delta functions are not, of course, physically realistic. The delta functions should be considered as an approximation for the actual physical distribution for polymer electrolytes. The actually physical distribution of polymer electrolytes would lead to an equation different than equation 8.1. A more complex distribution is probably warranted especially for C2000/PPO based systems.

In chapter 1 the close relation between polymer motion and conductivity was mentioned. This relation was presented by discussing the decoupling index and the α -relaxation. A possible reason for the similarity between microscopic structural relaxations/ α -relaxation and the conductivity is suggested.

The decoupling index is the ratio of a microscopic structural relaxation time and a characteristic time associated with the conductivity. The decoupling index indicates that there is a close relation between the microscopic structural relaxation time and

the conductivity. The microscopic structural relaxation time came from measuring the viscosity and then scaling the measured viscosity by the chain length. In the potential energy barrier picture presented in the previous section, a flow event entails the fluidizing of a locally ordered region. The rate of these flow events determines the viscosity. The conductivity is determined by the fluidizing of a locally ordered region which contains an ion. This fluidizing of locally ordered regions allows the ion to move, thus determining the conductivity, and allows segments of the polymer to move, thus allowing the microscopic structural relaxation. It is therefore not unexpected that the timescales associated with structural relaxations and the conductivity be similar.

The α -relaxation involves the relaxation of dipoles along the polymer backbone. In order for these dipoles to relax, a locally ordered region must fluidize. In the fluidized environment the dipoles can relax in response to the applied field. Again, in order for an ion to engage in long range motion the locally ordered region containing the ion must fluidize. Now it is expected that regions in which the cation are coordinated to the polymer would be in deeper wells than regions not coordinating a cation. This would lead to different timescales for the conductivity and the α -relaxation. Shifting the temperature by a characteristic temperature like the glass transition temperature would partially compensate for the shift to a deeper energy well caused by the presence of the cation. The similarity between the α -relaxation and conductivity can be understood by the necessity of disordering local regions, and the subsequent movement that can occur in a disordered region before a new locally ordered region is established.

8.4 Summary

In this chapter the empirical equation 8.1 has been generalized. It was shown that with the proper choice of $g(E)$ equation 8.2 is equivalent to the Vogel equation. The distribution $g_V(E)$ that yields the Vogel equation has many interesting properties. Depending on the mean and variance, $g_V(E)$ can display either Gaussian-like behavior or decaying exponential like behavior.

A possible microscopic picture that can be described by equation 8.2 is as follows. A small local region of a system is considered. This small region contains a number of atoms and molecules. The local region has a number of energy states depending on the arrangement of the constituent particles. The individual particles can not move or have very limited movement. In order for long range movement to occur the particles must move cooperatively. This cooperative movement can be pictured as a hop from a ordered state to a disordered/fluidized state. In this fluidized state the individual particles can move. After some particle rearrangement in the fluidized state, the particles “fall” into a random low energy state. The probability for being in a state with energy E is given by $g(E)$.

8.5 Mathematical Appendix

8.5.1 Derivation of $g_V(E)$

Problem Statement

The main body of this chapter discussed how equation (8.5) resulted from a generalization of the two Arrhenius equation. The goal in this section is to derive the distribution function $g_V(E)$ given equation (8.5).

$$\int_0^{\infty} e^{E(\frac{1}{T} - \frac{1}{T_e})} g_V(E) dE = e^{-\frac{B}{T_e - T_0}} e^{\frac{B}{T - T_0}} \quad (8.23)$$

Notice first of all that the L.H.S. of equation(8.23) resembles a Laplace transform. This connection can be made obvious by rewriting the temperature in terms of a new variable s .

$$-s = \frac{1}{T} - \frac{1}{T_e} \Rightarrow T = \frac{1}{-s + \frac{1}{T_e}} \quad (8.24)$$

Equation (8.23) therefore becomes

$$\int_0^{\infty} e^{-Es} g_V(E) dE = e^{\frac{B}{T_e - T_0}} e^{\frac{B(-s + \frac{1}{T_e})}{1 + sT_0 - \frac{T_0}{T_e}}} \quad (8.25)$$

Now that the relation between equation (8.23) and a Laplace transform has been made, the inverse Laplace transform can be used to find $g_V(E)$. The function $g_V(E)$ given in terms of a inverse Laplace transform is given in equation (8.26).

$$g_V(E) = \frac{1}{2\pi i} \int_{c-i\infty}^{c+i\infty} \left\{ e^{-\frac{B}{T_e - T_0}} e^{\frac{B(-s + \frac{1}{T_e})}{1 + sT_0 - \frac{T_0}{T_e}}} \right\} e^{Es} ds \quad (8.26)$$

In order to simplify the expression the following definitions are made.

$$\phi = \frac{1}{T_e} - \frac{1}{T_0}, \sigma = \frac{-B}{T_0}, \gamma = \frac{1}{T_e} \quad (8.27)$$

Equation (8.26) therefore becomes

$$g_V(E) = \frac{1}{2\pi i} \int_{c-i\infty}^{c+i\infty} \left\{ e^{-\frac{B}{T_e - T_0}} e^{\frac{\sigma(s-\gamma)}{s-\phi}} \right\} e^{Es} ds \quad (8.28)$$

Equation (8.28) will be used to find $g_V(E)$.

The inverse Laplace Transform

The inverse Laplace transform involves an integral along the line from $c-i\infty$ to $c+i\infty$.

The real number c is chosen so that the singularities of the integrand are to the left of it. The integrand in equation (8.28) is $e^{\frac{\sigma(s-\gamma)}{s-\phi}}$. There is a singularity at $s = \phi$.

This singularity is to the left of the imaginary axis as long as $T_e > T_0$. Assuming

this is the case, the real number c is set equal to zero. The integral therefore is along

the imaginary axis. What is desired, of course, is a closed contour integral so that

the theorems of contour integration from complex variable theory can be applied.

An infinite circular arc starting at $i\infty$ and ending at $-i\infty$ and oriented to the left

of the imaginary axis (in order to enclose the singularity) is appended to the original

contour from $-i\infty$ to $i\infty$. Integration is now along a closed contour. However before

the relevant theorems of contour integration can be applied, it must be shown that

the integral is zero along the circular half arc.

In order to show that the integral along the circular arc is zero, the variable

of integration s is written as $s = Re^{i\theta}$ where the radius $R \rightarrow \infty$. There are two

exponentials in equation (8.28) which involve s . These exponentials must be examined

individually as $R \rightarrow \infty$.

$$e^{\sigma \frac{(Re^{i\theta} - \gamma)}{(Re^{i\theta} - \phi)}} \rightarrow e^{\sigma \frac{Re^{i\theta}}{Re^{i\theta}}} \rightarrow e^{\sigma} \quad (8.29)$$

$$e^{ERe^{i\theta}} \rightarrow e^{ER(\cos\theta + i\sin\theta)} \rightarrow 0 \quad (\cos\theta < 0) \quad (8.30)$$

The integrand along the infinite circular half arc is therefore a constant times zero. The integral along the infinite circular half arc is therefore zero as desired. The complex variable theorems relevant to close contour integrals in the complex plane can therefore be applied.

The relevant complex variable theorem is, of course, that a closed contour integral is equal to the sum of the residues.

$$\int_C f(z)dz = 2\pi i \sum a_{-1} \quad (8.31)$$

However there is an additional complication associated with the integrand in equation (8.28). The complication involves the expression $e^{\frac{\sigma(s-\gamma)}{s-\phi}}$. The singularity at $s = \phi$ is an essential singularity as opposed to a pole of n^{th} order. The usual expression for the residue a_{-1} ,

$$a_{-1} = \frac{1}{(n-1)!} \left\{ \left(\frac{d}{dz} \right)^{n-1} [(z-z_0)^n f(z)] \right\}_{z=z_0}, \quad (8.32)$$

can not be used. What can be done instead is to expand the integrand in a Laurent series. A Laurent series is an expression for a function f about a singularity z_0 .

$$f(z) = \sum_{j=-\infty}^{\infty} a_j (z-z_0)^j \quad (8.33)$$

where

$$a_j = \frac{1}{2\pi i} \oint_C \frac{f(p)}{(p-z_0)^{j+1}} dp \quad (8.34)$$

The residue a_{-1} can therefore be found by expanding the integrand in a Laurent series and reading off the coefficient to the $(z-z_0)^{-1}$ or in our case $(s-\phi)^{-1}$ term.

The first step is to expand the first exponential in the integrand in a Taylor series.

$$e^{\frac{\sigma(s-\gamma)}{s-\phi}} = \sum_{m=0}^{\infty} \frac{1}{m!} \left[\frac{\sigma(s-\gamma)}{s-\phi} \right]^m \quad (8.35)$$

Inserting the Taylor series in equation (8.28) gives

$$g_V(E) = \frac{1}{2\pi i} \sum_{m=0}^{\infty} \frac{1}{m!} \int_C \left[\frac{\sigma(s-\gamma)}{s-\phi} \right]^m e^{Es} ds. \quad (8.36)$$

The integrand of equation (8.36) is what will be expanded into a Laurent series. The expansion is

$$\begin{aligned} \left[\frac{\sigma(s-\gamma)}{s-\phi} \right]^m e^{Es} &= \sigma^m \left[\frac{(s-\phi) + (\phi-\gamma)}{s-\phi} \right]^m e^{E(s-\phi+\phi)} \\ &= \sigma^m e^{E\phi} \sum_{k=0}^m \binom{m}{k} (s-\phi)^{m-k} (\phi-\gamma)^k (s-\phi)^{-m} \sum_{l=0}^{\infty} \frac{1}{l!} E^l (s-\phi)^l \\ &= \sigma^m e^{E\phi} \sum_{l=0}^{\infty} \sum_{k=0}^m \binom{m}{k} \frac{1}{l!} E^l (\phi-\gamma)^k (s-\phi)^{l-k} \end{aligned} \quad (8.37)$$

In the above expansion the binomial expansion has been used.

$$(a+b)^n = \sum_{k=0}^{\infty} \binom{n}{k} a^{n-k} b^k \quad (8.38)$$

The coefficient of $(s-\phi)^{-1}$ is required.

$$l-k = -1 \Rightarrow l = k-1 \quad (8.39)$$

The a_{-1} coefficient for Laurent series of the integrand of equation (8.36) is therefore

$$a_{-1} = \sigma^m e^{E\phi} \sum_{k=0}^m \binom{m}{k} \frac{1}{(k-1)!} E^{k-1} (\phi-\gamma)^k. \quad (8.40)$$

The result from the Laurent expansion

$$\int_C \left[\frac{\sigma(s-\gamma)}{s-\phi} \right]^m e^{Es} ds = 2\pi i \sigma^m e^{E\phi} \sum_{k=0}^m \binom{m}{k} \frac{1}{(k-1)!} E^{k-1} (\phi-\gamma)^k \quad (8.41)$$

can be inserted into equation (8.36) to give the expression for $g_V(E)$.

$$g_V(E) = e^{-\frac{B}{T_e - T_0}} \sum_{m=0}^{\infty} \frac{1}{m!} \sigma^m e^{E\phi} \sum_{l=0}^m \binom{m}{k} \frac{1}{(k-1)!} E^{k-1} (\phi - \gamma)^k \quad (8.42)$$

Normalization

Equation (8.23) required that $g_V(E)$ be normalized. Here is shown that $g_V(E)$ from equation (8.42) is indeed normalized, i.e.

$$\int_0^{\infty} g_V(E) dE = 1. \quad (8.43)$$

In equation (8.42) the terms involving the variable of integration E are of the form $E^{k-1} e^{E\phi}$. Integration of these terms gives

$$\begin{aligned} \int_0^{\infty} E^{k-1} e^{E\phi} dE &= \left(\frac{d}{d\phi} \right)^{k-1} \int_0^{\infty} e^{E\phi} dE = \left(\frac{d}{d\phi} \right)^{k-1} \left(\frac{-1}{\phi} \right) \\ &= \frac{(-1)^k (k-1)!}{\phi^k}. \end{aligned} \quad (8.44)$$

The integral of $g_V(E)$ is therefore

$$\begin{aligned} \int_0^{\infty} g_V(E) dE &= e^{-\frac{B}{T_e - T_0}} \sum_{m=0}^{\infty} \frac{1}{m!} \sigma^m \sum_{k=0}^m \binom{m}{k} \frac{1}{(k-1)!} (\phi - \gamma)^k \frac{(-1)^k (k-1)!}{\phi^k} \\ &= e^{-\frac{B}{T_e - T_0}} \sum_{m=0}^{\infty} \frac{1}{m!} \sigma^m \sum_{k=0}^m \binom{m}{k} (\gamma/\phi - 1)^k (1)^{m-k} \\ &= e^{-\frac{B}{T_e - T_0}} e^{\frac{\sigma\gamma}{\phi}} \\ &= e^{-\frac{B}{T_e - T_0}} e^{-\frac{B}{T_0 T_e} \left(\frac{1}{T_e} - \frac{1}{T_0} \right)^{-1}} \\ &= e^{-\frac{B}{T_e - T_0}} e^{-\frac{B}{T_0 T_e} \frac{T_e T_0}{T_0 - T_e}} \end{aligned}$$

$$\begin{aligned}
&= e^{\frac{-B}{T_e - T_0}} e^{\frac{B}{T_e - T_0}} \\
&= 1
\end{aligned} \tag{8.45}$$

where the binomial expansion (equation (8.38)) has been used in reverse.

8.5.2 Characteristic Function

The characteristic function was used in section 8.1 to show that $g_V(E)$ was independent of the characteristic energy T_e . The characteristic function of $g_V(E)$ has a closed form which is preferable to the infinite series form of $g_V(E)$ itself. In this section the details of the calculation of the characteristic function of $g_V(E)$ are given.

The definition of a characteristic function for some distribution $g(E)$ is

$$\phi(p) = \int e^{ipE} g(E) dE. \tag{8.46}$$

For $g_V(E)$, this involves integration of terms of the form $E^{k-1} e^{E(\phi+ip)}$. Similar to equation (8.44), integration of these terms gives

$$\int E^{k-1} e^{E(\phi+ip)} dE = (-1)^k \frac{(k-1)!}{(\phi+ip)^k}. \tag{8.47}$$

Using this result gives for $\phi_V(p)$

$$\begin{aligned}
\phi_V(p) &= e^{\frac{-B}{T_e - T_0}} \sum_{m=0}^{\infty} \frac{1}{m!} \sigma^m \sum_{k=0}^m \binom{m}{k} (-1)^k \left(\frac{\phi - \gamma}{\phi + ip} \right)^k \\
&= e^{\frac{-B}{T_e - T_0}} \sum_{m=0}^{\infty} \frac{1}{m!} \sigma^m \left(\frac{\gamma - \phi}{\phi + ip} + 1 \right)^m \\
&= e^{\frac{-B}{T_e - T_0}} \sum_{m=0}^{\infty} \frac{1}{m!} \sigma^m \left(\frac{\gamma + ip}{\phi + pi} \right)^m \\
&= e^{\frac{-B}{T_e - T_0}} e^{\sigma \frac{\gamma + ip}{\phi + pi}}.
\end{aligned} \tag{8.48}$$

Rewriting the terms appearing in the exponent of the exponential as

$$\frac{\gamma + ip}{\phi + ip} = \frac{\gamma}{\phi} + \frac{ip(\phi - \gamma)}{\phi(\phi + ip)} \quad (8.49)$$

and using the definition of ϕ , γ , and σ given in (8.27) gives after some algebraic rearrangement

$$\phi_V(p) = \exp\left(\frac{\langle E \rangle ip}{1 - \frac{\sigma_E^2}{2\langle E \rangle} ip}\right). \quad (8.50)$$

A part of the value of characteristic functions is that they are moment generating functions of distributions. To see this start with the definition of the characteristic function (8.46) and expand the exponential in a Taylor series.

$$\begin{aligned} \phi_V(p) &= \int g_V(E) \left(1 + ipE - \frac{1}{2!}p^2E^2 - \frac{i}{3!}p^3E^3 + \dots\right) dE \\ &= 1 + ip\langle E \rangle - \frac{p^2}{2!}\langle E^2 \rangle + \dots + \frac{(ip)^n}{n!}\langle E^n \rangle + \dots \end{aligned} \quad (8.51)$$

It is seen that all moments of a distribution $g(E)$ can be found from the formula

$$\langle E^n \rangle = \frac{1}{i^n} \left(\frac{d}{dp}\right)^n \phi(p) \Big|_{p=0} \quad (8.52)$$

As a consistency check, $\langle E \rangle$ will be computed using the above formula.

$$\begin{aligned} \langle E \rangle &= \frac{1}{i} \frac{d}{dp} \exp\left(\frac{\langle E \rangle ip}{1 - \frac{\sigma_E^2}{2\langle E \rangle} ip}\right) \Big|_{p=0} \\ &= \frac{1}{i} \exp\left(\frac{\langle E \rangle ip}{1 - \frac{\sigma_E^2}{2\langle E \rangle} ip}\right) \frac{d}{dp} \left(\frac{\langle E \rangle ip}{1 - \frac{\sigma_E^2}{2\langle E \rangle} ip}\right) \Big|_{p=0} \\ &= \frac{1}{i} \exp\left(\frac{\langle E \rangle ip}{1 - \frac{\sigma_E^2}{2\langle E \rangle} ip}\right) \left(\frac{\langle E \rangle i}{1 - \frac{\sigma_E^2}{2\langle E \rangle} ip} + \frac{\langle E \rangle ip \left(\frac{\sigma_E^2}{2\langle E \rangle} i\right)}{\left(1 - \frac{\sigma_E^2}{2\langle E \rangle} ip\right)^2}\right) \Big|_{p=0} \\ &= \frac{1}{i} \langle E \rangle i \\ &= \langle E \rangle \end{aligned} \quad (8.53)$$

Bibliography

- [1] K. H. Kim, D. R. Torgeson, F. Borsa, J. Cho, S. W. Martin, and I. Svare. *Solid State Ionics*, 91:7, 1996.
- [2] O. Bohnke, J. Emery, A. Veron, J. L. Fourquet, J. Y. Buzare, P. Florian, and D. Massiot. *Solid State Ionics*, 109:25, 1998.
- [3] C. Monthus and J. P. Bouchaud. *J. Phys. A: Math. Gen.*, 29:3847, 1996.
- [4] W. Kauzmann. *Chem. Rev.*, 43:219, 1948.
- [5] J. Jackle. *Rep. Prog. Phys.*, 49:171, 1986.
- [6] M. D. Ediger, C. A. Angell, and S. R. Nagel. *J. Phys. Chem.*, 100:13200, 1996.
- [7] C. A. Angell, K. L. Ngai, G. B. McKenna, P. F. McMillan, and S. W. Martin. *J. Appl. Phys.*, 88:3113, 2000.
- [8] P. G. Debenedetti and F. H. Stillinger. *Nature*, 410:259, 2001.
- [9] M. L. Ferrer, C. Lawrence, B. G. Demirjian, and D. Kivelson. *J. Chem. Phys.*, 109:8010, 1998.

- [10] M. L. Ferrer and D. Kivelson. *J. Chem. Phys.*, 110:10963, 1999.
- [11] J. T. Bendler, J. J. Fontanella and M. F. Shlesinger, and M. C. Wintersgill. *Electrochim. Acta*, 48:2267, 2003.
- [12] M. Goldstein. *J. Chem. Phys.*, 51:3728, 1969.
- [13] F. H. Stillinger. *Science*, 267:1935, 1995.
- [14] V. I. Arkhipov and H. Bassler. *J. Phys. Chem.*, 98:662, 1994.
- [15] J. C. Dyre. *Phys. Rev. B*, 51:12276, 1995.
- [16] S. A. Brawer. *J. Chem. Phys.*, 81:954, 1984.
- [17] M. D. Ediger. *Annu. Rev. Phys. Chem.*, 51:99, 2000.
- [18] R. Richert. *J. Phys.: Condens. Matter*, 14:R703, 2002.
- [19] I. Svare, S. W. Martin, and F. Borsa. *Phys. Rev. B*, 61:228, 2000.

Chapter 9

Summary and Future Work

9.1 Summary

This investigation into polymer electrolyte conductivity began with an examination of the frequency-dependent properties of the real part of the conductivity. There it was seen that the frequency-dependent conductivity of polymer electrolytes resembles the frequency-dependent properties of other disordered solid ionic conductors such as ionic glasses. These similarities include: (1) a power law dependence of the conductivity at high frequencies(see figure 3.2), (2) the BNN relation is found to hold(see figure 3.5), and (3) for a given salt concentration the temperature dependent conductivity can be scaled onto a master curve(see figure 3.6). Models that have been used to understand these frequency-dependent conductivity properties include: (A) a macroscopic model that considers a network of resistors each of which is in parallel with a capacitor, (B) a barrier hopping model with a distribution of barrier heights, and (C) Monte Carlo simulations that include a distribution of site energies and coulomb interactions. The

fact that similar frequency-dependent properties are seen in polymer electrolytes and other disordered ionic conductors suggest that a similar ionic transport mechanism might be operating.

A close examination of the frequency-dependent impedance of semicrystalline PEO LiTF 10-1 provided some interesting clues to the conductivity. What was seen in PEO LiTF 10-1 was two temperature dependent components that made up the DC conductivity. These components were seen as temperature dependent peaks in the plots of the imaginary part of the impedance versus the logarithm of frequency(see figure 4.2). Since the two peaks were fairly well resolved in frequency, non-linear curve fitting was used to deconvolve the two components. Non-linear curve fitting revealed that the high frequency component was consistent with the high temperature DC conductivity. The presence of the low frequency component was not detected at high temperatures. The results of the curve fitting suggested that there are two resistors in series and that each of the resistors have a Arrhenius like temperature dependence. This leads to the following equation for the conductivity:

$$\sigma = \frac{1}{\frac{e^{E_{\beta}/kT}}{\sigma_{\beta}} + \frac{e^{E_{\alpha}/kT}}{\sigma_{\alpha}}}. \quad (9.1)$$

It should be emphasized that figure 4.2 only reveals the presence of at least two components. Most likely there is a distribution of components, but these other components are not resolved. Since equation 9.1 only considers two components from a likely distribution of components, it can only be considered approximate.

Equation 9.1 was applied to the C2000 LiTFSI family of polymer electrolytes. The fits to the C2000 LiTFSI were satisfactory, but resulted in some physically unreason-

able values of σ_α . A plot of the logarithms of the prefactors versus the activation energies showed a straight line(see figure 5.9). A linear relationship between the logarithm of the prefactors and activation energy is known as the compensation effect. Incorporating the compensation effect, equation 9.1 becomes

$$\sigma = \frac{2\sigma_0}{e^{E_\beta(\frac{1}{kT} - \frac{1}{kT_e})} + e^{E_\alpha(\frac{1}{kT} - \frac{1}{kT_e})}}. \quad (9.2)$$

There are a number of theories that lead to the compensation effect. A common thread to many of these theories is that excitations are taken from the heat bath and used to overcome the barriers that limit the process.

A tentative microscopic picture was proposed for equation 9.2. This picture involves ion-ion interactions and ion-polymer interactions. For PEO-based systems it was suggested that E_α is due to ion-polymer interactions. However, it is necessary to consider a small region surrounding the ion, and the energy necessary to disorder this region. The region “hops” from a locally ordered configuration to a fluidized state. It was also suggested that E_β was due to ion-ion interactions. For C2000/PPO based systems a approximate separation of E_α and E_β into ion-polymer interactions and ion-ion interactions might not apply. In this case complicated structures involving ion aggregation and ion-polymer interactions and the energy necessary to fluidize these structures must be considered. The compensation effect temperature, T_e , was linked to peaks seen in the far IR spectra(see figures 7.4 and 7.5). These peaks are especially interesting since they involve torsions and bending vibrations of fairly long segments of the polymer backbone. These vibrations would seem an ideal source for the excitations that fluidize the regions surrounding the cation.

Two traditional arguments that lead to the Vogel equation were presented. These arguments are based on the ideas of free volume and configurational entropy. A third approach to understanding the Vogel equation was also presented. The approach considers the Vogel equation to be due to a distribution of activation energies. This approach was suggested because it is consistent with a hopping model approach to the frequency-dependent conductivity and because it is an obvious generalization of equation 9.2. While all three arguments lead to the Vogel equation, the physical interpretation of the different approaches is different. The free volume argument is the easiest to understand. It assumes that $v_f \propto T - T_0$ where v_f is the free volume and T_0 is the temperature at which the free volume vanishes. The configuration entropy argument uses the idea of cooperatively rearranging regions (CRRs). These CRRs can be in one of two states. The dramatic increases in some characteristic time of the system is associated with the growth of the CRRs. As the CRRs grow the time it takes to hop between the two states increases. In the approach presented in this thesis instead of two states a small region can be in one of a distribution of energy states. In order for the small region to adopt a new state it must “hop” from its current configuration to a more fluid like state. In this fluid-like state the constituent particles can rearrange. The fluid like state then falls into a lower energy state given by the distribution of energy states. The dramatic slowing down of the system as the temperature decreases is because the regions become trapped in deep well states. The distribution leading to the Vogel equation was found in this study, and some of its interesting properties were discussed.

9.2 Future Work

In order to further support the picture described in this work a number of projects can be undertaken.

First, a wider range of experimental data needs to be taken. Preferably the polymers would be amorphous and have a large molecular weight. Unfortunately the number of polymers that fit this description and are easily available are limited. Also a larger temperature range with low temperatures around -30°C is desirable. Again this is not easily done since the large resistances encountered at low temperatures are not easily measured. Recall that one low temperature study showed Arrhenius behavior at low temperatures (see figure 4.6). Once the amorphous conductivity data is obtained, fits to equation 9.2 can extract the value of T_e (if low temperature Arrhenius behavior is observed). For a given polymer salt system at low to medium salt concentrations the values of T_e should be similar. The far IR of the system should also be examined to see if T_e correlates with any vibrational peaks.

Second, it was suggested that E_{α} and E_{β} were related to ion-polymer and ion-ion interactions, respectively. This hypothesis can be tested by using different cations and anions. Specifically ions with higher valencies should give values for E_{β} and E_{α} quite different than the single valence lithium ion.

Third, related to the above experiment, the values of E_{α} and E_{β} can be compared to computer calculations. This would require knowledge of the local structures formed in the polymer electrolyte and of the transition state. Such local structures can be

guessed at from studies of small molecules that locally resemble the polymer. As for E_β , it was suggested that in PEO-“based system E_β might be primarily determined by ion-ion interactions. If this is so than molecular dyanamic or Monte Carlo simulations of positive and negative ions might provide reasonable estimates of E_β .

Fourth, since the hopping model approach to the Vogel equation was suggested based on the frequency-dependent conductivity, it would be desireable to connect the frequency dispersion to the non-Arrhenius DC conductivity. If, for example, a system shows non-Arrhenius behavior over a large temperature range, the Vogel equation rather than the two Arrhenius equation must be used for fitting. This fitting will then give values for $\langle E \rangle$ and σ_E . Once $g_V(E)$ is known, it should be possible to calculate the frequency-dependent conductivity $\sigma(\omega)$ (within some approximation). This calculated $\sigma(\omega)$ can then be compared to the measured frequency-dependent conductivity. This procedure is complicated by the possible presence of T_e and by the possible presence of percolation effects.

Fifth, a theory of the prefactor σ_0 (or x_0 in the generalized expression) is needed. The nature of the prefactor in conductivity and other rate process is a longstanding problem which will not be solved here. However, it is natural to suppose that the prefactor would depend on the concentration of free ions. An intriguing clue is provided by the BNN relation. The BNN relation states that $\sigma_{DC} \simeq \Delta\epsilon\epsilon_0\omega_m$. The dielectric loss strength is probably related to the movement and aggregation of ions and would seem to have some relation to the number of effective free ions. The characteristic frequency ω_m marks the start of frequency dispersion. It is therefore the smallest

time associated with normal diffusion, i.e. long range ion movement. More work on the nature of $\Delta\epsilon$ should prove worthwhile.